APPLICATION OF MACHINE LEARNING IN PACKAGING DYNAMICS AND DISTRIBUTION: CASE STUDIES ON PREDICTING DAMAGE FROM BUCKLING IN CORRUGATED PAPERBOARD STRUCTURES TO BRUISING IN TRANSPORTED PACKED APPLE FRUIT

By

Khadijeh Shirzad

A DISSERTATION

Submitted to
Michigan State University
in partial fulfillment of the requirements
for the degree of

Packaging – Doctor of Philosophy

2024

ABSTRACT

Understanding packaging dynamics and identifying hazards in physical distribution are essential for reducing damage risk to packages and products, thus improving their integrity. Evaluating the mechanical properties of package structures in different designs and environments through experimental tests is time-consuming and costly. While mechanics-based simulation models like the Finite Element Method have been used to address these challenges, they often rely on simplified assumptions due to the complex mechanical responses of composite structures.

Recent advancements in artificial intelligence, particularly machine learning, offer innovative solutions for efficient problem-solving, optimization, and predictive insights. In package dynamics and distribution, machine learning models provide significant cost and time advantages over traditional experimental testing by predicting performance without extensive physical trials. Machine learning learns from data and generates predictive models using advanced algorithms. This dissertation explores the use of machine learning techniques to predict damage to package structures and products after transportation vibrations, offering insights and predictive tools for future package designs. The machine learning solution is time and cost-efficient, eliminating the need for additional experimental tests once predictions are made. The application is demonstrated through three studies: a) analyzing and predicting the buckling behavior of corrugated paperboards with cutouts, b) predicting bruising damage to packaged apple fruits from vibrational forces during transportation, and c) forecasting the loss of compression strength in corrugated paperboard boxes post-transportation vibrations. Chapter 1 introduces the use of machine learning in package dynamics, outlines the algorithms used, and presents the research goals and case studies. While the studies are related to packaging dynamics, they differ in parameters, so the literature review is presented separately in each chapter. Chapter 2 investigates the relationship between cutout

characteristics and buckling loads in ventilated corrugated paperboard boxes using experimental tests and Finite Element Method simulations. The study found that larger cutouts reduce buckling resistance, while positioning holes closer to horizontal edges maintains higher strength. The machine learning model effectively predicts buckling strength, achieving 91.45 R^2 accuracy on experimental data for plates with single cutouts and 94.68 R^2 accuracy on simulation data for plates with multiple circular cutouts. Chapter 3 develops machine learning solutions to predict bruising damage to apples during transportation, identifying vibration intensity as the primary factor affecting damage. Chapter 4 examines the loss of compression strength in corrugated paperboard boxes due to transportation vibrations, using machine learning models that achieve an R^2 score of 0.93 to predict this degradation accurately. The analysis reveals that vibration characteristics have a more significant impact on compression strength than package dimensions. Chapter 5 summarizes the findings and suggests directions for future research to enhance the durability and performance of packaging systems. The novelty of this dissertation lies in demonstrating the application of machine learning in predicting dynamic damage in packaging dynamics and distribution through three case studies. While machine learning has been used for optimizing packaging geometry, its application in predicting mechanical failures is relatively limited. This research enhances the understanding of damage to package structures and products after transportation and provides a machine learning-based tool for predicting damage, which can be adapted for similar tests. In summary, the dissertation highlights the significant potential of machine learning in addressing challenges within packaging dynamics and distribution.

To my family, for their unconditional love and encouragement.
Thank you for believing in me and being my constant source of strength.

ACKNOWLEDGMENTS

Completing this dissertation has been a significant milestone in my academic journey, and it would not have been possible without the support and guidance of many individuals. First and foremost, I would like to express my gratitude to my advisor for his support, insightful guidance, and constant encouragement throughout my research. I am also grateful to my dissertation committee members for their valuable feedback, constructive criticism, and continuous support. I would also like to acknowledge the financial support from the School of Packaging, which provided the necessary resources to conduct this research. I am deeply appreciative of my family for their unwavering support and understanding. Their patience and belief in my abilities have been a constant source of motivation. Lastly, I extend my sincere thanks to my colleagues and friends who offered their assistance, shared their knowledge, and provided moral support during challenging times. Thank you all for making this achievement possible.

TABLE OF CONTENTS

Chapter 1: Introduction

Throughout the supply chain, from manufacturing facilities to end users, packaging plays a crucial role in protecting and preserving products (Ait-Oubahou et al., 2019; Natarajan et al., 2014; Sharma et al., 2021). Packaging not only ensures that products remain undamaged and functional upon delivery but also extends their shelf life by preventing contamination and degradation. Effective packaging provides protection against environmental factors like moisture, temperature fluctuations, and light, ensuring product quality remains preserved. Additionally, well-designed packaging enhances the consumer experience by providing convenience, ease of use, and clear information about the product. In the context of global trade, robust packaging solutions are essential for maintaining product integrity across long distances and varied transportation conditions.

1.1 Machine learning

Machine Learning (ML) Machine learning is essentially a type of applied statistics that places greater emphasis on using computers to estimate complex functions and less emphasis on determining confidence intervals for these functions (Goodfellow et al., 2016). These models learn patterns and make predictions or decisions based on data. ML encompasses various methods, including supervised learning, which involves learning from labeled data. It also includes unsupervised learning, which involves finding patterns in unlabeled data. Additionally, reinforcement learning involves learning optimal actions through trial-and-error interactions with an environment (Sutton & Barto, 2018). The purpose of ML models is to develop a mathematical approach to predict the complex patterns of sample data.

1.2 Application of ML model in packaging

ML has several applications in the packaging industry, addressing various challenges and enhancing overall efficiency. Here are some key areas where ML is making a significant impact:

- Optimizing Packaging Design: ML can be used to analyze historical data on packaging failures, helping engineers design more robust packaging solutions tailored to specific products (Mrówczyński et al., 2023)
- Predicting Potential Damage: ML models can predict the likelihood of damage under different scenarios, allowing for the anticipation and mitigation of risks associated with vibration, shock, and compression during transportation (Yin et al., 2024).
- Enhancing Performance and Sustainability: By identifying patterns and making accurate predictions, ML can enhance the overall performance and sustainability of packaging materials, leading to more efficient and environmentally friendly solutions. In other fields, ML is also used for sustainability, such as manufacturing (Kaur et al., 2023) and predicting scrapping inventory in environmental management, which helps reduce material waste and manage e-waste effectively (Huang & Liu, 2023). These applications demonstrate the broad potential of ML to contribute to sustainability across various industries.
- Produce Preservation: ML can determine optimal parameter combinations to maximize the shelf life of perishable goods, improving the preservation of produce during storage and transportation (Mohammed et al., 2023; Palumbo et al., 2022).
- Quality Control in Production: ML enhances quality control in production by continuously monitoring data from sensors and IoT (Internet of Things) devices (Ali et al., 2020), detecting anomalies (Jaramillo-Alcazar et al., 2023), and automatically adjusting production parameters to maintain consistent quality and reduce waste. This leads to more efficient, reliable packaging operations with fewer defects and lower production costs.

- Improving Supply Chain Processes: ML can analyze large volumes of data to identify patterns and make predictions that significantly improve supply chain processes and packaging operations, leading to increased efficiency and reduced costs (Min, 2010; Tan et al., 2017).

1.3 Packaging dynamics and challenges

Packages in distribution environments are exposed to various hazards (Dunno et al., 2016) including vibration, shock, and compression forces, which compromise the integrity and functionality of the package. Packaging dynamics involves the study of how packages behave under various environmental and mechanical stresses during handling and transportation. Key aspects of packaging dynamics include:

1. Shock: Sudden and intense forces resulting from drops or impacts can cause immediate damage to packaging and its contents. Understanding shock dynamics helps in designing packaging that can absorb energy to protect the product (Ficuspax, 2023).
2. Vibration: Continuous vibrations during transportation, especially over long distances, can lead to cumulative damage (Schmitz & Smith, 2012), such as fatigue in materials or loosening of components. Vibration analysis helps in creating packaging that can withstand or mitigate these effects.
3. Compression: Stacking and storage subject packages to compressive forces, which can deform or crush them (Testronix Instruments, 2023). Studying compression dynamics ensures that packaging can maintain its structural integrity under load.
4. Temperature Variation: Changes in temperature during transportation and storage can affect the integrity and performance of both the packaging and its contents (Hamm et al., 2018). Temperature fluctuations can cause materials to expand, contract, become brittle, or degrade. Understanding temperature dynamics is crucial for designing packaging that

provides thermal insulation or temperature regulation, ensuring product stability and longevity.

5. Humidity and Moisture: Exposure to humidity and moisture can weaken packaging materials, cause corrosion, promote mold growth, and lead to spoilage or degradation of the contents. Moisture dynamics involves studying how humidity levels and water exposure affect the packaging and product. Designing moisture-resistant packaging or incorporating desiccants can help protect against these adverse effects (Defraeye et al., 2015).

Packaging professionals face several challenges, including accurately predicting how different materials and designs will respond to dynamic forces, balancing protection with cost and sustainability, and adapting to varied and unpredictable transportation conditions. Traditional methods often rely on extensive physical testing, which can be time-consuming and costly.

To mitigate these risks and reduce the cost and time, innovative solutions are required to design and optimize packaging systems that can withstand the rigors of transportation and handling. This involves not only selecting appropriate materials and designs but also understanding and predicting the dynamic stresses that packages will encounter throughout the supply chain. In this context, the application of ML techniques presents a transformative approach to addressing the challenges in packaging dynamics and distribution hazards. ML algorithms can analyze vast amounts of data from past transportation scenarios to identify patterns and predict potential points of failure. By using predictive modeling, ML can simulate different packaging designs and transportation conditions, allowing engineers to optimize packaging solutions without the need for extensive physical testing. Moreover, predictive models developed using ML can reduce the need for extensive physical testing by simulating various stress conditions and predicting the

performance of packaging designs. This not only saves time but also allows for rapid prototyping and iteration. Additionally, ML can continuously learn and improve from new data, ensuring that packaging designs remain effective as transportation methods and conditions evolve. This capability not only enhances the resilience and reliability of packaging but also contributes to cost savings and sustainability by reducing material usage and minimizing product losses.

This dissertation explores the application of machine learning in packaging dynamics, focusing on predicting specific package damages during transportation through three specific studies. ML models might be able to enhance the overall efficiency and reliability of packaging systems, leading to reduced damage during transit, improved product quality, and increased cost-effectiveness in packaging logistics.

1.4 ML algorithms employed in this dissertation

This dissertation employs several ML algorithms, including Linear Regression, Support Vector Regression, K-Nearest Neighbor, Decision Tree Regressor, Random Forest Regression, Light Gradient Boosting Machine, and XGBoost, to predict the performance and integrity of packaging under various environmental and mechanical stresses. These algorithms are chosen for their ability to handle complex datasets and provide accurate predictions, enhancing the efficiency of packaging design and testing processes.

1.4.1 Linear regression model

Linear regression models are widely used for prediction in various fields, including business and industry due to their simplicity and interpretability. These models assume a linear relationship between the input variables and the output, typically represented by the Eq. 1:

$$y = \beta_0 + \beta_1 x_1 + \beta_2 x_2 + \cdots + \beta_p x_p + \epsilon \quad (1)$$

where y is the dependent variable, β_0 is the intercept, β_1, β_2, …, β_p are the coefficients of the input variables x_1, x_2, …, x_p, and ϵ is the error term. Linear regression models are particularly useful in situations with small training sets or sparse data (Montgomery et al., 2021). Despite their simplicity, linear regression models can outperform more complex models in certain prediction scenarios (Hastie et al., 2009). Furthermore, their coefficients provide insights into the relative importance of different predictors, aiding in feature selection and model interpretation. Additionally, linear regression serves as a foundation for more advanced statistical and ML methods, making it an essential tool for data analysts and researchers. Linear regression aims to find the best-fitting straight line through the data points, minimizing the differences between the observed values and those predicted by the model (Raschka & Mirjalili, 2017).

1.4.2 Support vector regression (SVR)

The SVR (Support Vector Regression) method is a well-established technique used for predicting both linear and non-linear regression problems. It is particularly useful when dealing with a limited amount of sample data. The fundamental principles of SVR formulated by Vapnik (Vapnik, 1964) follow the same methodology of support vector machines used in classification methods (Smola & Schölkopf, 2004). In a support vector machine classification algorithm, each labeled sample within the training dataset is treated as a data point within a multidimensional feature space. Within this feature space, a hyperplane is employed to classify the training data points. In contrast, the SVR model introduces an ε-insensitive loss function to determine a hyperplane that allows for an ε deviation between predicted and actual values within the training data (Zhang & O'Donnell, 2019).

1.4.3 K-Nearest Neighbor (KNN)

The KNN regression is a widely used ML method that is easy, simple, straightforward to interpret, and computationally cost-effective. In the KNN regression, the average values of k nearest neighbors are used to predict continuous values. The KNN regression estimates new data points based on the feature similarities (Mahmoodzadeh et al., 2021). In this method, each new data is given a distance value according to its similarity to the train data set. These distances (i.e., d) are calculated using various methods, including the Euclidian metric (Eq. 2), Manhattan metric (Eq. 3), and the Minkowski metric (Eq. 4) for continuous data value.

$$d = \sqrt{\sum_{i=1}^{n} (p_i - q_i)^2} \tag{2}$$

$$d = \sum_{i=1}^{n} |(p_i - q_i)| \tag{3}$$

$$d = \left\{ \sum_{i=1}^{n} (|p_i - q_i|)^m \right\}^{1/m} \tag{4}$$

where p_i is the new data point and q_i is the existing data point, n is the number of data points, and m is a positive value. Following the distance measurement of a new observation from the training set, the k nearest data points are to be considered. In this study, the KNN method is applied by 6 neighbors (i.e., k=6) as the optimal value of k.

1.4.4 Decision tree regression model

Decision tree regression is a powerful tool for data analysis, particularly in the context of categorical and continuous data (Olson & Wu, 2017). The representation of decision trees, including the use of different node representations, can significantly impact their performance (Czajkowski & Kretowski, 2016). Decision tree algorithms, such as ID3, C4.5, CHAID, and

CART, are widely used for classification and regression tasks, with pruning being a key method for improving accuracy (Olson & Wu, 2017). These algorithms are favored for their simplicity, effectiveness, and competitive performance (Jena & Dehuri, 2020). Classification trees are used when the dependent variable has a finite number of unordered values. They help in categorizing the data into distinct classes. In contrast, regression trees are designed for dependent variables that are continuous or have ordered discrete values, focusing on predicting a numerical outcome rather than a category. The decision tree regression algorithm works by first splitting the data into subsets based on the value of the features, seeking to find splits that minimize the variance in the target variable within each subset. This process continues recursively, creating a tree-like structure where each internal node corresponds to a decision based on a feature, and each leaf node represents a predicted value. Once the tree is built, it can be used to make predictions by traversing from the root to a leaf, following the decisions at each node, to arrive at a predicted value. In decision tree regression, the predicted value for a given input is typically the mean value of the target variable in the subset of the data that reaches the leaf node.

The key idea behind decision tree regression is to recursively partition the input space into smaller regions and fit a simple model, such as a constant or a linear function, within each region (Myles et al., 2004). The mathematical equation for decision tree regression can be expressed as a piecewise function, where each leaf node in the decision tree represents a distinct region of the input space, and the value associated with that leaf node represents the predicted output for any input that falls within that region. The decision tree regression model can be represented as a binary tree, where each internal node represents a split on a particular feature, and each leaf node represents a predicted output value (see Eq. 5).

$$y = f(x) = \sum_{i=1}^{M} c_i \cdot I(x \in R_i) \quad (5)$$

where *y* is the predicted output, *x* is the input vector, c_i is the constant or mean value associated with the *i*-th leaf node, $I(x \in R_i)$ is an indicator function that takes the value of 1 if the input *x* falls within the *i*-th region R_i, and 0 otherwise. *M* is the total number of leaf nodes.

1.4.5 Random forest regression model

Random forest regression is an ensemble learning method that builds multiple decision trees during training and merges their outputs to improve predictive accuracy and control overfitting. The algorithm begins by creating multiple bootstrap (i.e., dataset) samples from the training data, and for each sample, a decision tree is constructed using a subset of features selected at random. This process, known as bagging (bootstrap aggregating), helps to reduce variance and prevent overfitting. The final prediction $\hat{y}$ is obtained by averaging the predictions of all individual trees, represented by the Eq. 6:

$$\hat{y} = \frac{1}{T} \sum_{t=1}^{T} \hat{y}_t \quad (6)$$

where $\hat{y}_t$ is the prediction from the *t*-th tree and T is the total number of trees. Random forest regression is advantageous because it can handle large datasets with higher dimensionality, capture complex interactions between features, and is robust to outliers and noise. Additionally, it provides estimates of feature importance, which can be useful for understanding the underlying data structure. The implementation of random forest regression in this study follows the methodology outlined by (Breiman, 2001), utilizing the default parameters unless otherwise specified to ensure robustness and comparability of results.

1.4.6 Light Gradient Boosting Machine (LGBM)

Boosting is a specific technique within ensemble learning that iteratively improves the performance of a single model by focusing on difficult-to-predict instances. The boosting technique was originally devised to address classification challenges, and later, its application extended to regression models as well (Friedman, 2001; Marani & Nehdi, 2020). In a more general context, a boosting algorithm builds a sequence of models, each of which is trained on a dataset in which the individual samples are allocated different weights (Ibrahim et al., 2009). Patterns that are inaccurately predicted receive increased weight, while those predicted correctly have their weights reduced. Consequently, the model places greater emphasis on the patterns that were previously incorrectly predicted during each forward iteration. Subsequently, an ensemble of models is assembled, building upon these iterations (Erdal et al., 2013). LGBM, a gradient boosting framework rooted in decision trees, leverages multiple decision trees collaboratively, as described by Chen et al. (Chen et al., 2019). To effectively capture complicated non-linear patterns, LGBM employs a specialized variant of the decision tree, often referred to as a weak learner. Utilizing LGBM accelerates the training of conventional gradient boosting decision trees by up to 20 times as proven by Ke et al. (Ke et al., 2017). In the LGBM model, each subsequent model is trained to predict the errors of its predecessors in an additive manner. An iterative decision tree is constructed by fitting the residual to a negative gradient. To get the prediction from an ensemble of trees, all the predictions are added together.

The final prediction value of the output is estimated by aggregating the predictions made by each individual tree. Eq. 7 represents the prediction function in the LGBM.

$$\widehat{Y_n} = \sum_{j=1}^{H} f_j\,(x_m)\,, f_j \;\in\; F \tag{7}$$

where H, F, and f_j represents the count of trees, all possible tree structures, and the leaf score of the trees respectively. Multiple decision trees are combined in this ensemble approach to improve prediction accuracy and robustness. LGBM focuses on minimizing the loss function by integrating regularization techniques, which improve the generalization capabilities of the model. These methods prevent overfitting, enabling the model to make more accurate predictions on unseen data and ultimately enhancing its predictive performance. These regularization methods help prevent overfitting, allowing the model to better generalize unseen data, and ultimately improving its predictive performance. An overview structure of the LGBM for prediction procedure is presented in Figure 1.1.

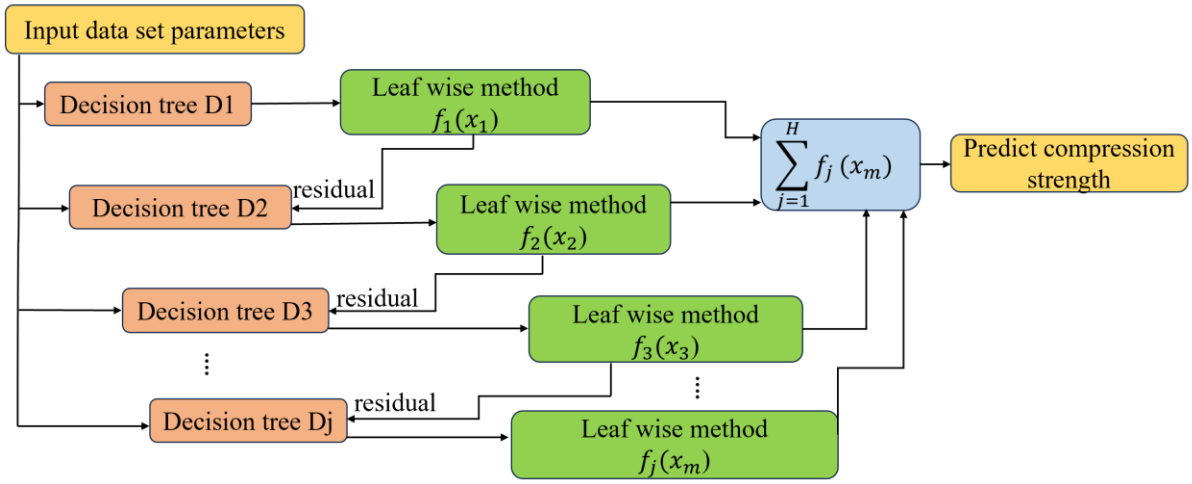

Figure 1.1. The structure of LGBM for the prediction of the output value

1.4.7 XGBoost regression model

Extreme Gradient Boosting (XGBoost) is an advanced version of the Gradient Boosting algorithm, is a powerful ML algorithm that has gained immense popularity in recent years due to its exceptional performance in a wide range of regression and classification tasks. This algorithm is built upon the principles of gradient boosting, a technique that combines multiple weak models to create a strong predictive model. At its core, XGBoost utilizes decision trees as the base learners,

which are then sequentially trained to minimize the residual error of the previous models (AL-Shatnwai et al., 2020; Chen & Guestrin, 2016; Hu & Chu, 2019). The algorithm employs various techniques to enhance its efficiency and effectiveness, such as regularization, gradient optimization, and stochastic boosting (Chen & Guestrin, 2016). One of the key advantages of XGBoost is its ability to handle sparse data and missing values, making it a versatile choice for a variety of real-world problems. Additionally, the algorithm is highly scalable and can be efficiently parallelized, enabling it to handle large-scale datasets with ease. The mathematical foundations of XGBoost are rooted in the gradient boosting framework, where the algorithm aims to minimize a loss function by iteratively adding new models to the ensemble. The objective function of XGBoost consists of two main components: the loss function that measures how well the model fits the training data, and a regularization term that penalizes model complexity to avoid overfitting. The objective function can be expressed as Eq. 8 (Chen & Guestrin, 2016):

$$\text{Obj}\ (\phi) = \sum_{i=1}^{n} l(y_i, \hat{y}_i) + \sum_{k=1}^{k} \Omega(f_k) \quad (8)$$

where $l(y_i, \hat{y}_i)$ is the loss function, measuring the difference between the actual value y_i and the predicted value $\hat{y}_i$. $\Omega(f_k)$ is the regularization term to penalize the complexity of the model, helping to prevent overfitting, *n* represents the number of training examples (or data points), *k* represents the number of trees in the model. Each f_k corresponds to an individual tree in the ensemble.

1.5 Overall goal and objectives

This study advances the understanding of packaging dynamics and distribution hazards and introduces a potential tool for improving packaging performance and durability. The goals of this dissertation are accomplished through the following objectives:

1) Investigate the structural stability of ventilated Corrugated Paperboard (CP) by predicting the buckling load of thin CP plates with cutouts using mechanics-based models and ML solutions, which a) enhance the knowledge of package ventilation design, b) measure the influence of each factor on the buckling results, and c) provide packaging professionals a potential predictive tool for effective packaging designs.

2) Develop ML solutions to predict mechanical damage to transported packed apple fruit during transportation and measure the influence of both packaging design elements and transportation vibration characteristics.

3) Predict the impact of transportation-induced vibrations on the compression strength of CP boxes with different sizes and top loads using a) an advanced ML method to incorporate more comprehensive factors into the analysis for more accurate predictions, and b) measure the influence of each factor on the compression strength reductions.

To systematically investigate the objectives of this dissertation, the following hypotheses have been outlined as:

Hypothesis 1:

- ML models can predict the buckling strength of ventilated CP with cutouts, enhancing both ventilation and mechanical performance for effective packaging.

Hypothesis 2:

- ML solutions can accurately predict mechanical damage to transported packed apple fruit during transportation, enhancing protection within the packages.

Hypothesis 3:

- The impact of transportation-induced vibrations on the compression strength of CP boxes can be predicted using ML models, leading to improved packaging configurations for better protection during transit.

By focusing on these specific aspects, the dissertation seeks to advance packaging technology through the integration of ML, ultimately leading to more resilient and efficient packaging solutions in dynamic distribution environments in the future.

The structure of this dissertation is organized into three chapters, each addressing a specific aspect of packaging dynamics and distribution hazards through the application of ML techniques. Chapter 2 examines critical buckling loads in ventilated CP boxes for food packaging. Ventilated CP boxes are widely used in the food packaging industry, featuring ventilation holes that reduce compression strength. Experimental tests and Finite Element Model (FEM) simulations establish correlations between hole characteristics and buckling loads, contributing to polynomial formulas for predictions. Note that experimental results for hole sizes in CPs may not consistently exhibit specific trends. This variability is due to the inherent complexity of CPs, including fluctuating glue quality between plate layers at different locations. Therefore, to enhance the accuracy of buckling load predictions for ventilated CP plates, in the second phase of this study, ML models, specifically Light Gradient Boosting Machine (LGBM), are employed to predict buckling loads. The model achieves high accuracy, providing a method for predicting compression strength across various hole sizes and locations. In addition, the ML model revealed the influence of each factor on the buckling results. Chapter 3 utilizes ML models to predict damage percentages of transported packed apple fruit during transportation vibrations and investigate the impact of various factors on the damage experienced by transported packed apple fruit and its packaging during transportation vibrations, utilizing ML models to predict damage percentages and optimize. Chapter 4

investigates the prediction of compression strength loss in CP boxes post-vibration, utilizing ML models to guide packaging design decisions and ensure product integrity during transportation.

In summary, these chapters demonstrate the transformative potential of ML in addressing critical challenges in packaging design and dynamics. By providing data-driven insights and predictive capabilities, this dissertation enhances the knowledge of packaging professionals and researchers, offering tools to inform and optimize future packaging designs for more efficient and reliable performance in dynamic distribution environments.

REFERENCES

Ait-Oubahou, A., Hanani, Z. A. N., & Jamilah, B. (2019). Packaging. *Postharvest Technology of Perishable Horticultural Commodities* (pp. 375–399). Elsevier. https://doi.org/10.1016/B978-0-12-813276-0.00011-0

AL-Shatnwai, A. M., Faris, M., & Amman, A. (2020). Predicting Customer Retention using XGBoost and Balancing Methods. *International Journal of Advanced Computer Science and Applications (IJACSA)*, 11(7). www.ijacsa.thesai.org

Breiman, L. (2001). Random forests. *Machine Learning*, 45, 5-32.

Chen, T., & Guestrin, C. (2016). XGBoost: A scalable tree boosting system. *Proceedings of the ACM SIGKDD International Conference on Knowledge Discovery and Data Mining*, 13-17-August-2016, 785–794. https://doi.org/10.1145/2939672.2939785

Chen, T., Xu, J., Ying, H., Chen, X., Feng, R., Fang, X., Gao, H., & Wu, J. (2019). Prediction of Extubation Failure for Intensive Care Unit Patients Using Light Gradient Boosting Machine. *IEEE Access*, 7, 150960–150968. https://doi.org/10.1109/ACCESS.2019.2946980

Czajkowski, M., & Kretowski, M. (2016). The role of decision tree representation in regression problems – An evolutionary perspective. *Applied Soft Computing Journal*, 48, 458–475. https://doi.org/10.1016/j.asoc.2016.07.007

Defraeye, T., Cronjé, P., Berry, T., Opara, U. L., East, A., Hertog, M., Verboven, P., & Nicolai, B. (2015). Towards integrated performance evaluation of future packaging for fresh produce in the cold chain. *Trends in Food Science & Technology*, 44(2), 201-225.

Dunno, K., Cooksey, K., Gerard, P., Thomas, R., & Whiteside, W. (2016). The effects of transportation hazards on shelf life of packaged potato chips. *Food Packaging and Shelf Life*, 8, 9–13. https://doi.org/10.1016/j.fpsl.2016.02.003

Erdal, H. I., Karakurt, O., & Namli, E. (2013). High performance concrete compressive strength forecasting using ensemble models based on discrete wavelet transform. *Engineering Applications of Artificial Intelligence*, 26(4), 1246–1254. https://doi.org/10.1016/j.engappai.2012.10.014

Ficuspax. (2023). Shock & Vibration Protection Importance in Packaging. Retrieved from https://ficuspax.com/blog/the-importance-of-shock-and-vibration-protection-in-packaging/

Friedman, J. H. (2001). Greedy function approximation: a gradient boosting machine. *Annals of Statistics*, 1189-1232.

Hamm, R., Whitlock, D., Eatinger, R., Stearns, J., & Ringwood, S. (2018, October). Implementation of a Temperature Ramp Rate Requirement and Impact on the Packaging Processes. *International Symposium on Microelectronics* (Vol. 2018, No. 1, pp. 000494-000507). International Microelectronics Assembly and Packaging Society.

Hastie, T., Tibshirani, R., Friedman, J. H., & Friedman, J. H. (2009). *The Elements of Statistical Learning: Data Mining, Inference, and Prediction* (Vol. 2, pp. 1-758). New York: Springer.

Hu, H., & Chu, P. (2019). Predicting Lake Erie Wave Heights using XGBoost. *arXiv preprint arXiv:1912.01786*.

Huang, S. M., & Liu, Y. Y. (2023). Machine Learning Improves Environmental Sustainability: A Teaching Case of Prediction about Scrapping Inventory. *International Journal of Computer Auditing*, 5(1).

Ibrahim, J., Chen, M.-H., & Sinha, D. (2009). Springer Series in Statistics. *The Elements of Statistical Learning* (Vol. 227, Issue 2). http://www.springerlink.com/index/D7X7KX6772HQ2135.pdf

Jaramillo-Alcazar, A., Govea, J., & Villegas-Ch, W. (2023). Anomaly Detection in a Smart Industrial Machinery Plant Using IoT and Machine Learning. *Sensors*, 23(19), 8286.

Jena, M., & Dehuri, S. (2020). Decision Tree for Classification and Regression: A State-of-the-Art Review. *Informatica*, 44(4).

Kaur, R., Kumar, R., & Aggarwal, H. (2023, June). Role of Machine Learning in Sustainable Manufacturing Practices: An Outline. *International Conference on Intelligent Manufacturing and Energy Sustainability* (pp. 541-551). Singapore: Springer Nature Singapore.

Ke, G., Meng, Q., Finley, T., Wang, T., Chen, W., Ma, W., Ye, Q., & Liu, T. Y. (2017). LightGBM: A highly efficient gradient boosting decision tree. *Advances in Neural Information Processing Systems, 2017-Decem (Nips)*, 3147–3155.

Mahmoodzadeh, A., Mohammadi, M., M Gharrib Noori, K., Khishe, M., Hashim Ibrahim, H., Farid Hama Ali, H., & Nariman Abdulhamid, S. (2021). Presenting the best prediction model of water inflow into drill and blast tunnels among several ML techniques. *Automation in Construction*, 127(April), 103719. https://doi.org/10.1016/j.autcon.2021.103719

Marani, A., & Nehdi, M. L. (2020). ML prediction of compressive strength for phase change materials integrated cementitious composites. *Construction and Building Materials*, 265, 120286. https://doi.org/10.1016/j.conbuildmat.2020.120286

Min, H. (2010). Artificial intelligence in supply chain management: theory and applications. *International Journal of Logistics: Research and Applications*, 13(1), 13-39.

Moh'd Ali, M. A., Basahr, A., Rabbani, M. R., & Abdulla, Y. (2020, November). Transforming business decision making with internet of things (IoT) and machine learning (ML). *2020 International Conference on Decision Aid Sciences and Application (DASA)* (pp. 674-679). IEEE.

Mohammed, M., Srinivasagan, R., Alzahrani, A., & Alqahtani, N. K. (2023). Machine-Learning-Based Spectroscopic Technique for Non-Destructive Estimation of Shelf Life and Quality of Fresh Fruits Packaged under Modified Atmospheres. *Sustainability*, 15(17), 12871.

Montgomery, D. C., Peck, E. A., & Vining, G. G. (2021). *Introduction to Linear Regression Analysis* (5th ed.). John Wiley & Sons.

Mrówczyński, D., Gajewski, T., & Garbowski, T. (2023). Sensitivity Analysis of Open-Top Cartons in Terms of Compressive Strength Capacity. *Materials*, 16(1), 412.

Myles, A. J., Feudale, R. N., Liu, Y., Woody, N. A., & Brown, S. D. (2004). An introduction to decision tree modeling. *Journal of Chemometrics*, 18(6), 275–285. John Wiley and Sons Ltd. https://doi.org/10.1002/cem.873

Natarajan, S., Govindarajan, M., & Kumar, B. (2014). *Fundamentals of Packaging Technology*. PHI Learning Pvt. Ltd.

Olson, D. L., & Wu, D. (2017). *Predictive Data Mining Models*. Springer Singapore. http://www.springer.com/series/8827

Palumbo, M., Attolico, G., Capozzi, V., Cozzolino, R., Corvino, A., de Chiara, M. L. V., Contò, F., Tolve, R., & Cefola, M. (2022). Emerging postharvest technologies to enhance the shelf-life of fruit and vegetables: an overview. *Foods*, 11(23), 3925.

Raschka, S., & Mirjalili, V. (2017). *Python ML: ML and Deep Learning with Python, Scikit-Learn, and TensorFlow*. Packt Publishing.

Sharma, B., Sadhu, S. D., Chopra, R., & Garg, M. (2021). Role of Packaging in Food Processing. *Food Chemistry: The Role of Additives, Preservatives and Adulteration*, 73-95.

Vapnik, V. N. (1964). A note on one class of perceptrons. *Automation and Remote Control*, 25, 821–837.

Schmitz, T. L., & Smith, K. S. (2012). *Mechanical Vibrations: Modeling and Measurement* (2nd ed.). Springer.

Smola, A. J., & Schölkopf, B. (2004). A tutorial on support vector regression. *Statistics and Computing*, 14(3), 199–222.

Tan, K. H., Ji, G., Lim, C. P., & Tseng, M. L. (2017). Using big data to make better decisions in the digital economy. *International Journal of Production Research*, 55(17), 4998-5000.

Testronix Instruments. (2023). What Is Box Compression Testing & Why Is It Critical for Packaging? Retrieved from https://www.testronixinstruments.com/blog/what-is-box-compression-testing-why-is-it-critical-for-packaging/.

Yin, M., Huo, L., Li, N., Zhu, H., Zhu, Z., & Hu, J. (2024). Packaging performance evaluation and freshness intelligent prediction modeling in grape transportation. *Food Control*, 110684.

Zhang, F., & O'Donnell, L. J. (2019). Support vector regression. *ML: Methods and Applications to Brain Disorders*. Elsevier Inc. https://doi.org/10.1016/B978-0-12-815739-8.00007-9

Chapter 2: Buckling Analysis of Corrugated Paperboards Comprising Cutouts Applied in Sustainable Ventilated Food Packaging Design Using Mechanics-based Models and ML

Part of this chapter was previously published in press as Shirzad, K., & Joodaky, A. (2023). Buckling analysis of thin plates with circular cut-outs for sustainable ventilated food packaging design. *Food Packaging and Shelf Life*, *40*, 101214.

Abstract

Thin plates with cutouts are commonly used in engineering structures such as bridges, construction, and ventilated CP boxes in food packaging. While ventilation holes aid air circulation, they also impact the material's buckling strength. In this chapter, we first investigate the importance of cutout geometry and location on buckling for single and multiple cutouts, followed by exploring how variations in hole geometry and location affect this strength, considering the complex, multi-layered structure of the material, and then apply ML model to enhance predictions. Experimental tests and finite element method (FEM) simulations reveal that the vertical location and diameter of the hole significantly impact the buckling results, showing a reasonable correlation between experimental and FEM data. Polynomial formulas were developed to predict buckling loads, using paperboard plates to demonstrate the application for ventilated food packaging designs. In the food packaging industry, ventilated CP boxes are crucial for the sustainable transport of fresh products. Traditional mechanical analyses, which often require simplifications, may not fully capture this complexity, leading to less accurate predictions of the paperboard's strength. To address these challenges, we employed a ML approach using the LGBM algorithm to develop a predictive model. This ML model, trained on a compression dataset from experimental tests for plates with a single cutout in three shapes and FEM simulations for plates with multiple circular cutouts, accurately estimates the buckling strength of the plates. It achieved 91.45% accuracy on experimental data for plates with single cutouts of different shapes and 94.68% on FEM simulation data for plates with multiple circular cutouts, demonstrating its reliability. An ML-based tool for predicting the buckling strength of corrugated paperboard is provided by this research, along with insights that can inform the design of more sustainable

packaging solutions. Moreover, the results of this chapter can be used for the buckling prediction of other elastic thin plate structures with cutouts applied in other industries like aerospace.

2.1 Introduction

Approximately 40% of the packaging market consists of paper and paperboard materials (Pathare & Opara, 2014). Specifically, within consumer packaging, food packaging is particularly significant, representing 70% of the market, with corrugated paperboard (CP) making up 48% of this segment (Fadiji et al., 2018a). The fundamental function of packaging is to protect the product from mechanical damage (Pathare & Opara, 2014). In fresh produce product packaging, ventilated CP (VCP) packaging has broad applications. The widespread use of VCP packaging is owing to its cost-effective material properties, recyclability, and effective protection of food products (Fadiji et al., 2019). The primary goal of VCP box design is to preserve the freshness of the food products and to provide adequate compression strength for the package (Mukama et al., 2020). The heat exchange control of the VCP packaging is critical for the consistent cooling or keeping warm the fresh products in a transportation system. The heat transfer between the food and air is facilitated by designing the vent holes in the box walls. The ventilation cutouts, however, compromise the strength of the package, which may cause mechanical damage to the product (Fadiji et al., 2018a).

Several researchers studied the design of the vent holes in the ventilated packages for fresh products (Berry et al., 2017; Fadiji et al., 2016; Opara & Fadiji, 2018; J. Singh et al., 2008). Berry et al. analyzed various package designs, finding that larger vent areas reduced package strength, while higher-grade corrugated fiberboard increased compression strength. Opara and Fadiji found that packages with smaller vent areas and lower length-to-height ratios suffered more mechanical damage. Singh et al. determined that rectangular or parallelogram-shaped vertical holes preserved the strength of corrugated boxes better than circular holes, with vent area and strength loss being

linearly correlated. Fadiji et al. also showed that increasing vent height and area reduced compression strength, with rectangular vents performing better than circular or oval ones, and vents placed at 45 degrees enhancing box strength.

Mechanical damage prevention is a critical component of effective packaging, especially for VCP (Gupta & Dudeja, 2017). The buckling collapse is the most common cause of mechanical damage and the buckling behavior of the VCP is directly associated with buckling strength of the vertical sidewall plate. Apart from the ventilation area, the structural strength of VCP can be influenced by the ventilation number, orientation, and shape (Mukama et al., 2020). There are few studies in the literature that examined the impact of the regarding location and size of the cutout on the buckling loads of the VCP. Fadiji et al., investigated the effect of vent hole design on the buckling loads of paperboard boxes using experimental tests and finite element analysis (Fadiji et al., 2016, 2019). Two VCP designs used in South Africa's fresh fruit industry were analyzed using a validated finite element model (FEM). The study found that the number, location, and shape of vents significantly affected the buckling load of the corrugated fiberboard cartons. A linear relationship was identified between vent height and buckling load. Additionally, the study concluded that the width side of the CP boxes is less susceptible to buckling than the length sides. In another study, Han & Park applied the FEM method to provide a comprehensive analysis of the key design factors for ventilation and hand holes in CP boxes (Han & Park, 2007). The study found that the optimal placement for vertically oblong holes on boxes is near the center and towards the upper section of both side faces. Incorrect vent positioning can cause misalignment of ventilation, especially in stacked VCP on pallets. The misalignment might disrupt airflow patterns during forced-air cooling (Berry et al., 2015). A study for apple bruise susceptibility in compression was conducted by Opara and Fadiji (Opara & Fadiji, 2018) with apples packed in two widely used VCP

packages MK4 and MK6. The MK4 package design, compared to the MK6, has a larger length-to-height ratio, longer trays, and a greater vent area. The study found that package design significantly affects apple vulnerability to bruising. MK6 packages experienced more damage than MK4 packages due to differences in bruise area and volume. Apples placed at the bottom of the package sustained less damage, irrespective of the package design. Beldie et al., (Beldie et al., 2001) aimed to examine the mechanical performance of paperboard packages under static compressive loads. They found that creases are the primary determinants of stiffness and recommended developing an accurate model for the creases, as they were modeled as hinges in the FEM. Garbowski et al. (2020) developed an analytical-numerical method to evaluate the static compressive strength of ventilated corrugated boxes with various openings and holes, achieving three times less estimation error compared to the McKee formula (Garbowski et al., 2020).

The majority of VCP package designs are primarily dependent on basic approaches developed from trial-and-error tests. In general, the buckling strength of VCP boxes is assessed by performing a sequence of controlled experimental compression tests utilizing a universal testing machine. The maximum force applied prior to the point of structural failure is then recorded. However, performing the experimental test is time and cost consuming. Thus, several computer simulation models are developed to provide more efficient solutions (Mukama et al., 2020).

FEM and mechanics-based approaches are used in analyzing composite structures even with dissimilar materials (A. Joodaky et al., 2013; I. Joodaky & Joodaky, 2019). These methods have been applied for studying CP used in food packaging designs (Fadiji et al., 2018b). Nevertheless, challenges remain in adopting FEM to model the VCP package due to the complexities in their composite structure such as the bonding quality of CP layers that are usually assumed to be perfect. The complex nonlinearities and additional properties of paper, like humidity

sensitivity and creep, further complicate modeling. The incorporation of these complexities and obtaining accurate material parameters present ongoing research needs for enhancing the applicability of FEM in modeling the VCP packages.

Alternatively, considering the progress made in artificial intelligence (AI) over the past few years, AI offers innovative solutions to engineering challenges. The ML models have been applied in various science and engineering applications such as predicting the compressive strength of concrete (Nguyen-Sy et al., 2020), predicting the stress-strain plots in material design (Pal & Naskar, 2021), predicting the mechanical properties of concrete (Ben Chaabene et al., 2020), detecting road shock (Lepine et al., 2017), reducing packaging costs (Zhao et al., 2017), analyzing the freshness of packaged meat products (Sun et al., 2022), and classifying the fish gelatin packaging film product (Silva et al., 2021). In packaging, there are some studies that applied ML to the packaging application such as Archaviboonyobul et al. (Archaviboonyobul et al., 2020) who used the artificial neural network method to analyze the effect of ventilation hole design and hand hole on the box compression strength. According to the study, the location of the hand holes is the main parameter that reduces the compression strength of the boxes.

In this chapter, a ML approach, specifically utilizing the LGBM algorithm, is presented to predict the buckling strength of VCP plates with single vent cutouts in various shapes, including circles, squares, 45-degree rotated squares (diamonds), and multiple circular cutouts of different sizes and locations. The ML models are trained on a limited number of actual experimental or simulation test results and can predict other potential, unseen designs. The ML models learn from a limited number of actual experimental or simulation test results and predict the other possible unseen designs. Notably, the compression behavior of a box is directly related to the compression

of its vertical side plates (Frank, 2014). Therefore, the findings for predicting the compression of VCP plates in this study can be applied to the design of VCP boxes.

The novelty of the present study is in 1) its comprehensive investigation of the critical buckling loads of thin elastic plates with circular cut-outs, specifically applied to VCP packaging design. This part of study uniquely combines experimental tests and finite element method simulations to analyze how the vertical location and diameter of the hole affect buckling behavior. Furthermore, it develops second and third order polynomial formulas for predicting buckling loads, providing a valuable predictive tool for similar elastic thin plate structures. By using CP plates as samples, the research directly addresses practical applications in VCP packaging, offering insights that can enhance the structural design and stability of VCP box; 2) using machine learning models to efficiently address the complexities inherent in the buckling load of CP by learning from a limited test data (experimental or simulational). Traditional mechanics-based models like finite element methods (FEM) struggle with CP complex properties such as the anisotropy, nonlinear deformations, and environmentally dependent conditions, often necessitating simplifying assumptions that compromise accuracy.

To this end, this chapter is divided into two main parts. For part I (plates with single cutouts), in the first phase the response of VCP plates with a circular cutout to buckling loads was analyzed first. To estimate these loads, two non-dimensionalized polynomials were developed based on the hole parameters and the buckling load of a perfect plate (without cutouts) using curve fitting to FEM results. The buckling load of the perfect plate can be obtained through experimental, analytical, or FEM approaches. An analytical formula for the buckling of a perfect plate was derived using classical plate theory in mechanics. The FEM results and developed formulas are based on simplified models, excluding the composite structure of CPs. In phase two of part I, ML

was applied to experimental test results, which include the real, complex, and relatively uncertain response of the plates, providing a more realistic predictive tool for buckling loads. In the subsequent phase, experimental data for two additional shapes square and diamond were collected, and ML models were applied to incorporate the shape feature into the analysis. Part II addresses the analysis of multiple circular cutouts. This section includes the collection of simulation data and the subsequent ML analysis of this data. Overall, the chapter provides a comprehensive examination of both single and multiple cutout configurations through a combination of simulation, experimental, and ML approaches. The results confirm that the buckling load of plates is related to the hole parameters. As the units of geometry dimensions and mechanical parameters presented in this study are nondimensional, the developed analysis can be applied to varied thin elastic plates of diverse dimensions, hole sizes, and hole locations. As a result of these findings, both packaging designers and manufacturers will gain valuable insights and an applicable tool for designing ventilated boxes for food packaging.

The remainder of this chapter is organized as follows. Section 2.3 and 2.4 details the data collection process, including the experimental test setup and analysis for single cutouts of circular, square, and diamond shapes. Additionally, Section 2.3.2 provides a description of the FEM model for the elastic plate with single circular cutouts. Section 2.5 details the data collection process for multiple plates with circular cutouts. An overview of the results from the ML models and a discussion of the performance of each model used in this chapter are presented in Section 2.5, 2.6, 2.7 and 2.8. Finally, Section 2.9 presents the conclusions of this chapter.

2.2 Buckling analysis of CP plates

This section discusses the concept of buckling, its relevance in packaging design, and the methods used to analyze and predict buckling behavior in structures such as VCP plates. Buckling

is an engineering term that refers to a collapse, usually caused by axial stresses, applied to a structure, such as beams or thin plates. The peak force that causes buckling is called the critical buckling load or simply buckling load. Analytical approaches in plate theory (Bloom & Coffin, 2000; Bulson, 1969), numerical methods such as FEM (Eiblmeier & Loughlan, 1995; Muc et al., 2018; Narayana et al., 2014), and experimental tests (Lin & Kuo, 1989) can be used to determine the buckling load of a plate. In many applications such as aerospace, bridge, and tunnel construction, plates might need to have one or more cutouts (Kim & Park, 2020). In packaging box designs, a pattern of cutouts is created on the box walls to facilitate handling (ASTM D6804, 2014) and ventilation for food products. The mechanical properties of corrugated boards are susceptible to environmental condition variations. The manufacturing processes (e.g., the quality of glue between the layers) add to the complexity of the plate properties evaluations. Both analytical and FEM approaches are limited in including some of the complexities in their models. McKee formula estimates the compression strength of corrugated board boxes (Kawanishi, 1989) as represented in Eq. 1,

$$F = 2.08\, P_m^{0.764}\left(\sqrt{D_x D_y}\right)^{0.254} Z^{0.492} \quad (1)$$

where Z is the box top perimeter, $D_x = \frac{E_x t^3}{12\,(1-\nu^2)}$ and $D_y = \frac{E_y t^3}{12\,(1-\nu^2)}$ are the flexural rigidities of the plate in x and y directions, t is the plates thickness, E_x and E_y are the plate elasticity modulus in x and y directions, ν is Poisson's ratio, and P_m is the Edge Crush Test (ECT) result of the plate sample. Figure 2.1 illustrates the ECT in which a plate sample (e.g., $2in \times 2in$) is placed vertically inside the top and bottom horizontal platens of the compression tester. The platens apply uniform displacement controlled quasi-static compression pressures until the plate collapses. The obtained peak load right before the collapse is recorded as the plate ECT.

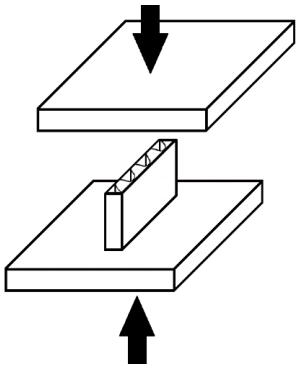

Figure 2.1. Schematic of ECT

The McKee formula is more applicable when it is simplified (Frank, 2014) as,

$$F = 5.87 \times P_m \sqrt{Z \times t} \quad (2)$$

The estimated results from the McKee formula are limited to specific conditions (e.g., relative humidity of 50%). Several studies investigated the buckling behavior of elastic thin plates with cutouts. Scheperboer et al., found that plates with a single centrally located hole had greater uniaxial compression resistance compared to plates with multiple holes of the same total size. Additionally, having five or more evenly distributed holes did not significantly impact the resistance (Scheperboer et al., 2016). Aydin Komur & Sonmez studied the effect of load location on the buckling load (Aydin Komur & Sonmez, 2008). No significant effect of plates with small holes on the buckling load ratio was reported by them. The plates with loading closer to their corners showed a higher buckling load. For simply supported plates with single or multiple cutouts, Moen and Schafer applied classical plate stability equations to develop an expression to predict elastic buckling stress and load (Moen & Schafer, 2009). El-Sawy et al., applied the FEM method to investigate the buckling stress of square and rectangular plates with holes at different slenderness ratios under uniaxial load (El-Sawy et al., 2004). The elasto-plastic buckling deformation was higher for thicker plates. Cheng & Zhao showed stiffeners can be applied for strengthening simply supported steel plates with various centric holes subjected to buckling

stresses during uniaxial compression (Cheng & Zhao, 2010). The reinforced perforated plates presented superior buckling strengths when compared to un-strengthened cases. Falkowicz et al. (Falkowicz, 2021; Falkowicz & Wysmulski, 2023; Falkowicz, 2023) investigated buckling and early post-buckling behavior and failure analysis (Falkowicz, 2023) of thin-walled epoxy/carbon composite asymmetric plates with a cutout. They applied both experimental and FEM methods. Moreover, the studies were conducted on the buckling behavior of thin-walled Carbon Fiber Reinforced Polymer composite plate with perforation (Falkowicz, 2022a, 2022b, 2022c). In a study by (Falkowicz, 2022a), they evaluated the effect of the parameters such as hole geometry, opening ratio, and spacing ratio on the buckling behavior. There was a decrease in the critical loads of the structure profiles due to the presence of cutouts. It was determined that the shape of the cutouts and opening ratio had the most impact on the buckling load of the channel cross-section profile. In (Falkowicz, 2022b), Falkowicz examined how the localization and geometric parameters of cutouts affect buckling load, finding that Z-cross-section perforated profiles remain stable even in the post-critical range. Additionally, a carefully selected hole arrangement can prevent weakening of mechanical properties.

2.3 Data collection: experimental, FEM, and plate theory for plates with single circular cutout

In this section, we detail the methodologies employed for data collection, encompassing both experimental and simulation-based approaches. Accurate and comprehensive data were gathered to facilitate the analysis of buckling behavior in thin plates with circular cutouts and to train the machine learning models for predicting the strength of VCP boxes. The advantage of using the experimental approach for the buckling of the perfect plate is that it includes the complex CP plate properties resulting from environmental factors (e.g., humidity) and manufacturing conditions (e.g., machinery effects) in the formula. Obtaining a single data point for the perfect

plate buckling from either of the three aforementioned approaches (i.e., experimental, analytical, or FEM) is substantially less expensive than performing experimental tests or FEM modeling for thousands of different holed plate cases required for the analysis. The analytical approach is limited in providing a solution for all holed plate cases. Similar to the approach used to derive the McKee formula based on ECT, one can formulate the compression strength of ventilated box based on the buckling of its comprised plates. Finally, we perform hundreds of experimental tests to study the buckling trends and to evaluate the accuracy of the developed formula.

2.3.1 Experimental test of CP plates with a single circular hole

C-flutes stand out as the predominant choice among different corrugated board grades, making up to 80% of the total corrugated packaging volume (American Box Company, 2023). The C-flute CP plates with ECT 32 *lbs./in* are selected for this study. Using an automatic cutting machine (Esko Kongsberg), the plates are cut in a random size of $15cm \times 15cm$, and circular holes were created on them. A same-sized plate without any vent holes is used as a control plate and is dubbed the perfect plate. The plates were conditioned in accordance with ASTM D642 test procedures (ASTM D642, 2000). A temperature of 23℃ and 50% relative humidity were applied to the plate specimens for 24 hours in an environmental chamber. A universal testing machine (Instron 5556) is used to conduct the compression tests. For each plate design, three samples are tested. The plate is compressed symmetrically. Therefore, either the right or left half of the plate is sufficient for creating the cutouts for testing. The left bottom corner of the plate is considered as the origin (0,0). The holes are placed along the x direction at 0, 3, 4.5, 6, and $7.5cm$ and along the y direction at 0, 3, 4.5, 6, 7.5, 9, 10.5, and $12cm$. Five samples with varying diameters of 1, 2, 3, 4, and $5cm$ were created and evaluated for each hole location. The number of samples are obtained by multiplying 5 (locations on the x direction) to 8 (locations on the y directions) to 5

(different diameters), and to 3 (number of repeats). Figure 2.2 shows three random examples of holed plates. All measurements are in centimeters (cm), indicating the x and y location from the left bottom corner of the plate, in addition to the diameter of holes (i.e., d). These dimensions are presented in the format of (x, y, d). The first mode buckling load is recorded for this study. At the origin, the hole could only have a quadrant shape, see Figure 2.2c. When either x or y coordinates are equal to zero, the hole becomes a semi-circle, see Figure 2.2b.

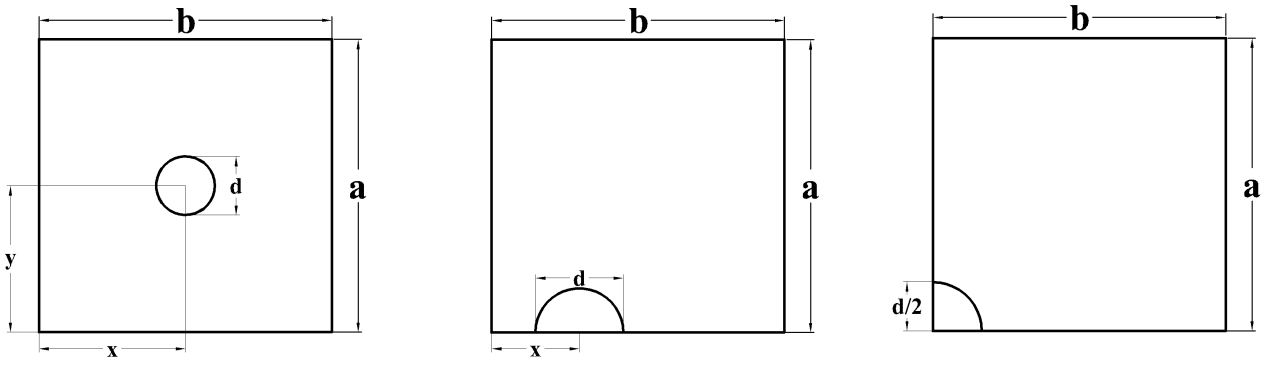

(a) (b) (c)

Figure 2.2. Sketch of three C-flute plates with random holes at different locations and with different diameters, (x, y, d) as (a) (7.5,7.5,3), (b) (4.5,0,4), and (c) (0,0,5)

The plate is placed between the two platens of the compression test machine, see Figure 2.3. The top platen compresses the plate at a rate of 1.27cm per minute, i.e., 0.5 in per minute (ASTM D642, 2000). The compression test machine used a fixed-platen design, in which the rotation of the platen was not permitted. To ensure the plate specimen remains in a vertical position during compression testing, two blocks, as shown in Figure 2.3a, are used. The blocks are removed when the top platen starts contacting the plate specimen. The specimens are compressed to 7.5mm, which is 5% of the plate height.

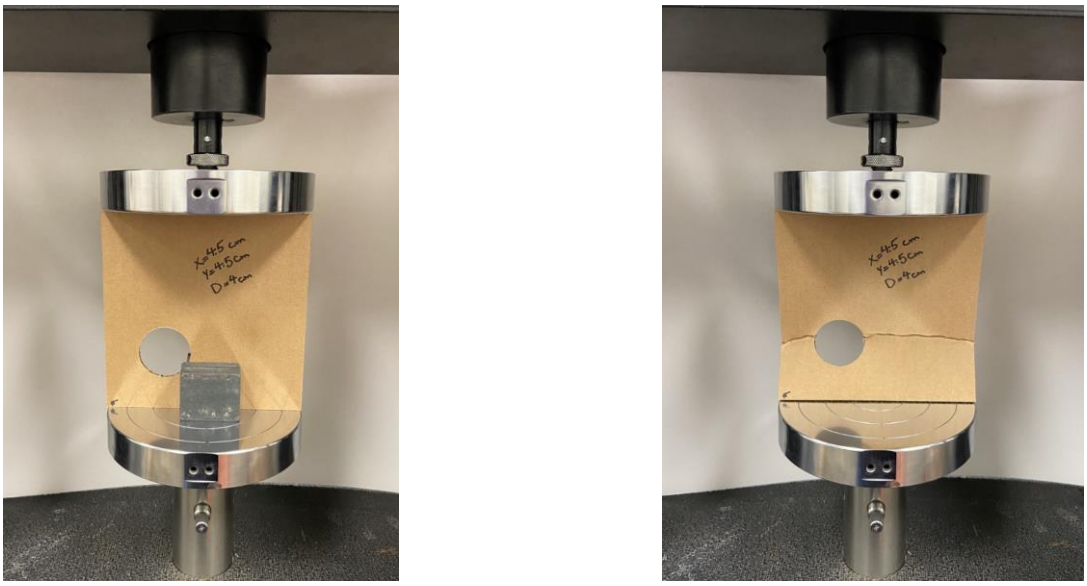

(a) (b)

Figure 2.3. Corrugated plate specimen under compression test: (a) before buckling, (b) after buckling

2.3.2 Buckling of thin elastic plates with single circular hole using FEM

To simulate the buckling load of a thin elastic plate comprising a single circular hole, a FEM model is created. A 15*cm* width (*w*) square plate with the thickness (*t*) of 3.8*mm* and a circular hole is modeled in ABAQUS software. To determine the equivalent elasticity modulus of the perfect plate, an experimental compression test was performed.

The recorded compression force and the vertical deformation are divided by the plate cross-section area ($t \times w$) and width to obtain the stress and strain respectively. The stress-strain curve shows a nearly linear response before the buckling, see Figure 2.4. The slope of the linear region is equal to the equivalent elasticity modulus of plate, 168.98*MPa*. With this approach, the composite CP plate is assumed to respond as an equivalent homogenous plate without any liner or flute layers. The obtained elasticity modulus and the Poisson's ratio of 0.33 (Fadiji et al., 2017) are provided to the FEM model of homogenous plate. The peak of the force-displacement curve is recorded as the experimental critical buckling load of the perfect plate, N_{exp}.

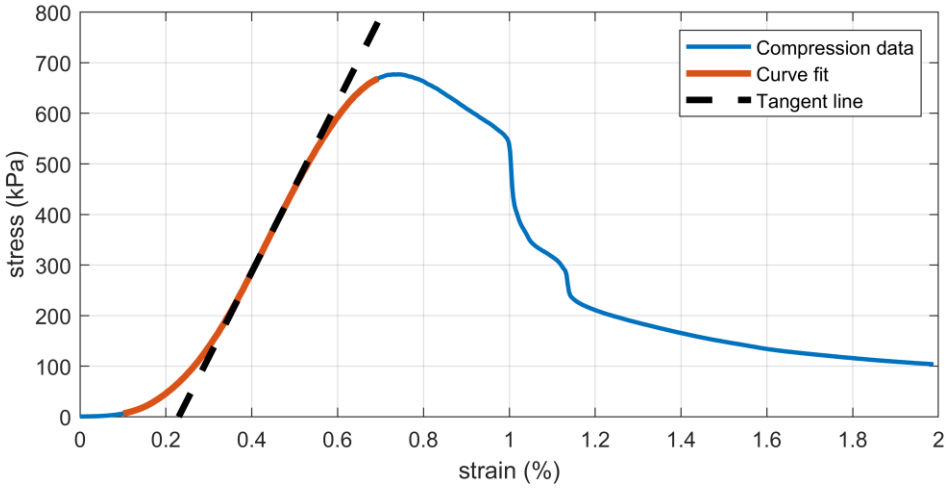

Figure 2.4. Stress-strain curve of the perfect plate in compression and fitted line for determining elasticity modulus

The deformable shell element and buckling perturbation analysis are selected in ABAQUS. The boundary conditions of the left and right edges are set to free. A simply supported boundary condition was selected for the top and bottom edges. Our FEM convergence study reported in Figure 2.5a shows that the mesh sizes smaller than 2% of the plate outer dimension obtain highly convergent buckling results. Figure 2.5b shows the von Mises stress distribution of the plate before buckling. As expected, the existence of the hole in the plate under compression results in stress concentration around the hole.

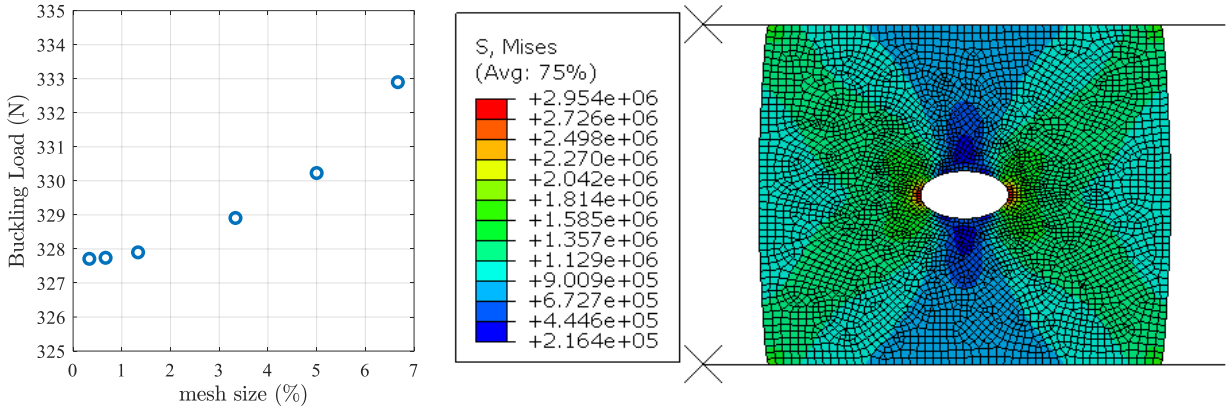

(a) (b)

Figure 2.5. (a) Mesh size convergence and (b) von Mises stress distribution from ABAQUS

Only the vertical left half of the plate is analyzed due to the geometry and loading symmetry. We non-dimensionalize the parameters and results to provide a size independent solution. For non-dimensionalizing the parameters, the size and location of the hole are divided by the plate width (i.e., 15*cm* in this case). The hole sizes of 0%, 10%, 15%, 20%, 25% and 30% of the width are considered. The results confirmed that the location variation in the x direction affects the buckling results by less than 1% due to the applied symmetry. Therefore, the location is only varied in y direction from 0% (semi-circle hole, see Figure 2.2b), to 50% of the plate with a 10% increment. By dividing the buckling loads of the holed plates by the buckling load of the perfect plate (386.15 *N/m)*, the buckling values are obtained in a non-dimesionalized percentage format.

In Figure 2.6, the non-dimensionalized buckling results are presented through a heat map that shows how they vary with different y locations and hole sizes. The map indicates that the closer the location is to the bottom or top edge, the larger buckling strength is preserved for all hole sizes. Additionally, as the size of the hole increases, the buckling strength decreases across all y locations.

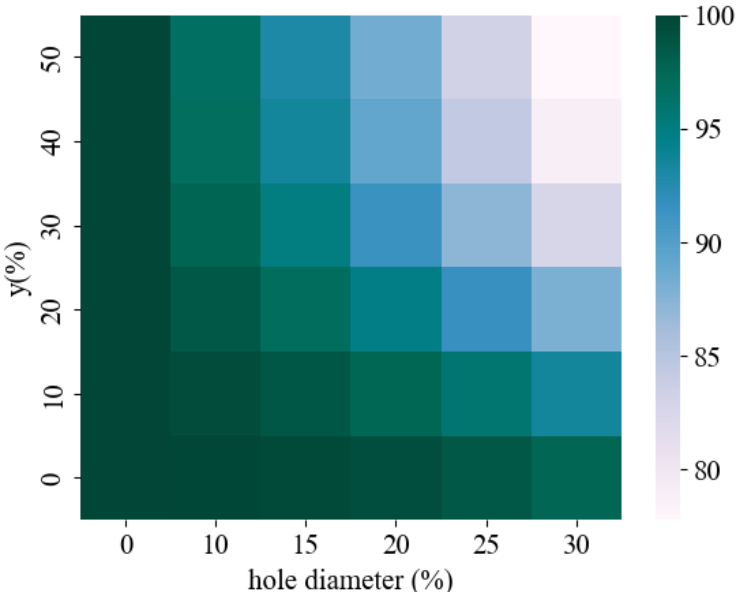

Figure 2.6. Heat map of buckling loads *N/m* for y locations versus hole diameters

2.3.3 Buckling load formula for plate with a circular hole

To develop a formula for predicting buckling load, the buckling loads resulting from FEM models are plotted for the y locations from 0 to 50% and hole diameters from 0 to 30% as shown in Figure 2.7. A second (O^2) and third order (O^3) polynomials are fitted on the curves. For the mentioned diameter range, the coefficients of terms in the fitted polynomials are examined.

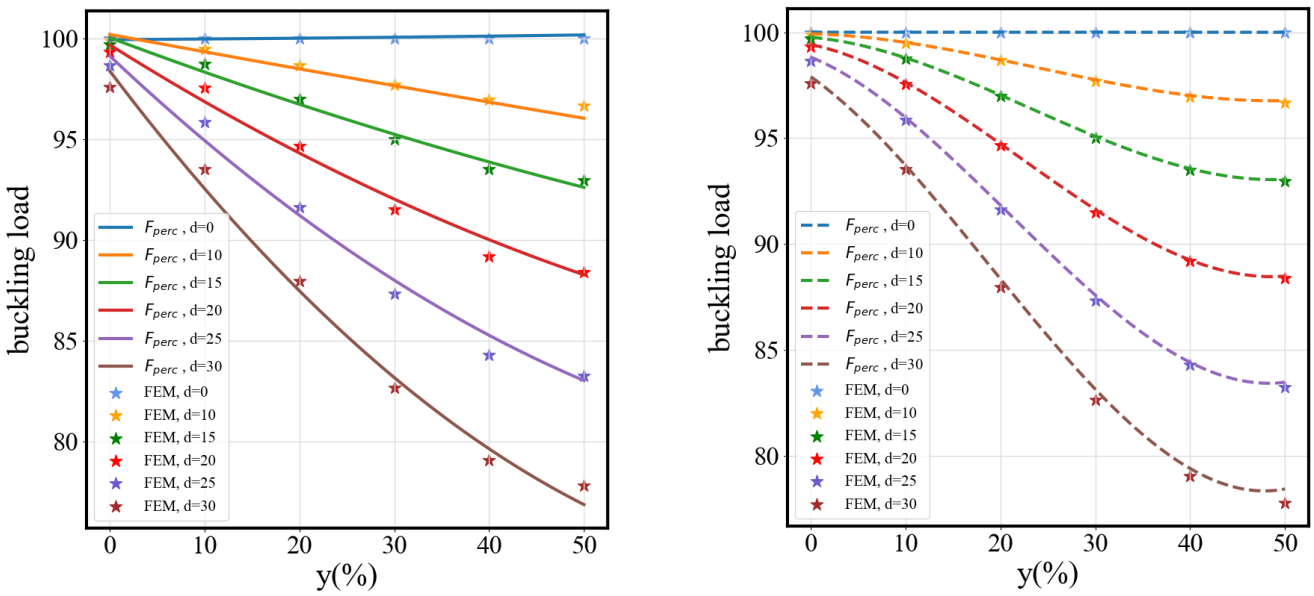

(a) Second order (b) Third order

Figure 2.7. Second and third order curve-fittings on the FEM results for the buckling of CP plates with a circular hole

Eq. 3 represents the second order polynomial,

$$F_{perc}\,(y,d) = C_{20} + C_{21}y + C_{22}y^2$$

$$C_{20} = -0.0039d^2 + 0.0651d + 99.994$$

$$C_{21} = -10^{-3} \times (0.592d^2 + 3.0923d - 2.9702) \quad (3)$$

$$C_{22} = 10^{-5} \times (0.613d^2 - 5.702d + 3.5238)$$

and Eq. 4 represents the third order polynomial,

$$F_{perc}(y,d) = C_{30} + C_{31}y + C_{32}y^2 + C_{33}y^3$$

$$C_{30} = 10^{-4} \times (-1.1d^3 + 8.5d^2 - 70.7d) + 100$$

$$C_{31} = 10^{-4} \times (-0.1101d^3 - 0.4069d^2 + 5.7533d - 1.0973) \quad (4)$$

$$C_{32} = 10^{-5} \times (0.118d^3 - 4.981d^2 + 1.847d + 0.155)$$

$$C_{33} = 10^{-7} \times (-0.14d^3 + 6.71d^2 - 2.21d + 0.19)$$

where d and y are in percentage (i.e., divided by the width of the plate then multiplied by 100). In order to convert the buckling load percentage to a buckling value, F_{perc} must be multiplied by the N_{cr}, the first mode buckling load of perfect plate as,

$$F = F_{perc} \times N_{cr} \quad (5)$$

Table 2.1 displays the R^2 values obtained from the second and third order polynomials. The error of the second order function is less than 2% while the third order function shows less than 0.0001% error compared to the FEM results.

Table 2.1. R^2 value for second and third order F_{perc}

Diameters		d=0	d=10	d=15	d=20	d=25	d=30	Average
R^2	O^2	1	0.981	0.983	0.985	0.987	0.990	0.988
	O^3	1	0.9999	0.9999	0.9999	0.9999	0.9999	0.9999

It is worth emphasizing that the obtained F_{perc} is non-dimensionalized and can be applied to thin elastic plates with different plate dimensions, hole dimensions, and hole locations. The first mode buckling load of perfect plate N_{cr} can be obtained from an analytical, FEM, or experimental test. The significant advantage of using the developed Eq. 5 is that obtaining one data for the N_{cr} from either of the mentioned methods costs substantially lower compared to the cost of performing thousands of tests for different scenarios that vary with plate dimension, hole dimensions, and hole location. For specific materials and structures such as corrugated boards that are highly susceptible to humidity and temperature, formulating an equation that comprises all variables is not feasible. By using the experimental buckling load of the perfect plate (N_{exp}) for N_{cr}, both the mechanical and environmental properties are incorporated into the equations. The thickness of the plate is a crucial factor that affects its buckling loads. The effect of plate thickness has already been

accounted for in the critical buckling load (i.e., N_{cr}) of the corresponding perfect plate in Eq. 5. Therefore, the obtained Eq. 3 and Eq. 4 do not need to include a thickness parameter. Table 2.2 compares the buckling load results for a 15*cm* square plate with a 2*cm* hole diameter in the center and varying plate thicknesses from 1.5 mm (1% of plate width) to 3*cm* (20% of plate width) to the buckling results from the corresponding plates with no holes. The ratio of N_s that is obtained from dividing the with-hole (i.e., w/) buckling by without-hole (i.e., w/o) buckling for each thickness, stays in the range of 81.3%$\pm$0.2%. Therefore, the plate thickness does not have a significant secondary effect on the buckling ratio.

Table 2.2. Comparison of plate buckling loads with 2 *cm* circular holes and different plate thicknesses

Thickness	Thickness/width	N_{cr} w/o hole	N_{cr} w/ hole	$N_s = \frac{N_{cr}\, w/}{N_{cr}\, w/o}$
0.0015	0.01	22.108	18.022	0.815
0.003	0.02	176.54	143.8	0.815
0.0075	0.05	2734.6	2223.6	0.813
0.015	0.1	21339	17330	0.812
0.03	0.2	157000	128000	0.815

In the following section, an analytical mechanics-based approach for calculating N_{cr} is explained.

2.3.4 Mechanics based approach for obtaining N_{cr} of perfect plates

Corrugated boards are considered orthotropic structures (Briassoulis, 1986). Based on the classical plate theory, the governing equation of a thin elastic orthotropic plate under uniform axial (N_x and N_y), torsional (N_{xy}), and transverse (q) loads shown in Figure 2.8, is given as (Bloom & Coffin, 2000),

$$D_{11}\frac{\partial^4 w}{\partial x^4} + 2(D_{12} + 2D_{66})\frac{\partial^4 w}{\partial x^2 \partial y^2} + D_{22}\frac{\partial^4 w}{\partial y^4} = \left[q + N_x \frac{\partial^2 w}{\partial x^2} + N_y \frac{\partial^2 w}{\partial y^2} + N_{xy}\frac{\partial^2 w}{\partial x \partial y}\right] \quad (6)$$

where w is the transverse displacement. The parameter D_{11}, D_{12}, D_{66}, and D_{22} (i.e., $D_{22} = \frac{E_{22}\, t^3}{12(1-\nu^2)}$) are the flexural rigidities of the plate with the thickness of t, and elasticity modulus of E_{11} and E_{22} in two plate non-thickness directions of x and y respectively, and Poisson's ratio of ν. Two vertical edges (see Figure 2.3) are free on the plates subjected to compression tests in this study. Consequently, the plate shows sinusoidal shape deformation only in the vertical direction (x direction) and not in the horizontal direction (y direction). The plate does not undergo any loads in horizontal or shear directions. As a result, the plate behaves like an isotropic plate and Eq. 6 is simplified to Eq. 7 (Bulson, 1969).

$$\frac{\partial^4 w}{\partial x^4} + 2\frac{\partial^4 w}{\partial x^2 \partial y^2} + \frac{\partial^4 w}{\partial y^4} = \frac{1}{D}\left[q + N_x \frac{\partial^2 w}{\partial x^2} + N_y \frac{\partial^2 w}{\partial y^2} + N_{xy}\frac{\partial^2 w}{\partial x \partial y}\right] \quad (7)$$

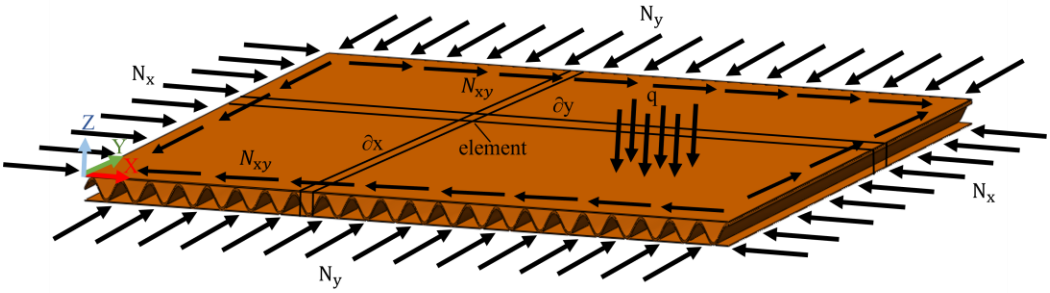

Figure 2.8. A CP plate under in-plane axial and torsional loads

When there is only one axial compression, then $N_y = N_{xy} = q = 0$. The Eq. 7 is reduced to

$$\frac{\partial^4 w}{\partial x^4} + 2\frac{\partial^4 w}{\partial x^2 \partial y^2} + \frac{\partial^4 w}{\partial y^4} = \frac{1}{D}\left[N_x \frac{\partial^2 w}{\partial x^2}\right] \quad (8)$$

The transverse deformation can be defined as a function of only x as,

$$w\,(x) = C\, sin\left(\frac{m\pi x}{a}\right) \quad (9)$$

where C is a constant value. As shown in Eq. 9. The horizontal width of plate, b, does not affect the buckling of the plate with two vertical free edges. After substituting Eq. 9 into Eq. 8 and performing some mathematical manipulations, the first buckling load is obtained as,

$$N_{cr} = \frac{\pi^2 D}{a^2} \tag{10}$$

where $D = \frac{E_{22}\, t^3}{12\,(1-\nu^2)}$. The N_{cr} in Eq. 10 can be applied in Eq. 5 to make it a totally computational approach. The computed buckling load in Eq. 10 is applicable to materials that are not affected by environmental conditions, such as aluminum. As mentioned before, for the structures such as corrugated boards that are susceptible to environmental conditions, using one experimental data for the N_{cr} in Eq. 5 will result in a highly accurate estimation for the buckling load F in Eq. 5.

2.3.5 Experimental results for buckling of CP plates with single circular cutout

In this section, the experimental results of the critical buckling load analysis for the CP plates with a single circular hole are discussed.

2.3.5.1 Pre-buckling and post-buckling behavior of CP plates with single circular cutout

Figure 2.9 shows the force-displacement curve from the experimental tests for the perfect plate described in Section 2 and the holed plates of the same outer dimensions with a circular hole located at the center (i.e., (7.5*cm*, 7.5*cm*)) and diameter sizes of 1, 2, …, 5*cm*. It can be observed that the maximum peak force is obtained from the perfect plate followed closely by the plates with the smallest hole diameter, 1*cm*. As the hole size increases the peak force decreases. The plates show approximately a linear compression stiffness before the buckling, see the pre-buckling region I in Figure 2.9(b). The post-buckling region II shows a nonlinear deformation behavior.

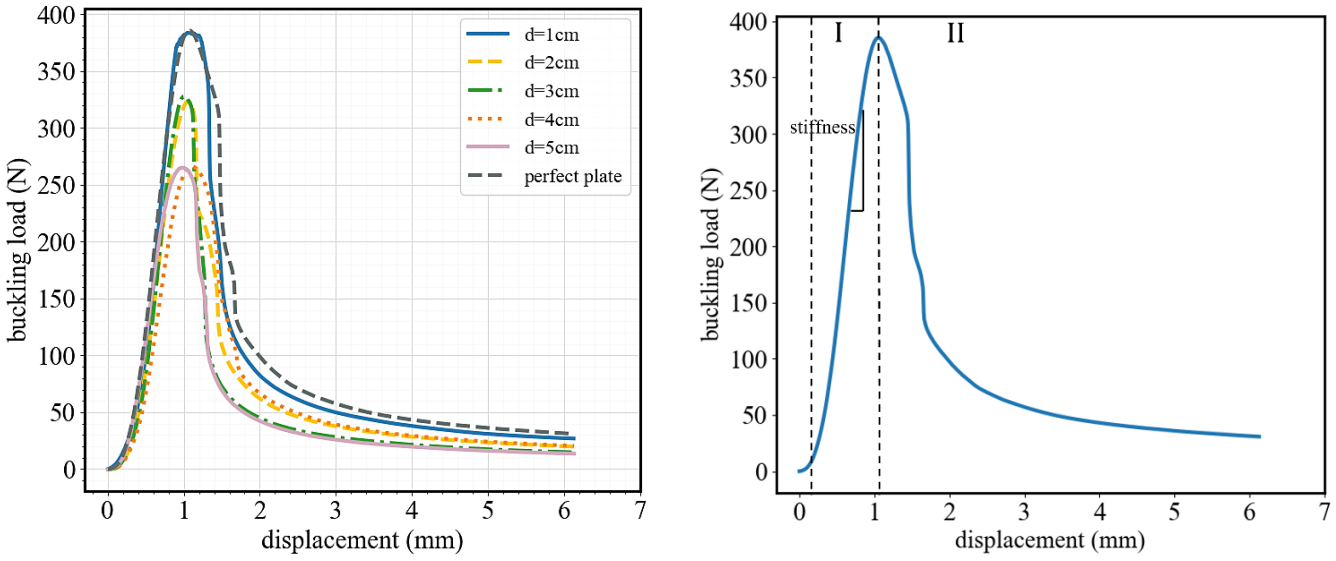

(a) (b)

Figure 2.9. Buckling behavior of C-flute plate with and without circular cutout

The slope of the nearly linear pre-buckling region I is considered as the linear stiffness of elastic plates. A line is tangentially fitted on the linear region and attached to the inflection point between the start and peak of the curve, see Figure 2.4. The slope of the line is recorded as the plate's linear stiffness. Figure 2.10 presents the linear stiffness of plates with various hole sizes. Error bars in Figure 2.10 indicate the standard deviation of the mean. As can be noted, increasing the size of the hole decreases the stiffness of holed plates. The ventilated corrugated plate with a hole diameter of d=1 *cm* shows the highest stiffness. The difference between stiffnesses of d=1*cm* and d=5*cm* cases is 36.31%.

An analysis of the t-test ($p < 0.05$) was used to determine the statistical difference between the hole size and plate stiffness. The p-value calculated for the different hole sizes indicate statistical significance in the stiffness differences, suggesting that the size of the hole has a significant effect on the stiffness of the plate. Table 2.3 presents data on the stiffness of different sizes of the holes, represented by their respective diameters. The table provides the mean values

along with their corresponding standard errors for each hole size. Additionally, it includes the results of t-tests comparing the stiffness values to a perfect plate. For the hole sizes equal or larger than 2cm, the size of the hole has a significant effect on the stiffness, as indicated by $p < 0.05$. However, for 1 cm hole diameter, the results do not provide sufficient evidence to suggest a significant effect on the stiffness of the CP.

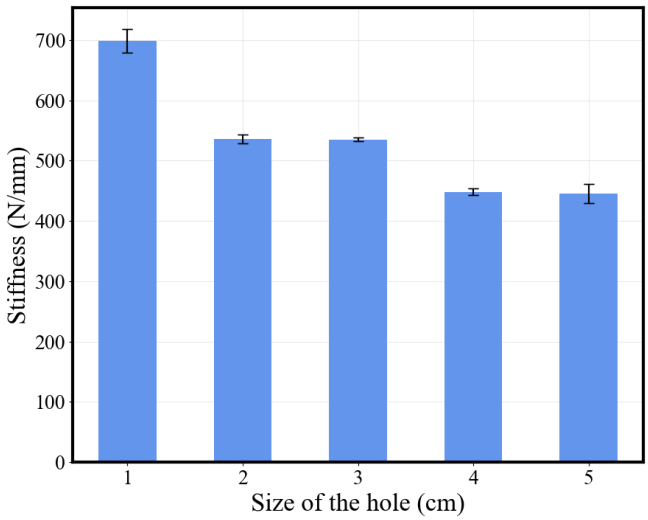

Figure 2.10. Stiffness of the plate with different sizes of the circular hole

Table 2.3. Statistical analysis of the stiffness of the circular holed plate

Size of the hole (cm)	Mean $\pm$ standard error of stiffness of the holed plate	t-value	p-value
d =1	698.52 $\pm$ 19.36	-0.85	0.4842
d =2	535.64 $\pm$ 7.40	-24.25	0.0016
d =3	535.31 $\pm$ 2.78	-64.67	0.0002
d =4	448.35 $\pm$ 5.25	-50.78	0.0003
d =5	444.88 $\pm$ 15.92	-16.97	0.0034

Furthermore, we conducted statistical analysis to assess the effect of hole size on buckling loads of the holed plate, considering that the hole is located at various locations (see Table 2.4). The results with $p < 0.05$ imply that the buckling loads of plates with various hole sizes is significantly different from the perfect plate that is 386.82 *MPa*. As the hole size increases, the buckling load tends to decrease, and this difference becomes more pronounced with larger hole sizes. Accordingly, there is strong evidence that the size of the holes impacts the buckling load of holed plates substantially.

Table 2.4. Mean buckling load of plate with a circular hole

Hole size (cm)	Mean $\pm$ standard error of buckling load	t-value	p-value
d =1	376.99$\pm$ 4.53	-2.16	0.0359
d =2	365.16$\pm$ 4.57	-4.73	1.9790×10^{-5}
d =3	338.44 $\pm$ 4.12	-11.73	1.0346×10^{-15}
d =4	288.18 $\pm$ 1.93	-50.99	1.8195×10^{-43}
d =5	257.62 $\pm$ 2.06	-62.59	1.1219×10^{-47}

2.3.5.2 Heat map of experimental data for the buckling of CP plates with single circular cutout

In Figure 2.11, the heat maps of the experimental data are shown for different hole sizes and locations of holes in x and y directions. The plates with larger hole sizes show lower buckling strength. When the holes are created closer to the horizontal edges, the buckling strength is higher. The effect of hole location on the buckling loads is less evident for plates with smaller hole sizes.

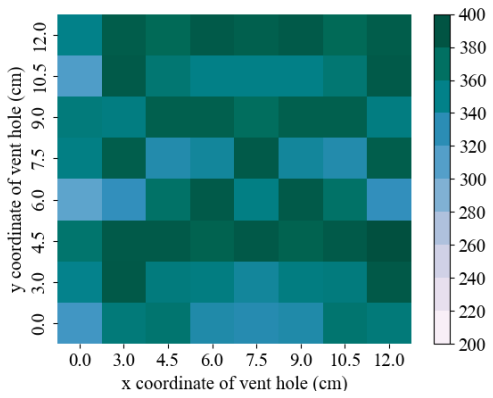

(a) *d=1cm*

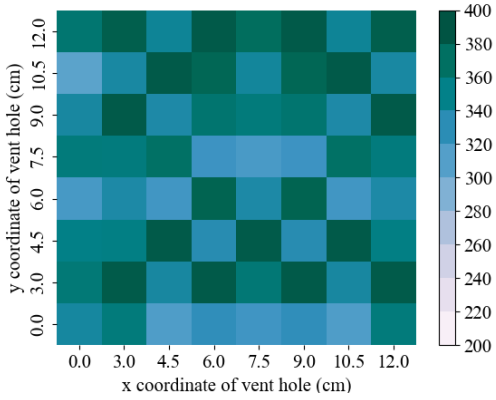

(b) *d=2cm*

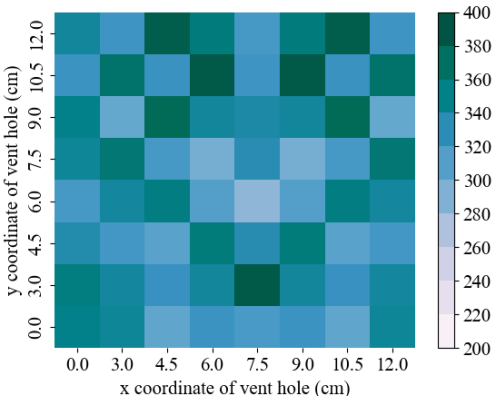

(c) *d=3cm*

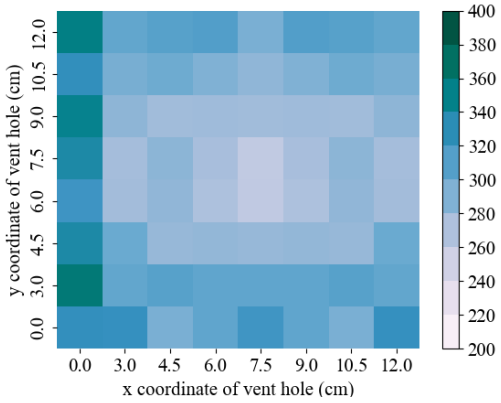

(d) *d=4cm*

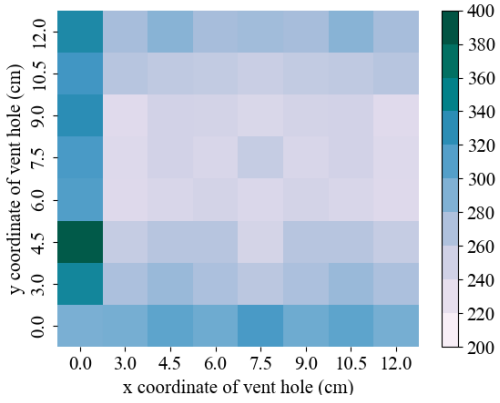

(e) *d=5cm*

Figure 2.11. Heat maps of experimental data with circular hole size (a) d =1 *cm*, (b) d =2 *cm*, (c) d =3 *cm*, (d) d =4 *cm*, and (e) d =5 *cm*

2.3.5.3 Effect of hole diameter in x direction

In Figure 2.12, the buckling loads of the holed corrugated plates are demonstrated for different hole sizes and y locations for each x location separately. The circular hole size varies from 1 to 5cm for different locations in x (3, 4.5, 6, 7.5cm) and y (3, 4.5, ..., 12cm) directions. The experimental results for plates with smaller hole sizes may contain unexpected trends due to the inherent complexities of the CP structures (e.g., manufacturing process) that can affect the mechanical properties of the plate. For example, the plot for x=7.5cm and y=3 cm shows an increase for the d=3cm compared to the corresponding smaller hole size cases while a reduction is expected. These uncertainties are significantly lower for the cases with larger hole size. It is evident that all cases exhibit an overall decreasing trend as the hole size increases. This decreasing trend is flatter for x=0 cases; the hole diameter parameter shows a lower effect on plate buckling for vertical edge holed cases.

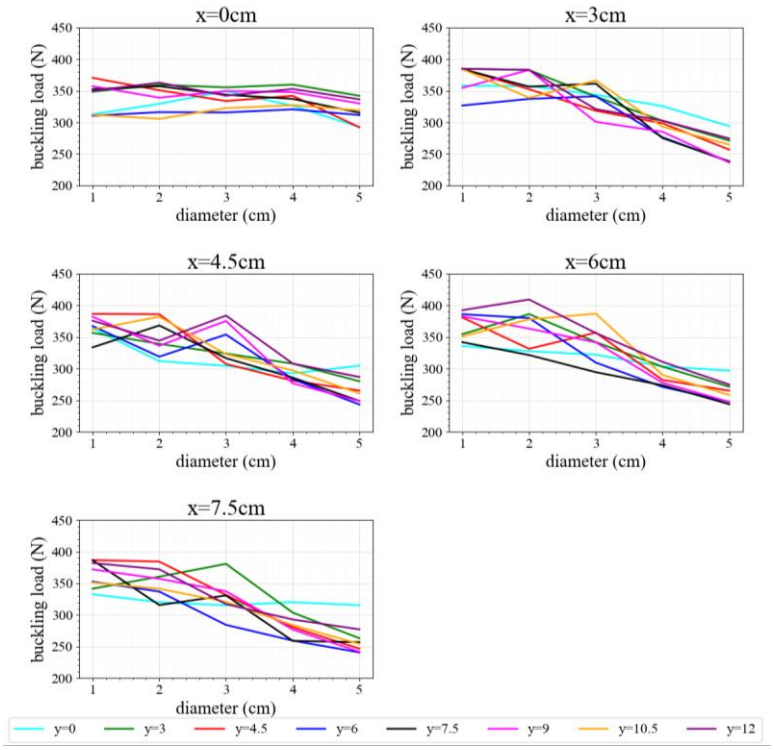

Figure 2.12. Experimental results: Effect of different hole size in x direction on buckling load of corrugated holed plates

2.3.5.4 Effect of hole diameter in y direction

Figure 2.13 illustrates the buckling load of the corrugated plate with circular holes of varying sizes in the x direction for each y location separately. Similar to Figure 2.12, 1) a general decreasing trend is observed as the size of the hole increases and 2) the plates with smaller hole sizes might exhibit unexpected results in their buckling loads.

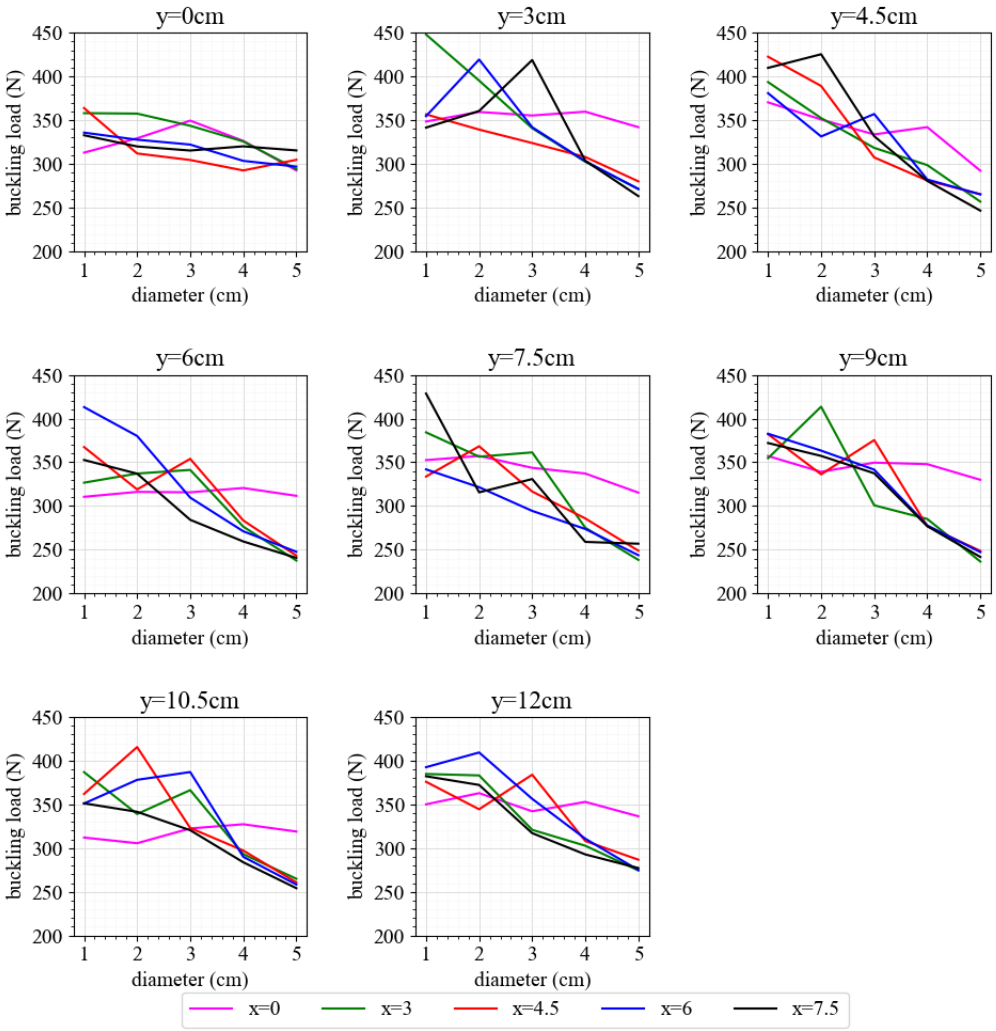

Figure 2.13. Experimental results: Effect of different hole size in *y* direction on buckling load of corrugated holed plates

2.3.6 Comparison between experimental and FEM

The buckling loads of the experimental test and FEM model results show variations ranging from 3% to 26% when comparing all cases. These variations may be attributed to the influences of temperature, environmental condition of the CP plate with cutout sample, glue quality of the flute in the CP, CP types (Fadiji et al., 2019), and potential pre-damage in the experimental samples. Due to the inherent complexity of corrugated boards, the experimental data could potentially lead to over- or under-estimated results. Importantly, the FEM analysis does not

account for these factors. Eq. 11 is used to calculate the statistical error between the experimental and FEM approach results.

$$\text{Error} = \left| \frac{F_{exp} - F_{FEM}}{F_{exp}} \right| \times 100\% \tag{11}$$

where F_{exp} is the experimental results and F_{FEM} is the results from FEM analysis.

2.4 Part I Buckling data collection for CP plates with three different cutout shapes

The widths of 1, 2, 3, 4, and 5*cm* are selected for the circular and squared holes. The widths of 1, 2, 3, and 4*cm* are determined for the diamond; the 5*cm* diamond hole does not fit into the locations that were close to the edge of the sample plate. The cutouts are made on the plates using a Kongsberg digital cutting table machine (see Table 2.5). The lower left corner of the plate is set as the origin (0,0). The location of the hole varies with a 1.5 *cm* increment, starting from point (3,3). Figure 2.14 shows three plates with three different cutout shapes. The plate samples are placed vertically inside a compression tester machine (Instron 5565 Universal testing machine). Vertical alignment of the samples is achieved by utilizing two small blocks within the compression tester machine. Once the top platen of the machine starts contacting the sample plate, the blocks are removed. The plates are compressed with 4% to 5% strains (6 to 7.5 *mm*). Figure 2.15 shows the plates and their buckling failure trace after performing the compression test.

Table 2.5 A summary of the experimental data set

Cutout Location		Diameter or side(*cm*)	Shape
(x (*cm*))	(y (*cm*))		
3, 4.5, 6, 7.5	3, 4.5, 6, 7.5, 9, 10.5, 12	1, 2, 3, 4, 5	Circle, square, diamond

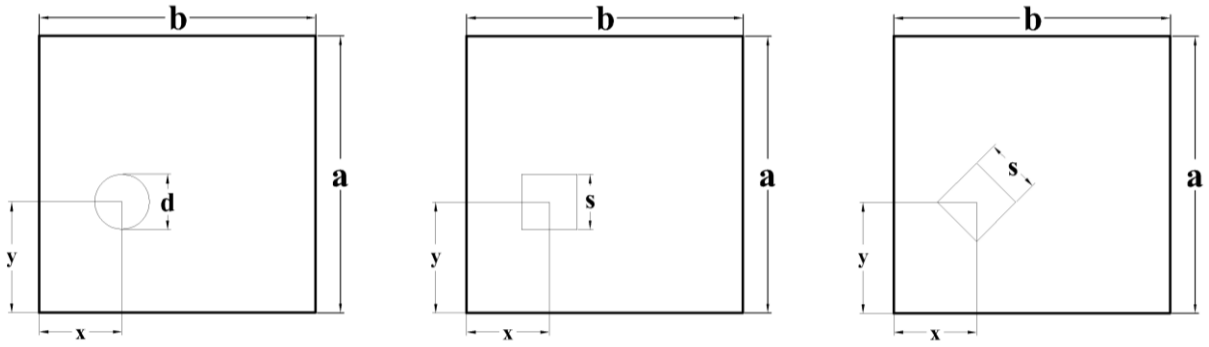

(a) (b) (c)

Figure 2.14. Sketch of three sample plates for experimental tests with a (a) circular hole, (b) square hole, and (c) diamond hole

(a) (b) (c)

Figure 2.15. Experimental compression test specimen with a (a) circular hole, (b) squared hole, and (c) diamond hole

As mentioned before, the average buckling strength of the plate without any holes (the perfect plate) is 386.83 *N*. The heatmaps in Figures 2.16 to 2.18 illustrate the buckling strength of plates as percentage of the buckling strength of perfect plate, for different vent hole locations and shapes. Figure 2.16 shows the buckling results of the plates comprising a circular vent hole while the diameter is equal to (a) 1 cm, (b) 2 cm, (c) 3 cm, (d) 4 cm, and (e) 5 cm. Figure 2.17 shows

the buckling results of the plates comprising a squared vent hole while the side is equal to (a) 1 cm, (b) 2 cm, (c) 3 cm, (d) 4 cm, and (e) 5 cm. Figure 2.18 presents the buckling results for plates with diamond vent shape while the side is equal to (a) 1 cm, (b) 2 cm, (c) 3 cm, and (d) 4 cm. For all cases in Figures 2.16-2.18, 1) despite some uncertainty, positioning the holes nearer to the top and bottom edges of the structure maintains higher buckling strength, and as the hole width increases, this observation becomes more evident, and 2) increasing hole sizes decreases buckling strength directly. One of the advantages of applying the ML approaches is finding a highly accurate prediction for such problems with uncertain trends as well as ranking the importance of each factor on the results.

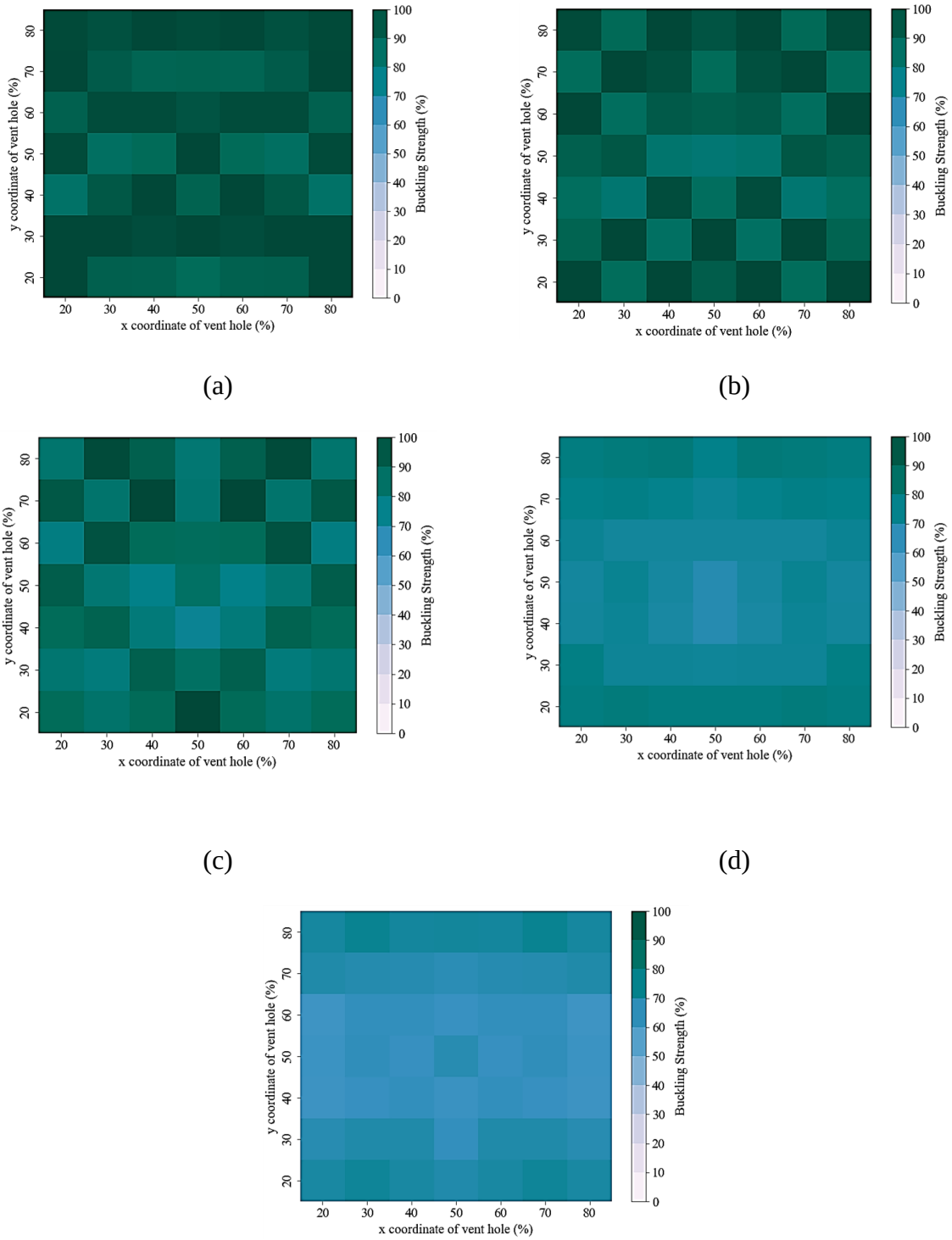

Figure 2.16. Heatmap of buckling data for plates with circle vent hole with sizes (a) *d*=1 cm, (b) *d*=2 cm, (c) *d*=3 cm, (d) *d*=4 cm, and (e) *d*=5 cm

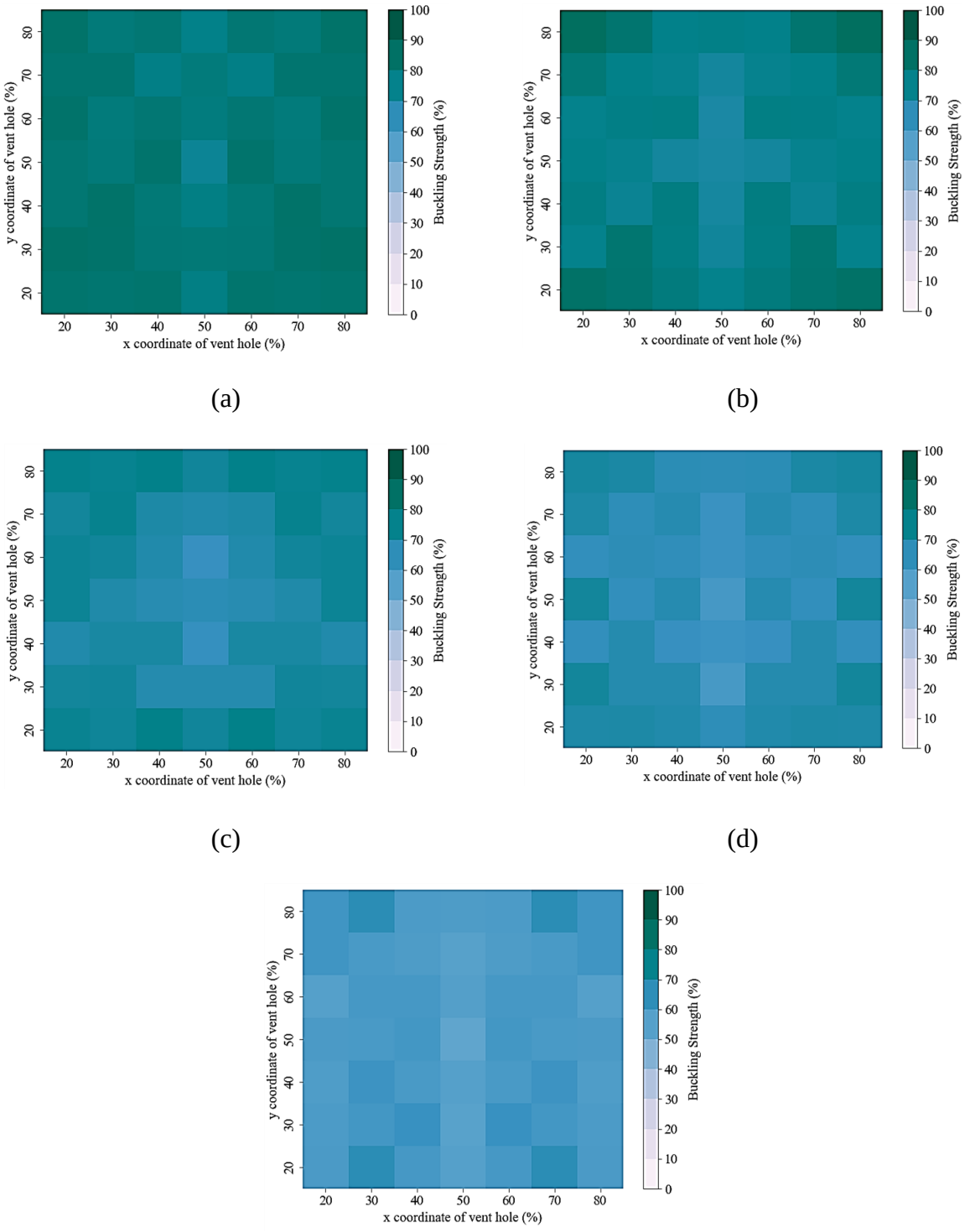

Figure 2.17. Heatmap of buckling data for the plates with square vent hole with sizes (a) *s*=1 cm, (b) *s*=2 cm, (c) *s*=3 cm, (d) *s*=4 cm, and (e) *s*=5 cm

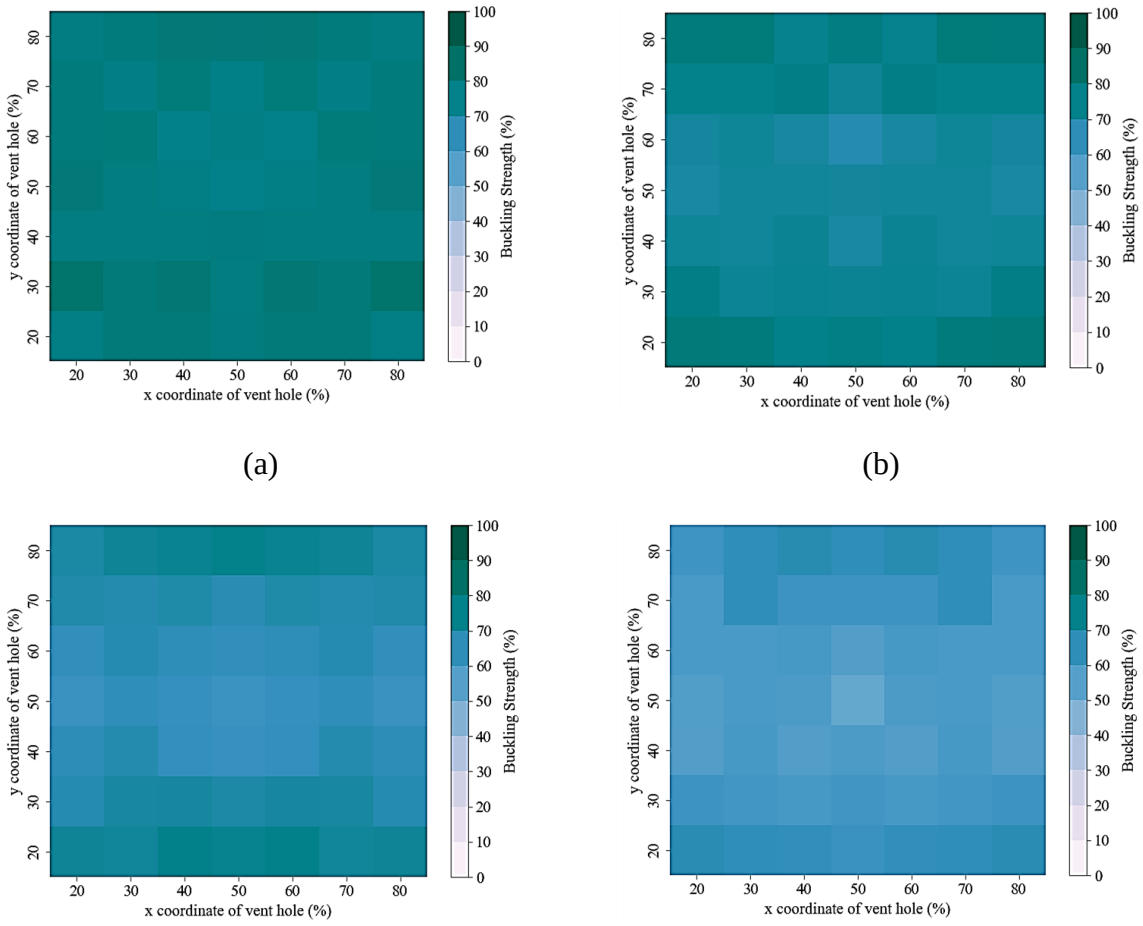

Figure 2.18. Heatmap of buckling data for plates with diamond vent hole with sizes (a) *s*=1 cm, (b) *s*=2 cm, (c) *s*=3 cm, and (d) *s*=4 cm

2.5 Part II data collection for plate with multiple circular cutouts using FEM simulation data

In the latter phase of our analysis, the process of gathering data involved the use of FEM environment of SolidWorks software for creating several patterned designs of the circular cutouts in the plates and collecting the buckling data. The Poisson's ratio and modulus of elasticity values used in this section are the same as those specified in section 2.3.2. These values were incorporated into the SolidWorks simulation model to estimate the critical buckling load of the VCP plates. The plates had holes arranged in different configurations of rows and columns, with specific parameters such as hole size and the initial margin of the hole pattern from the left side of the plate. Due to

the symmetric design all four side margins are equal. The simulation process involved subjecting the plate models to uniaxial compression and analyzing their buckling behavior.

The input data for the ML models included the hole pattern parameters (i.e., number of rows and columns), the hole diameter size, and the initial margin of the hole pattern from the plate side, which were specified for each plate design. The initial margin of the hole pattern from the plate side is considered 10, 15, 20, 25, and 30% of the plate dimensions (i.e., 15 *cm*). This margin variation includes 5 cases for the same pattern, size, and shape such as 2 by 2, 1 *cm* circular holes. When the margin is increased the distance between the holes is decreased. By systematically varying the hole patterns, and other parameters, a comprehensive dataset was generated, capturing the correlation between the input variables and the corresponding buckling loads. The buckling loads were measured as the output data for each configuration. The plate is designed with circular holes measuring 2%, 5%, 10%, and 15% of its width size (see Figure 2.19). The hole pattern consists of nine different variations, which are systematically varied starting from a 2×2 row and column arrangement. The pattern includes the following configurations: 2×2, 2×3, 2×4, 3×2, 3×3, 3×4, 4×2, 4×3, and 4×4. The dataset in this section comprises 175 data points in total.

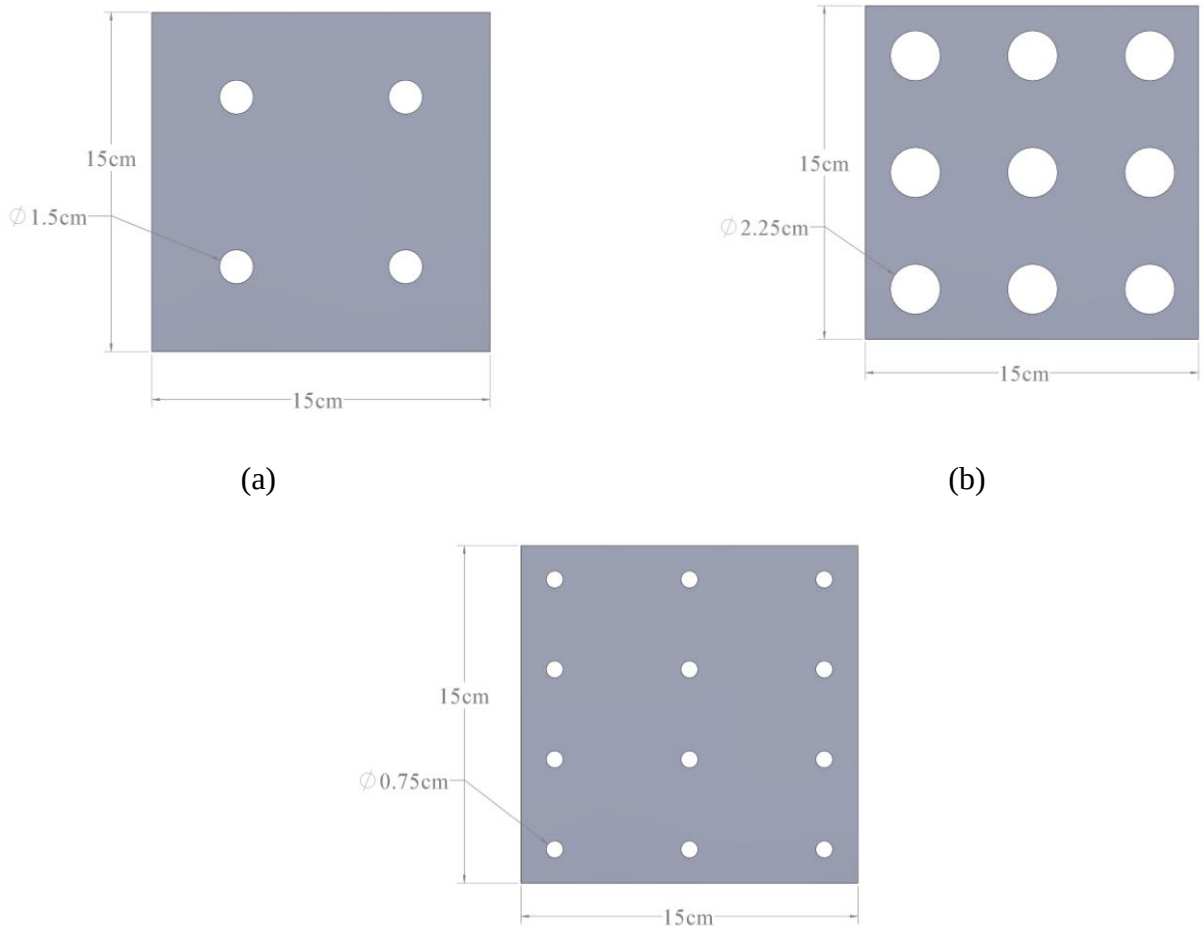

Figure 2.19. Sketch of three random 15×15 *cm* sample plates for simulation tests (a) 2×2 pattern with 25% margin with circular hole diameters of 1.5 *cm*, (b) 3×3 pattern with 15% margin with circular hole diameters of 2.25 *cm*, (c) 4×3 pattern with 10% margin with circular hole diameters of 0.75 *cm*

Figure 2.20-2.22 displays heatmaps of simulation data illustrating the buckling strength of various patterns across different sizes and distances from the left corner of the plate (i.e., margins). Designing a cutout pattern with the largest margin size of 4.5 cm and hole size of 2.5 in this study is unfeasible for the cases with higher number of holes due to reaching to the plate edges. The unfeasible designs are displayed on the heatmaps with green circles. The heatmaps reveal that plates with the same number of holes but different order of row and column (e.g., 2×4 and 4×2) exhibit different buckling strengths, indicating that factors like the order of rows and columns play

a crucial role. Additionally, an increase in the total number of holes correlates with a decrease in the buckling strength of the plate.

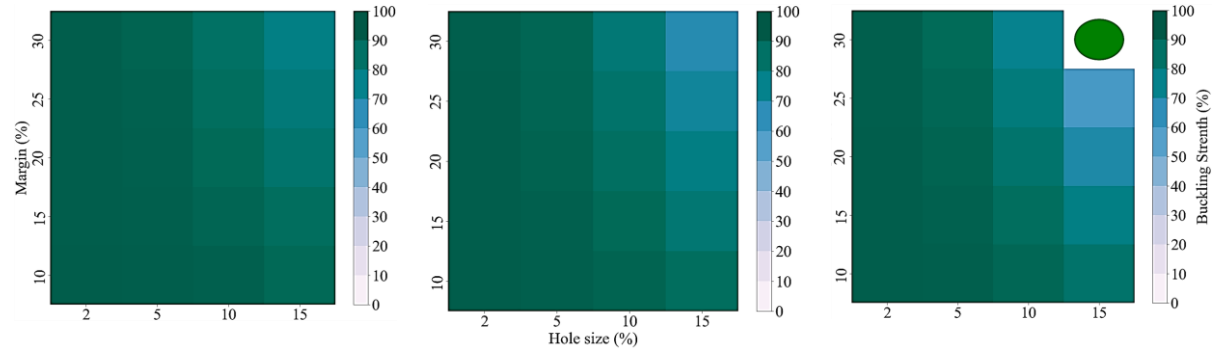

(a) (b) (c)

Figure 2.20. Heatmap of buckling strength of pattern (a) 2×2, (b) 2×3, and (c) 2×4

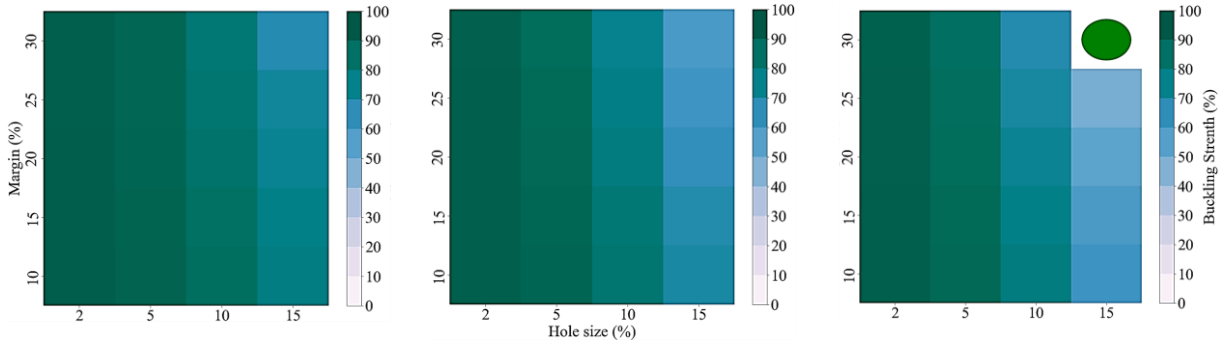

(a) (b) (c)

Figure 2.21. Heatmap of buckling strength of pattern (a) 3×2, (b) 3×3, and (c) 3×4

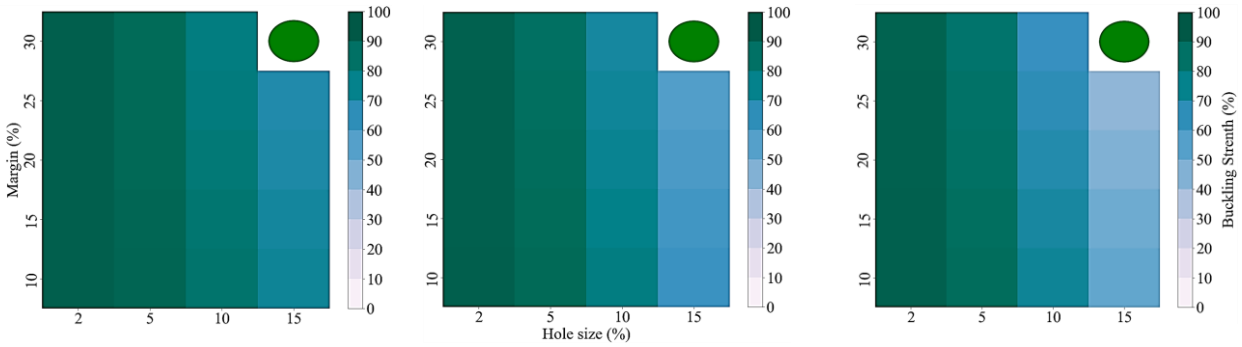

(a) (b) (c)

Figure 2.22. Heatmap of buckling strength of pattern (a) 4×2, (b) 4×3, and (c) 4×4

2.6 ML application on predicting buckling of VCP plate with single and multiple cutout

The buckling strength of a plate with single cutout (part I), as formulated in Eq. 5, is expressed as a percentage of the buckling strength of a perfect plate with no cutout. As discussed in Section 2.3.3, the formula for F_p was developed by analyzing the results from a FEM model. The N_{cr} part can be obtained from one either FEM, plate mechanics approach, or experimental test result. It is beneficial to apply the experimental approach for obtaining the N_{cr}, because one quick low-cost compression test can take the environmental and manufacturing complexities (e.g. adhesion effects between the corrugated board layers) effects into account. However, due to the simplified nature of our FEM model for simulating the VCP plates and the presence of environmental, manufacturing, and distribution hazards factors, the realistic buckling results contain uncertainties while following the expected trends. Several ML models are suggested to lower these uncertainties. In this chapter, to address these challenges, the F_p is predicted using ML models. Obtaining the N_{cr} follows the previously mentioned approaches. For CP plates with a matrix of multiple circular cutouts (Part II), the buckling strength is analyzed through machine learning models.

2.6.1 Data preprocessing for ML model

After the first step in the ML approach which is the acquisition of the sample data, the data is preprocessed for ML analysis. In part I of this section, the CP plates with single cutout in three shapes are analyzed. The location (i.e., x and y coordinates of the vent hole), size, and shape of the vent hole are considered the critical parameters that affect the compression strength of VCP packages (Han & Park, 2007b; Mukama et al., 2020; J. Singh et al., 2008; Thompson, 2008). The input ($X = \{x_1, x_2, x_3, x_4\}$) and output $\{Y\}$ variables in this study are presented in Table 2.6. An ASTM standard-based compressive test procedure was performed to determine the compressive strength of the VCP plates. The C-flute paperboard plates with a random dimension of $15cm \times 15cm$ and one either circular, square, or diamond cutout located at different locations on the plate are prepared. The samples were conditioned for 24 hours at 72°F and 50% RH as required in the test standard ASTM D642 (ASTM D642, 2020).

Table 2.6 An overview of parameters in this section

Parameter	Type	Unit
x_1: x coordinate of the vent hole	input	*cm*
x_2: y coordinate of the vent hole	input	*cm*
x_3: size of the vent hole	input	*cm*
x_4: shape of the vent hole	input	Circle, Square, Diamond
Y: Buckling strength (F_p)	output	*N*

In part II of this section, the CP plates with a pattern of multiple circular cutouts are analyzed. The number of rows and columns of holes, the size of the vent holes, and the margin of the hole from the plate side are considered critical parameters affecting the buckling strength of CP plates. The input variables ($X = \{x_1, x_2, x_3, x_4\}$) and output variable $\{Y\}$ used for part II, as presented in Table 2.7.

Table 2.7 Parameters in the ML data set used for the hole pattern design

Parameter	Type	Unit
x_1: number of the hole row	input	-
x_2: number of the hole column	input	-
x_3: size of the vent hole	input	*cm*
x_4: the margin of the hole from the plate side	input	*cm*
Y: Buckling strength (F_p)	output	*N*

2.6.1.1 Data preprocessing for Part I

For the second step of building up the ML models, data preprocessing in this work involves converting categorical input variables (i.e., the shape of the vent hole) to a numerical value, which can then be applied to the ML algorithms. Standardization of data that makes the input variables of the same scale is another part of data preprocessing. A unified scale of features generally improves the performance of ML and optimization algorithms. We applied non-dimensionalized values by dividing the dimensions to the plate width and dividing the buckling load to the buckling load of perfect plate to make our ML solution independent from the geometry dimensions and properties of the plate structure. The experimental test for part I is repeated three times for a case, each time on a new sample. The mean of the three maximum compression stress data for each case is collected and stored for the training of the ML models.

2.6.1.2 Data preprocessing for Part II

For part II where data is collected from FEM results, the tests do not need to be repeated as the simulation results do not vary for a case. The plate is compressed symmetrically from the top edge. Therefore, studying a vertical half (i.e., the left half) of the plate is sufficient; the results are duplicated symmetrically for the other half.

2.6.2 Data set splitting

In the third phase of our ML model development, we divided 686 experimental sample data in part I and 175 FEM simulation data in part II into two separate sets. These sets are used for training and testing to predict the buckling strength of VCP plates. The training set is used to train and optimize the ML models, while the test set is used to evaluate the performance of the ML models. In this study, a ratio of 90% of the data set was assigned to train the ML models and the residual 10% was employed for testing the models. Then a 5-fold cross-validation method is used to validate the ML prediction models. A comprehensive discussion of the 5-fold cross-validation technique is available in Section 2.8. Python programming language version 3.9.7 is used to implement the ML models. Figure 2.23 illustrates the workflow of the proposed ML method.

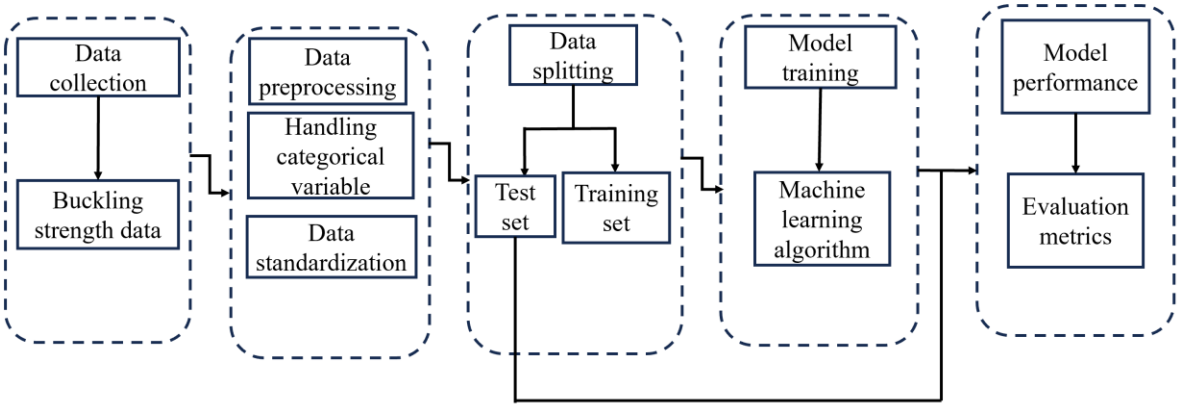

Figure 2.23. Schematic of proposed ML workflow in this study

2.7 ML models used in this chapter

To select the best ML models, we consider several factors such as the performance, the time and cost of training, and the robustness of the models. Prediction of the buckling strength is a type of regression problem due to the nature of the target variable (buckling strength), which is a continuous numerical quantity. The ML regression method is used to analyze the relationship between one or more independent variables and a dependent variable (de-Prado-Gil et al., 2022).

In this study, we employ three diverse methodologies for predicting the buckling strength of VCP plates. First, we apply the ensemble technique, specifically the LGBM. The ensemble technique is a ML model in which a learning algorithm combines the predictions of multiple differential ML models in order to enhance prediction accuracy (Al Daoud, 2019; Zhang & Ma, 2012). Chapter 1, Section 1.4 provides a comprehensive explanation of LGBM, a powerful gradient boosting framework that leverages tree-based learning algorithms. Subsequently, we compare the outcomes derived from the ensemble approach against those of the SVR and the well-established KNN method.

2.7.1 Customized loss function

Our general mechanics-based understanding suggests that as the size of a hole increases, the buckling strength of the plate should decrease. However, in 52 out of 686 cases of our experimental tests with different shapes, we observed that an increase in the hole size led to an increase in the buckling strength of the plates compared to the corresponding smaller hole size at the same location. This phenomenon was more pronounced in cases with circular shapes compared to those with square or diamond shapes. This result could be attributed to factors such as stress concentration, material quality, or the manufacturing process of the CP. In an attempt for enhancing our LGBM prediction model using ML technique, we implemented a customized loss function (Kashinath et al., 2021) based on the constraints in this study. This customized loss function penalizes the LGBM model for making predictions that contradict the known physics of the problem, specifically targeting predictions that indicate an increase in buckling strength with an increase in hole size. While Mean Squared Error (MSE) is a commonly used loss function for regression problems, we modified it in this context to include a penalty term ($\mathcal{P}$) to address this

specific issue. This penalty term is added to the regular MSE to increase the loss for predictions that violate the physics-based expectation (see Eq. 12).

$$\mathcal{P}_{penalty} = max\ (0, y_{pred}\ -\ y_{true}) \tag{12}$$

where y_{pred} is the predicted buckling strength, y_{true} is the true buckling strength. The penalty is the positive difference between the predicted and true values. Finally, we combine the regular MSE with the penalty term to create the custom loss function (i.e., $\mathcal{L}$). This combined loss function will be used to train the LGBM model. The combined loss function can be written as:

$$\mathcal{L}_{LGBM} = \text{MSE} + \lambda \times \mathcal{P} \tag{13}$$

where λ is a hyperparameter that controls the strength of the penalty. By incorporating this custom loss function, we explicitly integrate domain-specific knowledge, in this case, physics-based constraints, into the training process. Ultimately, this approach encourages the model to make predictions that not only align with the observed data but also adhere to the underlying physics, resulting in predictions that are not only accurate but also physically meaningful.

2.8 Comparing ML methods: a comparative analysis

In order to highlight the capabilities of the LGBM algorithm, an ensemble learning approach, this study incorporates well-established single learning methods, namely KNN, and SVR. This section provides a brief description of these methods. Chapter 1 thoroughly explains the KNN algorithm, a simple yet effective method used for classification and regression tasks. Similarly, an in-depth exploration of SVR, a powerful regression technique derived from support vector machines, is provided in Chapter 1.

2.8.1 Hyperparameters tuning of ML models

As ML models are trained on different datasets, the hyperparameters (i.e., tuning parameters) have a significant effect on their predictability, reliability, and generalizability to

various datasets. The purpose of hyperparameter tuning is to achieve optimal hyperparameter values while applying a learning algorithm to a specified data set. Therefore, all models were initially tuned so that the best performance accuracy was obtained for predicting the buckling strength of VCP plates. Table 2.8 presents the summary of three different ML model hyperparameters. In the LGBM method, the maximum depth sets a boundary on the depth of the tree, the learning rate controls the amount of contribution that each model has to the ensemble prediction, and the number of leaves indicates the number of leaves in a tree, which are parameters to be tuned. As mentioned earlier, *k* is the number of the nearest neighbors in the KNN model. In the case of the SVR method, the kernel and ε are the essential parameters to be tuned, where the kernel determines the data transformation strategy and the choice of ε defines the tolerance for prediction errors.

Table 2.8 An overview of the ML model hyperparameters for the prediction of buckling strength of plates with cutouts

Algorithms	Hyperparameters	Setting
LGBM	maximum depth	2
	learning rate	0.094
	number of leaves	15
	tree learner	feature
KNN	*k* number of nearest neighbors	6
SVR	kernel	'rbf'
	ε	0.1

2.8.2 Model development

A 5-fold cross-validation algorithm is implemented along with Grid Search algorithms to optimize the performance of all models applied in this study. As a first step, the parameter ranges

are evaluated based on findings in previous studies in the literature (e.g., Fadiji et al., 2019; Feng et al., 2020; Mukama et al., 2020). After the initial range of values has been determined, a grid search method is applied to find the specific values for parameters in the ML models. The cross-validation is then used to find the parameter set with the best performance iteratively training and testing the model (Kohavi, 1995). The process of the cross-validation method involves splitting the original data into training and validation sets iteratively to assess the predicted performance of a model. The 5-fold cross-validation involves dividing the data set into five parts, four of which are used for training, and one for evaluation.

2.8.3 Accuracy results analysis for ML section

To verify the performance of the ML regression models, the following four evaluation metrics including coefficient of determination (R^2), root mean square error (RMSE), mean absolute error (MAE), and mean absolute percentage error (MAPE) are used. The four metrics are defined in Eqns. 14-17 respectively:

$$R^2 = 1 - \frac{\sum_{i=1}^{n}(BS_i - BS_i')^2}{\sum_{i=1}^{n}(BS_i - \overline{BS})^2} \tag{14}$$

$$RMSE = \sqrt{\frac{1}{n}\sum_{i=1}^{n}(BS_i - BS_i^{'})^2} \tag{15}$$

$$MAE = \frac{1}{n}\sum_{i=1}^{n}\left|BS_i - BS_i^{'}\right| \tag{16}$$

$$MAPE = \frac{1}{n}\sum_{i=1}^{n}\left|\frac{BS_i - BS_i'}{BS_i}\right| \times 100 \tag{17}$$

where BS_i represents the buckling strength of the i-th sample in the dataset, obtained either from experimental testing or FEM computation; BS_i' is the buckling strength for i-th sample in the dataset predicted by the proposed ML models; $\overline{BS}$ in Eq. 14 is the averaged value of the buckling

strength of samples; and n is the total number of the sample in the dataset. The metric R^2 represents how well the original values fit the predicted values by applying the regression ML models. The RMSE shows the difference between a predicted value and an original value. The MAE is a measure of prediction error based on the actual situation. The MAPE metric presents the error-to-original value ratio and the error of the prediction. A summary of the evaluation metric results is presented in Table 2.9 and Table 2.10 for experimental test data in part I and II, respectively. The high value (i.e., higher than 90%) of R^2 for LGBM model indicates a comparatively good performance of the models in predicting the buckling strength of the VCP plates that shows a significant correlation with the actual data.

Table 2.9 The summary of the results from ML models for experimental data in Section 2.4 (Part I)

Method	Performance measures			
	R^2	RMSE	MAE	MAPE (%)
LGBM	0.917	3.30	2.56	3.34
KNN	0.868	4.23	2.93	3.83
SVR	0.829	4.81	3.84	5.41

Table 2.10 The summary of the results from ML models for FEM simulation data in Section 2.5 (Part II)

Method	Performance measures			
	R^2	RMSE	MAE	MAPE (%)
LGBM	0.946	3.47	2.23	3.35
KNN	0.873	5.13	3.24	4.73
SVR	0.698	7.92	7.27	8.76

The scatter plots of predictions and actual values of buckling strength of the VCP plates based on LGBM, SVR, and KNN models are illustrated in Figures 2.24 and 2.25. The actual values of buckling strength of VCP plates are plotted on the x-axis and the predicted values by ML models are plotted on the y-axis. The scatter points are the results, and the solid line indicates the condition

where the predicted and actual values are ideally equal. As can be seen, comparing the results of the three models, the LGBM model predicts results more accurately than the other two models. The LGBM is considered more accurate because it uses the leaf-wise tree growth method rather than depth-wise tree growth algorithms as in other ML algorithms.

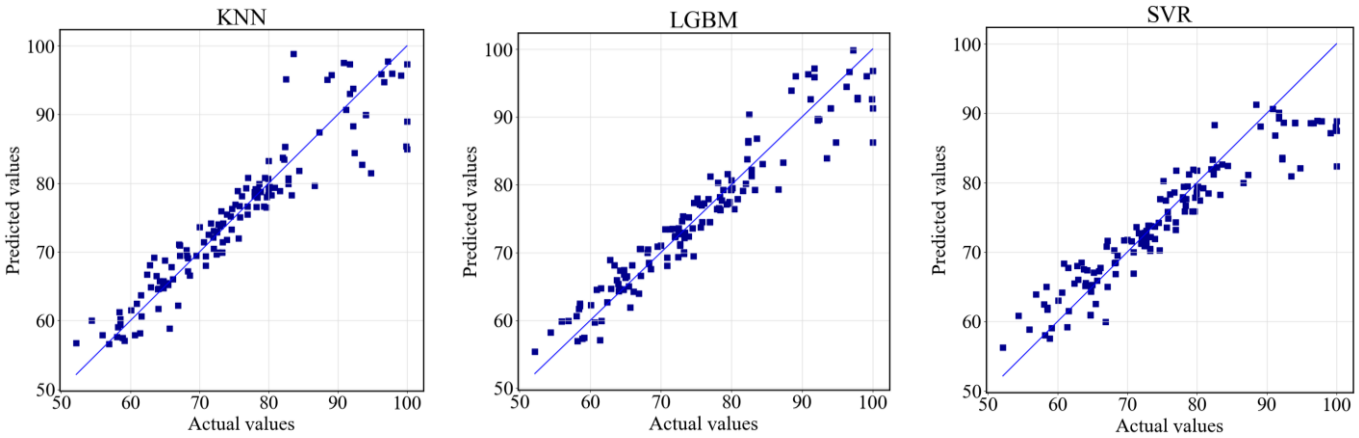

Figure 2.24. Buckling strength prediction results of ML models from experimental data in Section 2.4

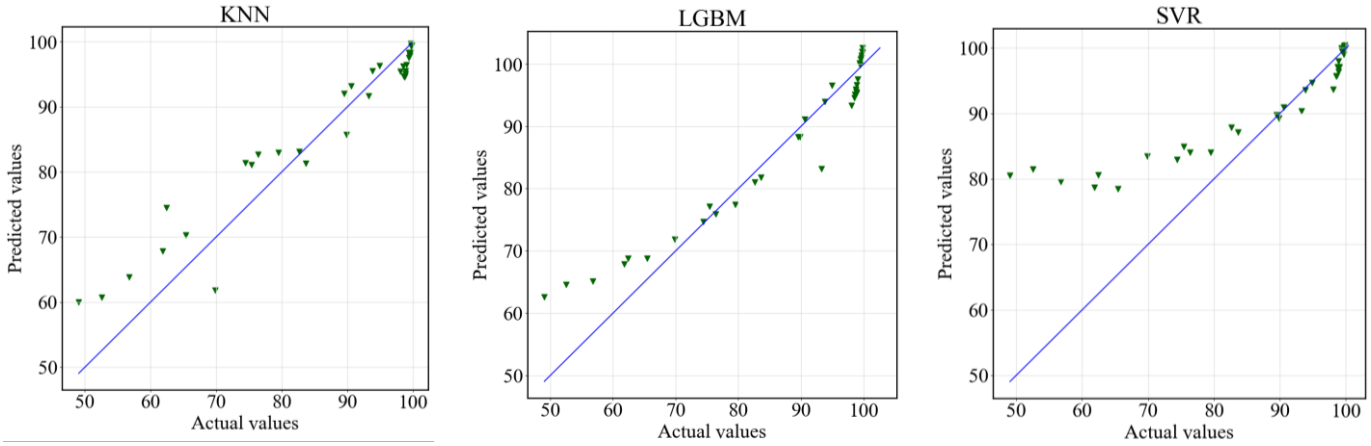

Figure 2.25. Buckling strength prediction results of ML models from FEM simulation data in Section 2.5

2.8.4 Effect of training and testing set ratio

The performance of an ML model is influenced by factors such as dependent and independent variables, the number of variables, and the size of the training dataset. To this end, we analyze how the size of the training data influences the results. We apply different split ratios

of training and testing sets including 90-10, 85-15, 80-20, and 70-30 on the LGBM model which shows the highest accuracy in our analysis. Table 2.11 shows the comparative results of the LGBM model with various training and testing sets for experimental test data in Section 3.1. As observed, all testing sets achieve nearly identical accuracy. The model achieved high R^2 scores ranging from 0.9143 to 0.9170, indicating a strong correlation between the predicted and actual values. Similarly, the RMSE values ranged from 3.30 to 3.41, showing consistent accuracy in predicting the variability of the target variable. Overall, the model demonstrated robust performance across different training and test set percentages, with minor variations in the MAPE values.

Table 2.11 LGBM model accuracies for different training and testing sets ratios for experimental test data for plates with a single different shape cutout in Section 2.4 (Part I)

Data set		Performance measures			
Training set (%)	Test set (%)	R^2	RMSE	MAE	MAPE (%)
90	10	0.9145	3.40	2.65	3.55
85	15	0.9143	3.41	2.61	3.44
80	20	0.9170	3.30	2.56	3.34
70	30	0.9152	3.34	2.62	3.48

Table 2.12 presents the effect of different training and test set ratios on the FEM simulation data in Section 3.2. Increasing the volume of training data leads to an apparent trend of reducing prediction error and deviation. To illustrate, as the proportion of training data expands from 70% to 90% of the entire dataset, the R^2 value exhibits growth, rising from 0.92 to 0.94. The data reveals a clear relationship between the size of the training set and the performance of the model on the test set. Specifically, as the training set size increases, the model exhibits higher R^2 values, indicating its ability to explain a significant portion of the variance in the data, while simultaneously reducing RMSE, MAE, and MAPE values. This underscores the importance of adequately sized training sets for enhancing the performance of the model overall.

Table 2.12 LGBM model accuracies for different training and testing sets ratios for FEM simulation data for plates with multiple circular cutouts in Section 2.5 (Part II)

Data set		Performance measures			
Training set (%)	Test set (%)	R^2	RMSE	MAE	MAPE (%)
90	10	0.9468	3.47	2.23	3.35
85	15	0.9058	4.11	2.70	3.92
80	20	0.9328	3.42	2.42	3.53
70	30	0.9202	3.79	2.50	3.52

2.8.5 Size and area of the hole analysis

We examined the factors affecting the buckling load of VCP plates by analyzing the size and shape of holes using the results from the FEM model. Figure 2.26a shows a comparison between the buckling loads of plates with different cutout shapes and the same size located at the plate center (7.5, 7.5). For a hole size of 1 *cm*, the circle shape exhibits a buckling load of 354.77 *N*, while the square and diamond shapes have buckling loads of 352.88 *N* and 352.81 *N*, respectively. This suggests that, at this size, the square and diamond shapes perform comparably to the circle in terms of buckling load. However, as the size of the hole increases, the buckling load decreases for all shapes, with the circle case consistently having the highest buckling load among the three shapes at each size increment. In ventilation and air circulation analysis for designing packages in cold chain, the total area of the cutout might be a more important factor than the cutout width. The area of the circle cutout becomes different from the area of corresponding square and diamond cutout with the same width. Figure 2.26b shows a comparison of the buckling loads of plates with different cutout shapes and same areas. We used the same 1, 2, 3, and 4 cm diameter for the circle cutout diameter and matched the required cutout width for the square and diamond. Figure 2.26b reveals that when the areas are equal, circle cutout is not superior anymore in retaining the buckling strength compared to square and diamond, the three shapes show approximately same results. For example, for a circle with a diameter of 1 *cm* and a square and

diamond both with a width of 0.886 *cm* (all three cases provide same area of 0.78 cm^2), the buckling loads are obtained as close values of 354.77 *N*, 354.37 *N*, and 354.33 *N* respectively. This indicates that the importance of shape factor is negligible when the areas of the different cutout shapes are equal. Here again, as the cutout sizes increase, the buckling loads decrease for all shapes.

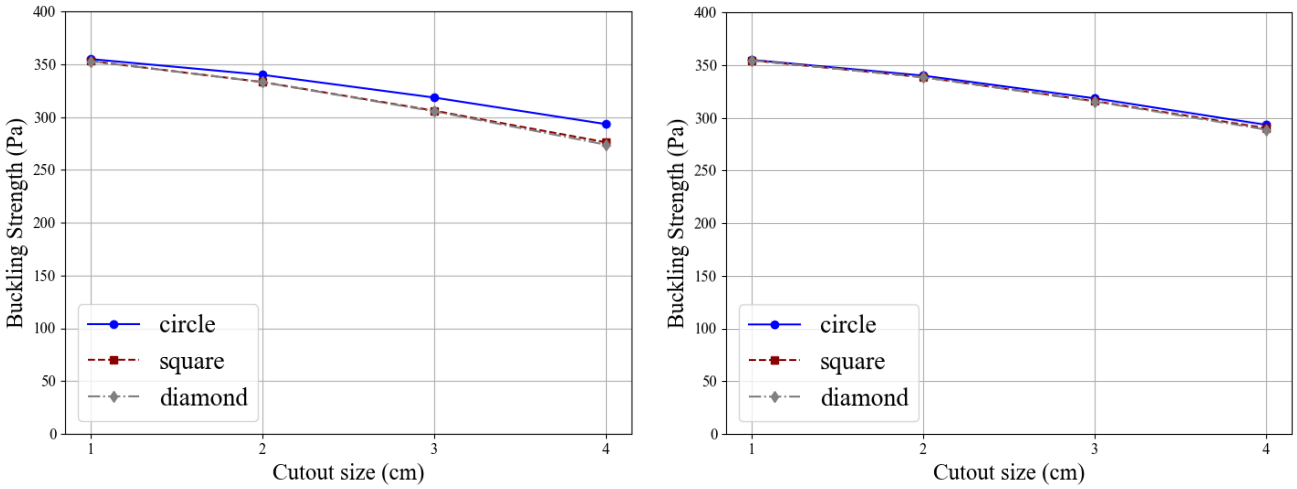

Figure 2.26. Comparison of buckling load of VCP plates with different cutout shapes and (a) same hole width, (b) same hole area

2.8.6 Input variables sensitivity analysis

The LGBM method provides a high accuracy in predicting the buckling strength of the VCP plates. In this section, we analyze the basic mechanical phenomena underlying the prediction of the LGBM model for the buckling strength of the VCP plates by studying the effect of each input variable on the buckling strength of the VCP plates. The input variables (i.e., features) for experimental data include the x and y location of the vent hole, the shape of the vent hole, and the size of the vent hole. The input variables (i.e., features) for FEM simulation data include the number of the hole row and column, the size of the hole, and the margin of the hole from the plate side. In the feature importance method, the model assigns a score to each feature by evaluating the

importance of the feature for predicting the outcome. By evaluating the importance of features for predicting the outcome, input features are given a score. The score will be higher as the feature contributes more to predicting the output. Figure 2.27 shows the score of each feature in the feature importance analysis. In the case of experimental data for single cutout with three shapes, it can be found that the shape of the vent hole has the most impact on the buckling strength of the VCP plates. The shape of the vent hole was investigated by (Han & Park, 2007b; J. Singh et al., 2008) and comparable effects were reported. The size and y-coordinate location of the vent hole can also have a significant impact on the buckling strength of the VCP plates. This is reasonable since the axial load was applied in the y direction. The x-coordinate location of the vent hole has the least importance. Moreover, the analysis of feature importance in the FEM simulation data for a pattern of cutouts highlights the significance of both the size and the distance of the hole from the corner and to the center of the plates.

We expanded our investigation to include the cases of three shapes with equal areas and found consistent results when analyzing their feature importance. This expanded investigation allowed us to compare how different shapes, despite having the same area, influenced the feature importance in our analysis. Understanding these subtleties is crucial for gaining insights into how geometric factors impact the overall behavior of the structures under study.

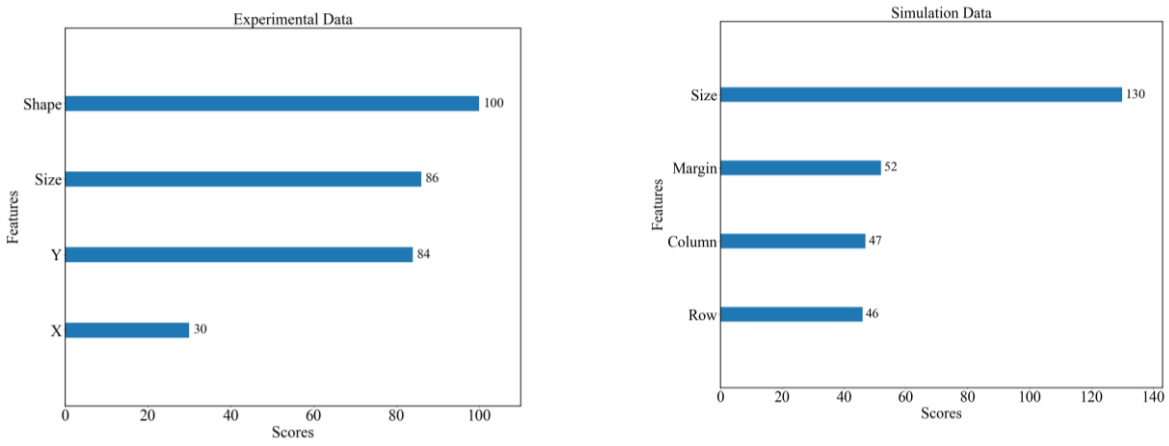

(a) (b)

Figure 2.27. Importance of various input (i.e., feature) variables in (a) experimental test for single cutout and three shapes in section 2.4, (b) FEM simulation for pattern of circular cutouts in section 2.5

2.9 Conclusion

The use of perforated plates extends across various engineering structures, such as bridges, airplane fuselages, and ventilated food packaging boxes. In this chapter, we employed a combination of experimental, FEM, analytical, and ML approaches to predict the buckling load of thin elastic plates with A) a single circular, square, or diamond hole and B) multiple circular cutouts. While these models are adaptable to perforated plates made of other elastic materials, our primary focus was on VCP widely used in the packaging industry. Conducting these evaluations is essential for package designers to create efficient packages that achieve both optimal airflow within the package and sufficient mechanical strength while using minimized package materials, ensuring reliable performance throughout the cold chain supply.

Through the proposed methods, we successfully predicted the buckling loads of plates with two free vertical edges under vertical compression loads, simulating compressions in package stacks. First, we measured the compression stiffness of a random sized (e.g., 15cm × 15 cm) CP composite plate with no cutout using experimental tests to obtain a modulus of elasticity for the

equivalent homogenous plate. Then the CP plate was modeled in FEM software (ABAQUS) as a solid shell plate. Utilizing FEM results for a range of hole sizes and locations, we formulated two nondimensionalized buckling load equations for thin elastic plates comprising a single circular hole. The outcomes from the developed model aligned well with the experimental results. It was observed that increasing the hole size results in decreased buckling resistance of the plates while positioning the hole closer to the horizontal top or bottom edges retained higher buckling strength. The variation of hole location in the x direction had no significant impact on the results due to the existing symmetries. Then, we measured the buckling of CP plates with a single circular cutout for a range of hole sizes and locations experimentally. It is essential to note that the experimental results for smaller hole sizes may not always follow the trends mentioned. This inconsistency can be attributed to the inherent complexity of CPs, such as variable glue quality between the plate layers at different locations of the paperboard due to the applied distribution hazards. Therefore, to enhance the accuracy of buckling load predictions for VCP plates, the integration of AI and ML methods becomes imperative for future studies. Furthermore, the plate theory utilized in Eq. 8 is developed based on linear elasticity. Hence, for structures that exhibit nonlinear deformations and plastic pre-buckling behavior, alternative analysis methods like ML should be employed to provide more accurate results. ML models typically analyze the entirety of data using advanced algorithms without searching for physics-based reasons.

The ML approach for predicting the buckling strength of VCP applied in designing sustainable food packages offers a promising alternative to the current time- and cost-consuming experimental tests and computational methods. This chapter adopts ML models to predict the buckling strength of VCP plates using a small dataset from experimental tests or simulations to train the algorithms. The initial application of ML on the experimental buckling results of CP

plates with a single circular hole showed reasonably accurate predictions which include the uncertain results. Predicting these anomalies could not be expected from our simplified FEM models. Then we further expanded our experimental data by testing the VCP plate with two more cutout shapes to include hole's shape feature in the ML analysis. In Section 2.4, experimental compression tests were conducted on 15 *cm* square plates with a single hole in three shapes: circle, square, and diamond. We observed that placing holes near the top and bottom edges of the structure preserves higher buckling strength, especially as hole width increases, while larger hole sizes directly reduce buckling strength. The location, size, and shape of the vent hole were considered as input variables and the buckling loads were labeled as output for the ML models. In many food package designs, VCP packages comprise several cutouts in a patterned design on their walls. Section 2.5 investigates the buckling strength of VCP plates with multiple circular cutouts using the FEM environment of SolidWorks software. The FEM simulation data includes the rows and columns of the holes, the size of the holes, and the initial margin of the hole pattern from the side of the plate, all of which collectively influence the buckling strength of the VCP packages for the ML models. The models are trained on the collected data and evaluated using statistical measurements such as R^2, RMSE, MAE, and MAPE. We used a customized loss function to include the expected physics constraints of the problem to take advantage of the ML which improves the predictions accuracy. The results indicate that all ML models provide reasonably accurate predictions for the buckling strength of the VCP packages. In particular, the LGBM approach demonstrates remarkably accurate predictions for the compression strength of the VCP packages. The study also discusses different training and testing sizes of the dataset, finding that the most accurate results are achieved by training 90% of the total dataset. Furthermore, the impact of different input variables on buckling strength is analyzed. The sensitivity analysis of the LGBM

model reveals that the shape of the vent hole in plates with single cutout is the main variable influencing the buckling strength, followed by the size of the vent hole for VCP plates with a single hole. For plates with a pattern of holes, the size of the hole is the most influential variable. These insights provide valuable information about the relative contributions of each input variable in determining the buckling strength. In conclusion, the results of this study demonstrate that ML models align with established knowledge regarding the factors affecting buckling strength. This alignment highlights the potential of ML methodologies as a viable and efficient means of predicting the buckling strength of VCP packages. These findings offer a promising avenue for improving the efficiency and accuracy of buckling strength assessments, thereby reducing material waste in package designs while enhancing package protection properties. Additionally, the analysis conducted in this study can be extended to plate structures with cutouts in other engineering disciplines such as aerospace and construction.

2.10 Limitations and future study

For future research and further analysis, it will be interesting to conduct failure mode analysis, explore other shapes of the holes like oblong, and apply the other types of CP such as flute B. This comprehensive investigation will facilitate a deeper understanding of the behavior of perforated plates and contribute to the advancement of packaging design and engineering. The analysis can be applied to the other engineering plate structures with cutouts applied in industries such as aerospace and construction.

Acknowledgment: The work was supported under the MTRAC Program by the State of Michigan 21st Century Jobs Fund received through the Michigan Strategic Fund and administered by the Michigan Economic Development Corporation.

REFERENCES

Al Daoud, E. (2019). Comparison-Between-Xgboost-Lightgbm-and-Catboost-Using-a-Home-Credit-Dataset. *International Journal of Computer and Information Engineering, 13*(1), 6–10.

American Box Company. (2023). Understanding Corrugated Board Grades. Retrieved from https://Amboxkc.Com/Board-Grades-Flutes/.

Archaviboonyobul, T., Chaveesuk, R., Singh, J., & Jinkarn, T. (2020). An analysis of the influence of hand hole and ventilation hole design on compressive strength of corrugated fiberboard boxes by an artificial neural network model. *Packaging Technology and Science, 33*(4–5), 171–181. https://doi.org/10.1002/pts.2495

ASTM D642. (2000). Standard Test Method for Determining 1 Compressive Resistance of Shipping Containers, Components, and Unit Loads 1. *Test, 00*(November), 1–6. https://doi.org/10.1520/D0642-20.Development

ASTMD6804. (2014). Standard Guide for Hand Hole Design in Corrugated Boxes.

Aydin Komur, M., & Sonmez, M. (2008). Elastic buckling of rectangular plates under linearly varying in-plane normal load with a circular cutout. *Mechanics Research Communications, 35*(6), 361–371. https://doi.org/10.1016/j.mechrescom.2008.01.005

Beldie, L., Sandberg, G., & Sandberg, L. (2001). Paperboard packages exposed to static loads-finite element modelling and experiments. *Packaging Technology and Science, 14*(4), 171–178. https://doi.org/10.1002/pts.546

Ben Chaabene, W., Flah, M., & Nehdi, M. L. (2020). ML prediction of mechanical properties of concrete: Critical review. *Construction and Building Materials, 260*, 119889. https://doi.org/10.1016/j.conbuildmat.2020.119889

Berry, T. M., Delele, M. A., Griessel, H., & Opara, U. L. (2015). Geometric design characterisation of ventilated multi-scale packaging used in the South African pome fruit industry. *Agricultural Mechanization in Asia, Africa, and Latin America, 46*(3), 1–19.

Berry, T. M., Fadiji, T. S., Defraeye, T., & Opara, U. L. (2017). The role of horticultural carton vent hole design on cooling efficiency and compression strength: A multi-parameter approach. *Postharvest Biology and Technology, 124*, 62-74. https://doi.org/10.1016/j.postharvbio.2016.10.005

Bloom, F., & Coffin, D. (2000). Handbook of Thin Plate Buckling and Postbuckling. *Handbook of Thin Plate Buckling and Postbuckling.* Chapman and Hall/CRC. https://doi.org/10.1201/9781420035650

Briassoulis, D. (1986). Equivalent orthotropic properties of corrugated sheets. *Computers and Structures, 23*(2), 129–138. https://doi.org/10.1016/0045-7949(86)90207-5

Bulson, P. S. (1969). The Stability of Flat Plates. Elsevier Publishing Company. NY.

Cheng, B., & Zhao, J. (2010). Strengthening of perforated plates under uniaxial compression: Buckling analysis. *Thin-Walled Structures*, *48*(12), 905-914. https://doi.org/10.1016/j.tws.2010.06.001

da Silva e Silva, N., de Souza Farias, F., dos Santos Freitas, M. M., Pino Hernández, E. J. G., Dantas, V. V., Enê Chaves Oliveira, M., Joele, M. R. S. P., & de Fátima Henriques Lourenço, L. (2021). Artificial intelligence application for classification and selection of fish gelatin packaging film produced with incorporation of palm oil and plant essential oils. *Food Packaging and Shelf Life*, *27*(May 2020). https://doi.org/10.1016/j.fpsl.2020.100611

de-Prado-Gil, J., Palencia, C., Silva-Monteiro, N., & Martínez-García, R. (2022). To predict the compressive strength of self-compacting concrete with recycled aggregates utilizing ensemble ML models. *Case Studies in Construction Materials*, *16*, e01046. https://doi.org/10.1016/j.cscm.2022.e01046

Eiblmeier, J., & Loughlan, J. (1995). The buckling response of carbon fibre composite panels with reinforced cutouts. *Composite Structures*, *32*(1–4), 97–113. https://doi.org/10.1016/0263-8223(95)00049-6

El-Sawy, K. M., Nazmy, A. S., & Martini, M. I. (2004). Elasto-plastic buckling of perforated plates under uniaxial compression. *Thin-Walled Structures*, *42*(8), 1083–1101. https://doi.org/10.1016/j.tws.2004.03.002

Fadiji, T., Coetzee, C., & Opara, U. L. (2016). Compression strength of ventilated CP packages: Numerical modelling, experimental validation and effects of vent geometric design. *Biosystems Engineering*, *151*, 231–247. https://doi.org/10.1016/j.biosystemseng.2016.09.010

Fadiji, T., Berry, T., Coetzee, C., & Opara, L. (2017). Investigating the Mechanical Properties of Paperboard Packaging Material for Handling Fresh Produce Under Different Environmental Conditions: Experimental Analysis and Finite Element Modelling. *Journal of Applied Packaging Research*, *9*(2), 3.

Fadiji, T., Berry, T. M., Coetzee, C. J., & Opara, U. L. (2018a). Mechanical design and performance testing of corrugated paperboard packaging for the postharvest handling of horticultural produce. *Biosystems Engineering*, *171*, 220-244.

Fadiji, T., Coetzee, C. J., Berry, T. M., Ambaw, A., & Opara, U. L. (2018b). The efficacy of finite element analysis (FEA) as a design tool for food packaging: A review. *Biosystems Engineering*, *174*, 20–40. https://doi.org/10.1016/j.biosystemseng.2018.06.015

Fadiji, T., Coetzee, C. J., Berry, T. M., & Opara, U. L. (2019). Investigating the role of geometrical configurations of ventilated fresh produce packaging to improve the mechanical strength – Experimental and numerical approaches. *Food Packaging and Shelf Life*, *20*. https://doi.org/10.1016/j.fpsl.2019.100312

Falkowicz, K. (2021). Composite plate analysis made in an unsymmetric configuration. *Journal of Physics: Conference Series*, *2130*(1). https://doi.org/10.1088/1742-6596/2130/1/012014

Falkowicz, K. (2022a). Numerical Buckling Analysis of Thin-Walled Channel-Section Composite Profiles Weakened by Cut-Outs. *Advances in Science and Technology Research Journal*, *16*(6), 88–96. https://doi.org/10.12913/22998624/155397

Falkowicz, K. (2022b). Numerical Investigations of Perforated CFRP Z-Cross-Section Profiles, under Axial Compression. *Materials*, *15*(19). https://doi.org/10.3390/ma15196874

Falkowicz, K. (2022c). Stability Analysis of Thin-Walled Perforated Composite Columns Using Finite Element Method. *Materials*, *15*(24). https://doi.org/10.3390/ma15248919

Falkowicz, K. (2023). Experimental and numerical failure analysis of thin-walled composite plates using progressive failure analysis. *Composite Structures*, *305*(November 2022), 116474. https://doi.org/10.1016/j.compstruct.2022.116474

Falkowicz, K., Wysmulski, P., & Debski, H. (2023). Buckling analysis of laminated plates with asymmetric layup by approximation method. *Materials*, *16*(14), 4948.

Feng, D. C., Liu, Z. T., Wang, X. D., Chen, Y., Chang, J. Q., Wei, D. F., & Jiang, Z. M. (2020). ML-based compressive strength prediction for concrete: An adaptive boosting approach. *Construction and Building Materials*, *230*, 117000. https://doi.org/10.1016/j.conbuildmat.2019.117000

Frank, B. (2014). Corrugated box compression - A literature survey. *Packaging Technology and Science (Vol. 27, Issue 2, pp. 105–128)*. https://doi.org/10.1002/pts.2019

Garbowski, T., Gajewski, T., & Grabski, J. K. (2021). Estimation of the compressive strength of corrugated cardboard boxes with various openings. *Energies*, *14*(1), 1–20. https://doi.org/10.3390/en14010155

Gupta, R. K., & Dudeja, P. (2017). Food packaging. *Food Safety in the 21st Century* (pp. 547-553). Academic Press.

Han, B. J., & Park, J. M. (2007). Finite Element Analysis of Vent / Hand Hole and Science. *Packaging Technology and Science*, June 2006, 39–47.

Joodaky, A., Joodaky, I., Hedayati, M., Masoomi, R., & Farahani, E. B. (2013). Deflection and stress analysis of thin FGM skew plates on Winkler foundation with various boundary conditions using extended Kantorovich method. *Composites Part B: Engineering*, *51*, 191–196. https://doi.org/10.1016/j.compositesb.2013.03.010

Joodaky, I., & Joodaky, A. (2019). Bending of edge-bonded dissimilar rectangular plates. *Meccanica*, *54*(3), 565–572. https://doi.org/10.1007/s11012-019-00969-6

Kashinath, K., Mustafa, M., Albert, A., Wu, J. L., Jiang, C., Esmaeilzadeh, S., Azizzadenesheli, K., Wang, R., Chattopadhyay, A., Singh, A., Manepalli, A., Chirila, D., Yu, R., Walters, R., White, B., Xiao, H., Tchelepi, H. A., Marcus, P., Anandkumar, A., Prabhat. (2021). Physics-informed ML: Case studies for weather and climate modelling. *Philosophical Transactions of the Royal Society A*, *379*(2194). https://doi.org/10.1098/rsta.2020.0093

Kawanishi, K. (1989). Estimation of the compression strength of corrugated fibreboard boxes and its application to box design using a personal computer. *Packaging Technology and Science, 2*(1), 29-39.

Kim, Y., & Park, J. (2020). A theory for the free vibration of a laminated composite rectangular plate with holes in aerospace applications. *Composite Structures, 251*(May), 112571. https://doi.org/10.1016/j.compstruct.2020.112571

Kohavi, R. (1995). A Study of Cross-Validation and Bootstrap for Accuracy Estimation and Model Selection. *International Joint Conference of Artificial Intelligence (Vol. 14, No. 2, pp. 1137-1145)*.

Lepine, J., Rouillard, V., & Sek, M. (2017). On the use of ML to detect shocks in road vehicle vibration signals. *Packaging Technology and Science, 30*(8), 387–398.

Li, F., Zhang, L., Chen, B., Gao, D., Cheng, Y., Zhang, X., Yang, Y., Gao, K., Huang, Z., & Peng, J. (2018). A Light Gradient Boosting Machine for Remainning Useful Life Estimation of Aircraft Engines. *IEEE Conference on Intelligent Transportation Systems, Proceedings, ITSC, 2018-Novem*, 3562–3567. https://doi.org/10.1109/ITSC.2018.8569801

Lin, C. C., & Kuo, C. S. (1989). Buckling of Laminated Plates with Holes. *Journal of Composite Materials, 23*(6), 536–553. https://doi.org/10.1177/002199838902300601

Moen, C. D., & Schafer, B. W. (2009). Elastic buckling of thin plates with holes in compression or bending. *Thin-Walled Structures, 47*(12), 1597–1607. https://doi.org/10.1016/j.tws.2009.05.001

Muc, A., Chwał, M., & Barski, M. (2018). Remarks on experimental and theoretical investigations of buckling loads for laminated plated and shell structures. *Composite Structures, 203*(July), 861–874. https://doi.org/10.1016/j.compstruct.2018.07.094

Mukama, M., Ambaw, A., & Opara, U. L. (2020). Advances in design and performance evaluation of fresh fruit ventilated distribution packaging: A review. *Food Packaging and Shelf Life (Vol. 24)*. https://doi.org/10.1016/j.fpsl.2020.100472

Narayana, A. L., Rao, K., & Kumar, R. V. (2014). Buckling analysis of rectangular composite plates with rectangular cutout subjected to linearly varying in-plane loading using fem. *Sadhana, 39*, 583-596.

Nguyen-Sy, T., Wakim, J., To, Q. D., Vu, M. N., Nguyen, T. D., & Nguyen, T. T. (2020). Predicting the compressive strength of concrete from its compositions and age using the extreme gradient boosting method. *Construction and Building Materials, 260*, 119757. https://doi.org/10.1016/j.conbuildmat.2020.119757

Opara, U. L., & Fadiji, T. (2018). Compression damage susceptibility of apple fruit packed inside ventilated CP package. *Scientia Horticulturae, 227*, 154–161. https://doi.org/10.1016/j.scienta.2017.09.043

Pal, S., & Naskar, K. (2021). ML model predict stress-strain plot for Marlow hyperelastic material design. *Materials Today Communications*, *27*(February), 102213. https://doi.org/10.1016/j.mtcomm.2021.102213

Pathare, P. B., & Opara, U. L. (2014). Structural design of corrugated boxes for horticultural produce: A review. *Biosystems Engineering (Vol. 125)*. https://doi.org/10.1016/j.biosystemseng.2014.06.021

Scheperboer, I. C., Efthymiou, E., & Maljaars, J. (2016). Local buckling of aluminium and steel plates with multiple holes. *Thin-Walled Structures*, *99*, 132–141. https://doi.org/10.1016/j.tws.2015.11.009

Shirzad, K., & Joodaky, A. (2022). Predicting the Compression Strength in Ventilated Corrugated Paperboard Packages Using ML Models. *The 23rd IAPRI World Packaging Conference IAPRI Bangkok 2022, Survival and Sustainability, June*.

Shirzad, K., & Joodaky, A. (2023). Buckling analysis of thin plates with circular cutouts for sustainable ventilated food packaging design. *Food Packaging and Shelf Life*, *40*(November), 101214. https://doi.org/10.1016/j.fpsl.2023.101214

Singh, J., Olsen, E., Singh, S. P., Manley, J., & Wallace, F. (2008). The effect of ventilation and hand holes on loss of compression strength in corrugated boxes. *Journal of Applied Packaging Research*, *2*(4), 227.

Sun, Y., Zhang, M., Adhikari, B., Devahastin, S., & Wang, H. (2022). Double-layer indicator films aided by BP-ANN-enabled freshness detection on packaged meat products. *Food Packaging and Shelf Life*, *31*(December 2021), 100808. https://doi.org/10.1016/j.fpsl.2021.100808

Thompson, J. F. (2002). Commercial cooling of fruits, vegetables, and flowers (Vol. 21567). University of California, Division of Agriculture and Natural Resources.

Zhang, C., & Ma, Y. (2012). Ensemble machine learning (Vol. 144). New York: Springer.

Zhao, C., Johnsson, M., & He, M. (2017). Data mining with clustering algorithms to reduce packaging costs: A case study. *Packaging Technology and Science*, *30*(5), 173–193.

Chapter 3: Machine Learning Solutions for Predicting Mechanical Damage to Apple Fruit and Packaging under Vibrational Forces in Transportation

Abstract

This chapter investigates the impact of various factors on the damage experienced by apple fruit and its packaging during transportation vibrations, including vibration intensity, duration, profile, package type, and apple variety. Utilizing ML models, we predict the percentage of damage in packaged apple fruit. By leveraging ML solutions, we not only predict damage percentages but also identify key areas for improvement in packaging design and transportation protocols, ultimately contributing to more efficient and damage-resistant packaging solutions for apple fruit. Our analysis reveals that vibration intensity is the most significant factor affecting damage, followed by duration and package type. The vibration profile and apple variety have relatively minor impacts. These findings underscore the importance of considering intensity, duration, and package type in predicting and mitigating damage during transportation vibrations. Furthermore, employing a random forest model, we achieved a high accuracy in predicting damage, outperforming other models in predictive power and accuracy. This research provides valuable insights for enhancing packaging design and transportation practices to reduce damage to apple fruit and packaging during transit.

3.1 Introduction

Consumer trends toward healthier food, eating out (i.e., eating out influences consumer products as the trend drives restaurants to offer healthier, minimally processed food options, boosting demand for fresh produce), and minimally processed foods have increased the demand for fresh produce in recent decades (Li & Thomas, 2014). Based on market data for 2023, fruits and vegetables were valued at USD 96.26 billion, with a projected compound annual growth rate of 4.1% in 2030 (Grand View Research, 2018). Transporting agricultural products, including apples, presents challenges like potential mechanical damage to the produce and its packaging.

This damage, including bruises, cuts, and blemishes, occurs during transportation and postharvest handling due to impact, compression, and vibration forces, affecting the quality and marketability of the produce.

Mechanical damage caused by vibration is one of the most common quality challenges to fresh produce during transit (Al-Dairi et al., 2022). Horticultural products like apples are highly susceptible to mechanical damage, leading to significant losses (Fadiji, Coetzee, Chen, et al., 2016). Bruising represents the most frequently occurring form of mechanical damage throughout the stages of harvesting, sorting, packaging, storage, transportation, and retailing (Du et al., 2020). During transportation, damage often results from fruits colliding with each other or with packaging, as well as from abrasion when fruits rub against surfaces (Van Zeebroeck et al., 2007). These visual defects significantly impact the quality and profitability of both growers and retailers (Al-Dairi et al., 2022). Moreover, such damage diminishes consumer desirability and contributes to resource wastage (M. Lin et al., 2023). Therefore, minimizing mechanical damage is crucial for preserving fruit quality, extending shelf life, reducing food waste, and sustaining profitability for growers and distributors.

There are several studies in the area of damage during transport and handling of apples. Some of them focused on the dynamic forces during apple transport and handling cause by far the most bruise damage. Mehl et al., (Mehl et al., 2004) developed a hyperspectral imaging system to detect surface defects such as bruises, side rots flyspecks, scabs and molds, fungal diseases (e.g., black pox), and soil contaminations in apple fruits. Detecting apple defects by non-destructive spectroscopy and imaging an overview of common defects in apples, encompassing physiological disorders, mechanical damage, pathological disorders, and contamination.

A range of non-destructive methods have been explored for detecting mechanical damage in apples. Solovchenko et al., (Solovchenko et al., 2010) and He et al., (He et al., 2022) both highlight the potential of visible/near-infrared spectroscopy, with the latter also discussing the applicability of other techniques such as chlorophyll fluorescence, computer vision, and imaging. Lu and Y. Lu (Lu & Lu, 2017) provides a comprehensive review of spectroscopic and imaging technologies for defect detection in apples, including those related to mechanical damage. Bratu et al., (Bratu et al., 2021). These studies highlight the potential of non-destructive methods, such as laser photoacoustic spectroscopy and multispectral imaging, for evaluating fruit quality and detecting degradation, emphasizing their value in detecting mechanical damage in apples and their potential for further research and application. Assessing the firmness and quality of apples using non-destructive methods has been a significant focus in recent research. Tian & Zu (Tian & Xu, 2023) provides a comprehensive overview of the current state of nondestructive firmness evaluation methods for fruits and the challenges and prospects in achieving accurate on-line measurement of fruit firmness. Hosoya et al., (Hosoya et al., 2017) used a high-output pulsed laser to generate a laser-induced plasma shock wave, which was then applied to apples as an excitation force. The firmness of the apples was evaluated by analyzing the vibration response spectra using a Laser Doppler Vibrometer (LDV). LDV sensors detect the Doppler effect of the reflected laser, caused by the movement of the sample, to measure the vibration velocity of the object. Lee et al., (Lee et al., 2022) predict the soluble solid content in Fuji apple. In Kim et al., (K. B. Kim et al., 2009) study with ultrasonic velocity and attenuation models, they detected firmness in apples and built prediction models for firmness.

The impact of vibration on various characteristics of apple fruit has been extensively studied using simulation techniques. Walkowiak-Tomczak et al., (Walkowiak-Tomczak et al.,

2021) utilized vibration simulation techniques to investigate the effect of vibration on various characteristics of apple fruit, including color, firmness, total soluble solids, pH value, titratable acidity, dry matter content, and total polyphenol content. Their findings indicated that vibrations reduced the firmness of the fruit while enhancing its antioxidant capacity and polyphenol content across different cultivars. Jung and Park (Jung & Park, 2012b) employed a vibration simulation in their investigation, focusing on the impact of transportation vibration on various attributes of apples inside the package. Their study revealed that the vibration stress led to increased total soluble solids, weight loss, CO_2 concentration, and ethylene production rate, while also decreasing the firmness of the apples during storage. Vursavus and Ozguven (Vursavuş & Özgüven, 2004) assessed the impact of vibration frequency, vibration acceleration, vibration duration and packaging type on mechanical damage during the transportation of Golden Delicious Apples. Their study considered packaging methods such as paper pulp tray, pattern packing, and volume packing. Interestingly, they discovered that volume packaging resulted in the most significant levels of damage to the apples during transportation. Fadiji et al., (Fadiji, Coetzee, Chen, et al., 2016) examined the sensitivity of apple fruit inside packages during simulated transport. They specifically focused on two commonly used ventilated CP packages in the South African fresh produce industry, namely, MK4 and MK6. Due to the increasing peak acceleration of the packaging container from the bottom to the top, they observed high bruise damage on apple fruit on the top layer of the package. The damage ranged from 50% to 74% bruise damage. Singh et al., (S. P. Singh et al., 1992) examine the impact of truck vibration and packaging systems on apple bruising. The study evaluated four interior packaging options: foam trays, paper pulp trays, and two paperboard partition/box combinations. Testing was conducted on a vibration table using a random controller, which mimicked the vibrations experienced by truck trailers with leaf-spring

and air-cushion suspensions on expressways. The results indicated that foam trays provided the best protection, followed by paperboard partitions. Paper pulp trays resulted in the highest damage levels. Additionally, the Air-ride truck suspension caused greater damage compared to the leaf-spring suspension across all package types.

While various studies have assessed the damage caused by vibration on different species of fruits and vegetables, there is limited information available on the interaction between packaging and fruits during vibration (Al-Dairi et al., 2022). To ensure the safety of packaged produce and to optimize packaging designs to minimize damage and costs, it is essential to understand how packages and produce react under static and dynamic loads (Fadiji, Coetzee, Chen, et al., 2016).

ML has demonstrated potential for non-destructive product defect detection in recent studies. Nturambirwe and Opara (Nturambirwe & Opara, 2020) and Suprijono et al., (Suprijono et al., 2022) both highlight the role of ML methods in addressing technical challenges and achieving fast, early, and quantitative assessments. Image processing and artificial neural networks have been successfully used to detect defects in agricultural commodities, with high accuracy rates (Suprijono et al., 2022). Furthermore, deep learning technology has been applied to detect defects in tomatoes, leading to increased speed, accuracy, and cost-effectiveness in the grading process. Shi and Wu (Shi & Wu, 2019) and Mahanti et al, (Mahanti et al., 2022) reviews the application of the different image processing technique to detect the mechanical damage in apple fruits. These studies collectively underscore the potential of ML in enhancing quality assessment and defect detection in agricultural products.

To address the issue of transportation vibrations causing damage to apples, ML solutions can be employed to optimize transport methods and minimize risk. These advanced algorithms

and predictive models analyze factors such as road conditions, vehicle dynamics, and packaging characteristics to develop strategies that reduce mechanical stress on apples. ML techniques provide detailed insights into how packages and produce interact under different loads, allowing for accurate prediction and grading of apple maturity and quality. By identifying factors that contribute to damage, ML enables packaging engineers to design more effective packaging solutions, ensuring safer and more efficient transportation.

This chapter examines the bruising of apples in four different packaging types under simulated transportation vibrations. It aims to predict vibration damage and analyze influential factors and bruise severity. ML methods were used to predict mechanical damage to transported packed apple fruit, aiming to develop models for optimal transportation conditions. The study highlights the transformative potential of ML in improving the efficiency and sustainability of packaging systems, reducing waste, and enhancing product quality. By considering factors such as vibration intensity, duration, vibration level (truck suspension system), apple type, and packaging type, the research provides valuable insights for designing more resilient and effective packaging solutions, addressing an underexplored area in predicting packed apple bruising during transit. The novelty of this study lies in its application of ML models to predict and analyze mechanical damage to packed apple fruit under transportation vibrations, considering various influential factors such as vibration intensity, duration, profile, package type, and apple variety. In addition, the applied ML model ranked the influence of each factor, which is highly beneficial for efficient package design.

This chapter is organized as follows: Section 3.2 outlines the data collection process for the sample dataset obtained from experimental tests. In Section 3.3, we investigate the experimental data analysis, uncovering key insights and trends. Section 3.4 evaluates the

performance of each ML model, comparing their effectiveness in predicting outcomes based on the experimental data. Finally, Section 3.5 presents the conclusions drawn from the research and outlines potential directions for future work.

3.2 Data collection

In this section, we provide a detailed description of the data collection process, including the description of simulating conditions utilizing the vibration table. Additionally, we present the ML models employed in this chapter.

3.2.1 Plant source

Two varieties of "Jonagold" and "Fuji" fresh apples were collected from MSU Clarksville Horticultural Experiment Station (MSU Clarksville Research Center, Clarksville, MI), based on their consistency in size, weight, firmness, and lack of physical damage. A truck transported the apples designated for testing to the laboratory following harvest. These specific apple cultivars were chosen for their high susceptibility to bruising, which is easily observable. The mean weight and diameter of the apples were 141.9 ± 3.1 g and 67 ± 4.0 mm respectively. Only uniformly sized and mature apples, assessed by firmness, and free from physical damage, were selected.

3.2.2 Package configuration

Figure 3.1 presents four different packaging configurations referenced in this study. These configurations, denoted as A, B, C, and D, represent common designs employed within the U.S. fruit industry for the handling of apples. Package A included a single wall CP Regular Slotted Container (RSC) along with a molded paper pulp tray. The box measured 480×320×105 mm, with each tray containing 20 apples, resulting in a total carrying capacity of 9±1.5 lbs. (see Figure 3.1a). Package B was like Package A, but instead of the molded paper pulp tray, it used plastic bags, referred to as volume packing. Each bag can contain 5 to 6 apples, with each bag weighing 3 ± 0.5

lbs. (see Figure 3.1b). Package C featured a Reusable Plastic Container (RPC) paired with a molded paper pulp tray. The container measured 580×395×190 mm, and each tray could hold 30 apples. The container had a total weight capacity of 16±6 lbs. (see Figure 3.1c). Package D closely resembled Package C in many aspects. Instead of molding paper pulp trays, it used volume packing. This approach increased its average weight capacity to 18±5 lbs. providing enhanced flexibility in accommodating larger quantities of produce.

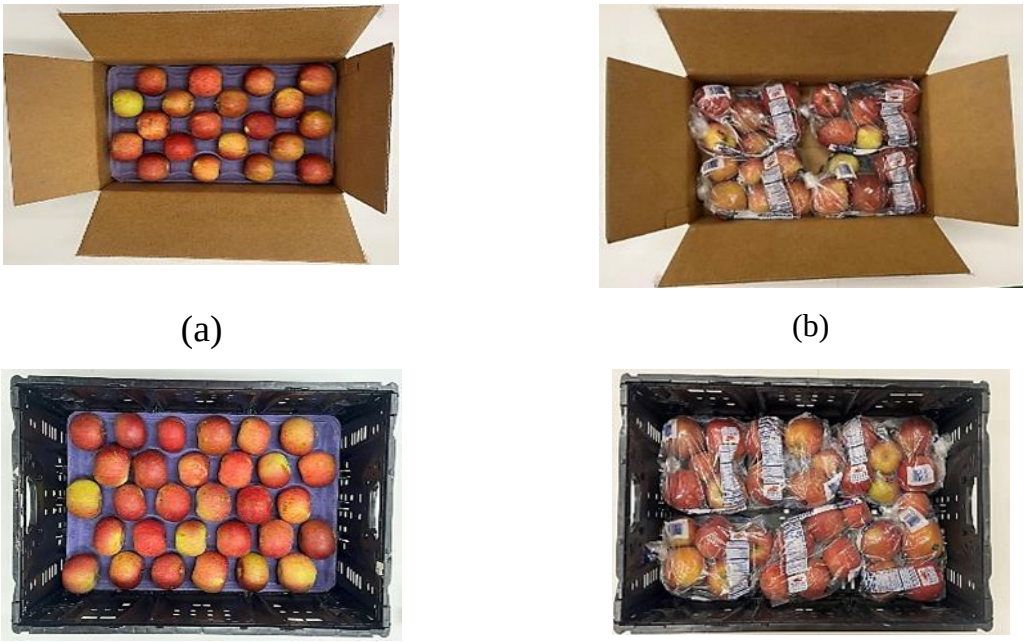

(a) (b)

(c) (d)

Figure 3.1 package type. (a) RSC + molded paper pulp tray; (b) RSC + plastic bag; (c) RPC+ molded paper pulp tray; (d) RPC+ plastic bag

3.2.3 Vibration simulation

The laboratory simulation involved utilizing an electrohydraulic vibration table (Model 10000 Vibration Test System, Lansmont) to conduct rigorous testing on packaging integrity. Two distinct vibration profiles were employed: ISTA 3A, representing an Over-the-road profile, and ISTA 3H, simulating an Air-ride profile. A random vibration controller was utilized to execute the

vibration spectrums depicted in Figure 3.2. Vibration tests were conducted with varying durations of 1, 3, and 5 hours and intensities of 0.2, 0.3, 0.5, and 0.7 *Grms* for each profile. These parameters aimed to replicate real-world transportation conditions comprehensively including both smooth and rough roads.

All tests were conducted under standard conditions (70°F, 50% RH), ensuring consistency across experiments. Following the vibration testing, packages were stored for 72 hours to allow any resulting bruises to become visible. Fresh produce, especially susceptible to mechanical damage, may take a few hours for visible bruises to appear on the injured area, depending on the degree and type of mechanical damage incurred. This delayed indication implies that bruising in some produce may remain undetected until it reaches the retail store or consumer, underscoring the importance of robust packaging (Fadiji et al., 2023). The severity of bruising was meticulously recorded, considering the diameter of the bruise.

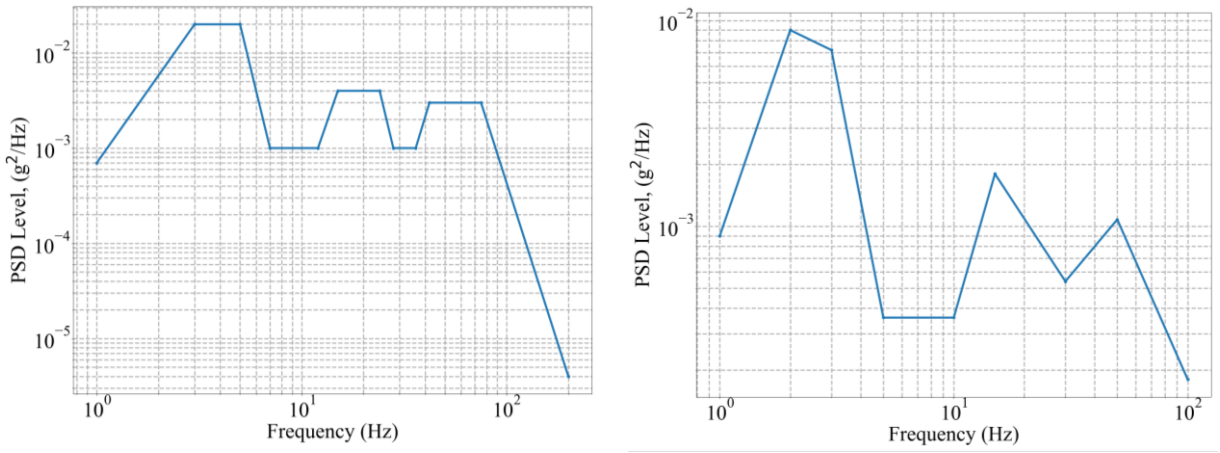

(a) (b)

Figure 3.2. Vibration level in trailer with suspension system of (a) Over-the-road, (b) Air-ride

The percentage of bruised fruit represents the fraction of apples in a package that have experienced any bruising (Singh et al., 1992). This data was crucial in assessing the efficacy of packaging designs and transportation strategies in minimizing product damage. Quantifying the extent of bruising was imperative in evaluating the performance of packaging under varied vibration conditions. According to (Pathare & Al-Dairi, 2021), the depth of damage in apples is directly correlated with the surface area of the bruising and external bruise. In this study, we considered an apple 'damaged' if the bruise diameter was more than 0.25 inches, measured using a caliper; otherwise, it was categorized as 'undamaged'. We recorded the damage incidence for each packaging type and vibration scenario, allowing us to accurately determine the percentage of apples bruised within each packaging condition. Each external bruise was assessed by determining the average diameter determined by digital caliper measurements (Singh et al., 1992). This measurement facilitated a systematic approach to assessing the impact of vibration duration and intensity on bruise severity. Furthermore, the correlation between vibration parameters and bruise characteristics could provide valuable insights for optimizing packaging designs and transportation protocols. Understanding how different vibration profiles affect bruise development aids in mitigating product losses and maintaining product quality throughout the supply chain, ultimately benefiting both producers and consumers alike.

3.3 Experimental data analysis

The box plot in Figure 3.3 illustrates the distribution of the percentage of damage for two different vibration profiles, Over-the-road and Air-ride. The horizontal line inside each box represents the median percentage of damage, which is around 30% for the Over-the-road profile and around 20% for the Air-ride profile. The plot reveals that the Over-the-road vibration profile not only has a higher median percentage of damage but also exhibits greater variability, indicating

more significant and inconsistent damage levels. In contrast, the Air-ride vibration profile results in a lower median percentage of damage and less variability, suggesting more consistent and less severe damage to the packages. This indicates that the Air-ride profile is less damaging and more reliable compared to the Over-the-road profile, likely due to the smoother and more controlled nature of the Air-ride transportation method. Consequently, the Air-ride profile may be preferable for transporting packages that are sensitive to damage.

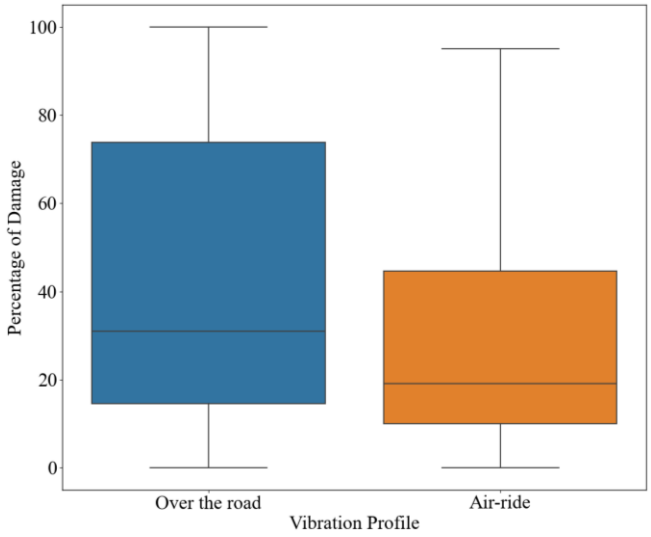

Figure 3.3. Bar plot for percentage of apple damage by vibration profile

The statistical analysis indicates that several factors have a statistically significant effect on the percentage of damage to apples, with *p*-values < 0.005. Specifically, the parameter profile, intensity, duration, and package type significantly influence the percentage of damage. The 'Intensity' factor, with a p-value of 7.24×10^{-45}, indicates an extremely strong influence of vibration intensity on the damage percentage, highlighting the importance of controlling vibration levels during transport.

The bar chart in Figure 3.4, the effect of package type on percentage of damage illustrates the mean percentage of damage for different package types (A, B, C, and D), with error bars

representing the standard deviation. Package type C exhibits the highest mean percentage of damage at approximately 50%, suggesting it is the least effective in preventing damage. In contrast, Package types A, B, and D have lower mean damage percentages, around 30-40%, indicating better performance in reducing damage. Notably, all package types show significant variability, with Package types A and C displaying the most inconsistency, as evidenced by their extensive error bars. The high variability across all package types implies that factors beyond the type of packaging might be influencing the damage percentage. This analysis suggests that while Package Type C is less effective, other underlying factors need further investigation to fully understand and mitigate the damage.

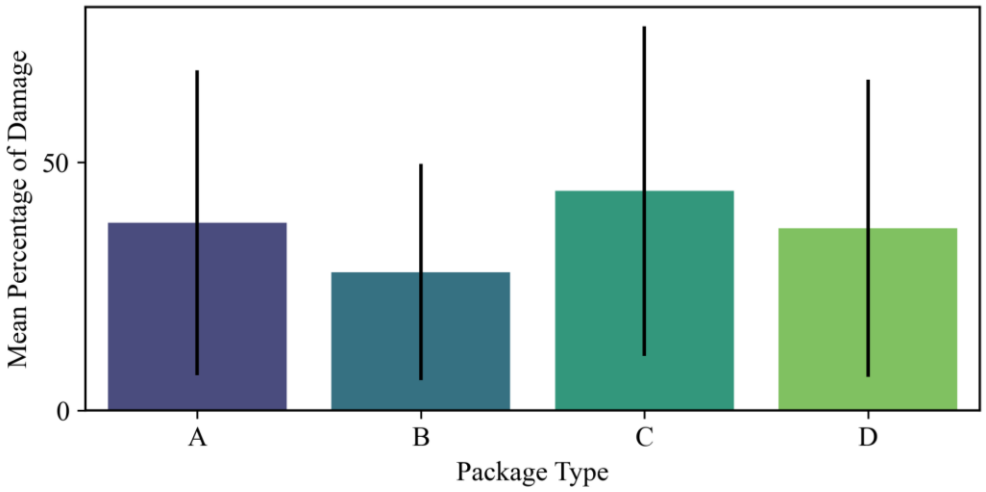

Figure 3.4. Effect of package type on percentage of damage

3.3.1 Data preprocessing for ML models

As the first step in setting the data for the ML models, the input and output data sets are determined. Table 3.1 shows the input variables ($X = \{x_1, x_2, x_3, x_4, x_5\}$) and the output variable $\{Y\}$ used in this research.

Table 3.1. An overview of the variables in this study

Parameter	Type	Unit
x_1: vibration profile (Air-ride and Over-the-road)	input	ISTA-random-vibration profile
x_2: vibration intensity (0.2, 0.3, 0.5, 0.7)	input	G*rms*
x_3: vibration duration (1, 3, 5)	input	hour
x_4: type of package	input	A, B, C, D
x_5: type of apple	input	Jonagold, Fuji
Y: percentage of bruised apple	output	%

In this chapter, the dataset was divided into three subsets: a training set, a validation set, and a test set. The training set, comprising (70%) of the data, is used to train the ML models by allowing it to learn the underlying patterns and relationships within the data. The model adjusts its parameters during this phase to minimize errors and improve prediction accuracy. The validation set, which includes (15%) of the data, is utilized to tune the hyperparameters of the model and evaluate its performance during the training phase. This helps in selecting the best model configuration that generalizes well to unseen data by checking for overfitting and refining hyperparameters. Finally, the test set, also (15%) of the data, is used to evaluate the performance of final model after training and validation are complete. This provides an unbiased assessment of the predictive accuracy and generalizability of model on new, unseen data, ensuring that the model performs well in real-world scenarios. By splitting the data into these three sets, we ensure a robust and effective training process that results in a model capable of making accurate predictions on new data.

3.4 ML models used in this chapter

In this chapter, we apply three ML models: linear regression, decision tree regression, and random forest regression, as previously explained in Chapter 1. Linear regression is used due to its simplicity and interpretability, providing a baseline for understanding relationships between variables. Decision tree regression is employed because of its ability to handle non-linear relationships and capture interactions between features effectively. Random forest regression, an ensemble learning method, is included for its robustness and ability to reduce overfitting by averaging multiple decision trees, thereby improving prediction accuracy. By using these diverse models, we aim to comprehensively evaluate and compare their performance in predicting vibration damage to apple fruit and packaging during transportation. Each model is assessed for its effectiveness in predicting the percentage of bruised apples, considering the unique characteristics of our dataset. Linear regression, a fundamental and widely used model, serves as a baseline to understand the relationship between the variables. Decision tree regression, known for its ability to handle non-linear relationships and interactions between variables, is employed to capture the complexity of the dataset. Finally, the random forest regression model, an ensemble learning method that builds multiple decision trees and merges them for a more accurate and stable prediction, is utilized to enhance the robustness of the predictions.

Next section provides a detailed evaluation of the ML models. Through this comprehensive evaluation, we aim to determine the most suitable model for accurately predicting the percentage of bruised apples based on the given dataset.

3.5 Results

This section presents and interprets the prediction plots for three different regression models: linear regression, decision tree regression, and random forest regression, comparing their performance in terms of predicting the percentage of damage across various data points.

3.6 Comparison of regression model predictions

Figure 3.5 presents the prediction plots for three different regression models: (a) linear regression, (b) decision tree regression, and (c) random forest regression. Each plot compares the predicted values against the actual values, providing insight into the performance of each model. In Figure 3.5a, the prediction plot for the linear regression model shows the predicted values closely following the actual values, although there are notable deviations, particularly at certain peaks and troughs. This indicates that while the linear regression model captures the overall trend, it struggles with accurately predicting the extreme values. This can be attributed to the assumption of the model in a linear relationship between the input variables and the output, which may not hold true for the more complex patterns in the data. Figure 3.5b displays the prediction plot for the decision tree regression model. This model shows a closer alignment with the actual values compared to the linear regression, particularly at the peaks and troughs. The step-like patterns are evident, reflecting the nature of decision trees, which partition the data into distinct regions. Although the decision tree model handles the non-linearities in the data better than the linear regression model, it still shows some overfitting, particularly in regions with sparse data points, as evidenced by the sharp changes in predicted values. The prediction plot for the random forest regression model is shown in Figure 3.5c. This model combines the predictions of multiple decision trees, smoothing out the step-like patterns seen in the single decision tree model. The random forest regression model provides a more accurate and consistent prediction across the

entire range of actual values, with fewer extreme deviations. This suggests that the random forest model effectively captures the underlying patterns in the data while mitigating the overfitting issue observed with the single decision tree. The distribution of the residuals appears more uniform, indicating a better fit overall.

(a)

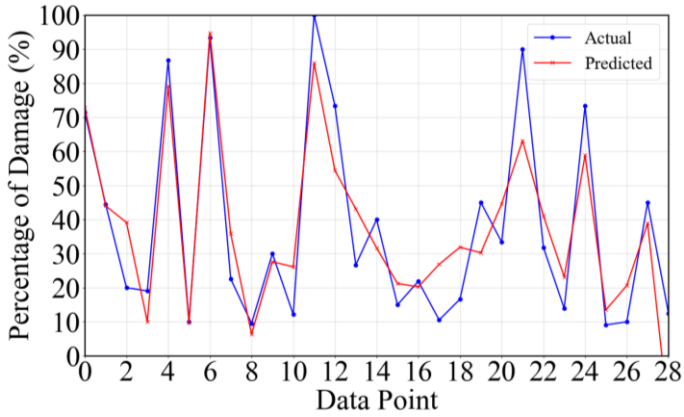

(b)

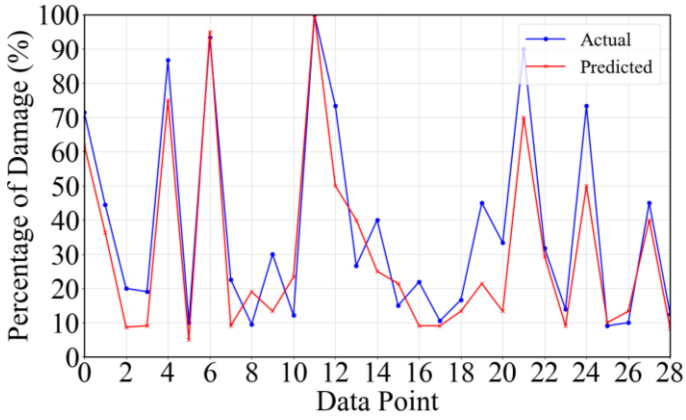

(c)

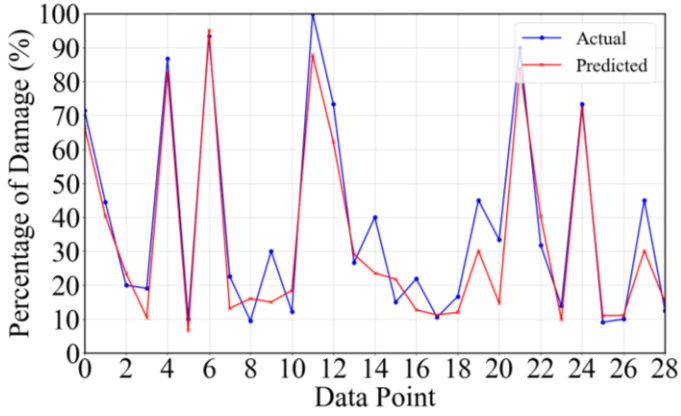

Figure 3.5. Prediction accuracy plot for (a) linear regression, (b) decision tree regression, and (c) random forest regression ML models

3.6.1 Feature importance for random forest model

Figure 3.6 depicts the relative importance of various features in predicting minimizing vibration damage to apple fruit and packaging. The features assessed include vibration intensity, duration, profile, package type, and apple type. Intensity stands out as the most significant feature, with a score significantly higher than all other features. This indicates that the intensity of vibrations has the greatest impact on the damage experienced by the apple fruit and packaging. Duration is the second most influential feature, though its score is notably lower than that of intensity, suggesting that the length of time the apples are exposed to vibrations also plays a crucial role in the extent of damage, but to a lesser extent than intensity. Package type ranks third, indicating that the type of packaging used has a meaningful impact on damage levels, as different packaging solutions might offer varying degrees of protection against vibration. The profile of the vibration, while still relevant, has a lower importance score compared to intensity, duration, and package type, implying that the specific characteristics of the vibration profile are less critical but still contribute to the overall damage. Apple type is the least influential feature, with a score close to zero, suggesting that the type of apple has minimal impact on the damage caused by vibrations, indicating that the other factors are more critical in determining the extent of damage. Overall, the analysis underscores the dominant importance of vibration intensity and duration in predicting and mitigating damage to apple fruit during transportation, with package type also playing a significant role, while vibration profile and apple type have relatively minor impacts.

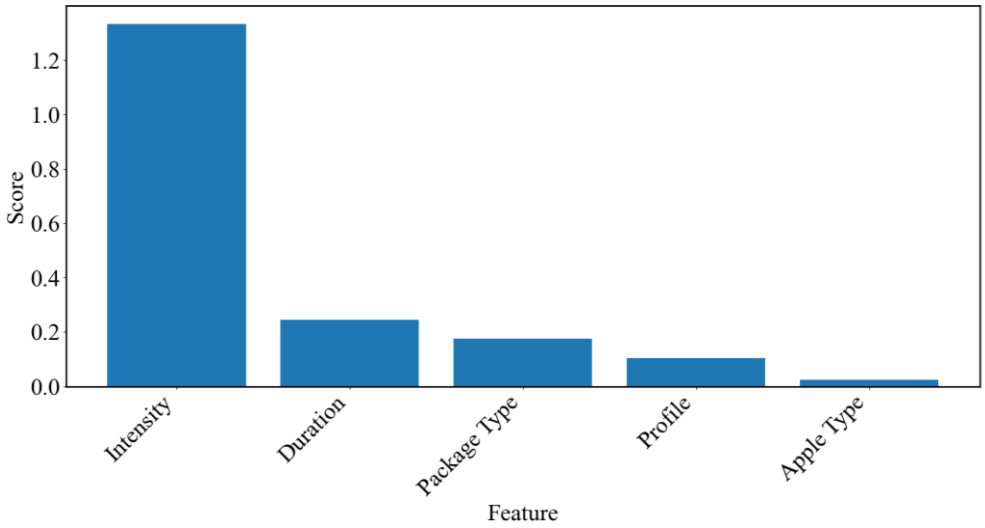

Figure 3.6. Feature importance

3.7 Comparative analysis of model performance using evaluation metrics

Table 3.2 compares the performance of three ML models. Linear regression, decision tree, and random forest using four evaluation metrics: R^2, Mean Squared Error (MSE), Root Mean Squared Error (RMSE), and Mean Absolute Error (MAE). Random Forest outperforms the other models across all metrics. It achieves the highest R^2 value of 0.927, indicating it explains 92.71% of the variance in the data, compared to 0.825 for the decision tree and 0.797 for linear regression. Additionally, random forest has the lowest MSE (65.339), RMSE (8.083), and MAE (6.381), suggesting it produces the smallest average prediction errors both in terms of squared differences and absolute differences. The decision tree performs better than linear regression but not as well as random forest, with moderate values for MSE (144.591), RMSE (12.024), and MAE (9.871). Linear regression, while the least accurate, still provides reasonable predictions with an R^2 of 0.797, MSE of 167.65, RMSE of 12.94, and MAE of 10.565. Overall, the random forest model is the most effective for this dataset, demonstrating superior predictive power and accuracy.

Table 3.2. Performance metrics

	Linear Regression	Decision Tree	Random Forest
R^2	0.7975	0.825	0.927
MSE	167.657	144.591	65.339
RMSE	12.948	12.024	8.083
MAE	10.565	9.871	6.381

3.7.1 Training data size

The line plot in Figure 3.7 shows the relationship between the number of training examples and the RMSE for both training and cross-validation sets in a random forest model. As the number of training examples increases from 25 to 100, both training and cross-validation errors decrease, indicating improved model performance. The training error (red line) starts at around 9 and stabilizes just above 5, showing increased accuracy with more data. The cross-validation error (green line) starts higher at 25, indicating initial overfitting, but decreases significantly to around 15 as more data is added, improving generalization. The shaded areas represent confidence intervals, showing reduced variability in RMSE with more training examples. Overall, the plot underscores the importance of sufficient training data for enhancing the Random Forest model's performance and generalization.

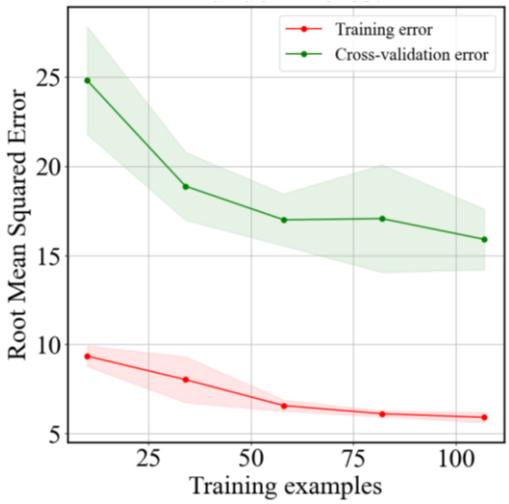

Figure 3.7. Learning curve of random forest model

3.8 Conclusion and future work

This study examines the various factors influencing the damage to apple fruit and its packaging during transportation vibrations. We investigated variables such as vibration intensity, duration, profile (suspension system), package type, and apple variety to assess their impact. Employing ML techniques like linear regression, decision tree, and random forest, we were able to predict the damage levels experienced by the transported packed apple fruit. Our findings emphasize the critical significance of vibration intensity and duration in foreseeing and mitigating damage to apple fruit during transportation. Additionally, the type of packaging used becomes a crucial factor in protecting against vibration damage. While the specific characteristics of the vibration profile and the type of apple have minor impacts, they should still be considered when designing packaging solutions. Furthermore, our application of ML models, including linear regression, decision tree, and random forest, revealed that the random forest model outperformed the others, achieving an R^2 of 0.927. This underscores the superior predictive power and accuracy of the random forest model in this context, further highlighting its efficacy in predicting and mitigating damage during transportation vibrations. These ML predictive models not only aid in

anticipating the percentage of damage for transported packed apple but also allow us to identify potential areas for improvement in packaging design or transportation conditions, ultimately contributing to the reduction of damage to packaged fruit. Overall, this chapter offers valuable insights for enhancing packaging design and transportation practices to predict damage to transported packed apple fruit during transit as well as highlighting the benefit of applying ML in food packaging dynamics area. Thoughtful selection of improved solutions to this critical issue can significantly reduce the vulnerability of fresh produce to vibration damage during road transport, thereby lowering the incidence of postharvest losses of fresh commodities (Al-Dairiet al., 2022). As for future research, we recommend exploring more apple types with additional layers for apple packaging and incorporating factors such as temperature and humidity in the analysis. Moreover, a comprehensive understanding of the internal package design factors contributing to damage would be beneficial in developing even more effective packaging solutions. Last but not least, it is suggested to update the study to apply multi-axis vibration tables (like an IMV's multi-axis shaker recently installed in the School of Packaging at MSU), which simulates transportation vibration more realistically than the current vertical single axis in this study.

REFERENCES

Al-Dairi, M., Pathare, P. B., Al-Yahyai, R., & Opara, U. L. (2022). Mechanical damage of fresh produce in postharvest transportation: Current status and future prospects. *Trends in Food Science and Technology, 124*(March), 195–207. https://doi.org/10.1016/j.tifs.2022.04.018

Bratu, A. M., Popa, C., Bojan, M., Logofatu, P. C., & Petrus, M. (2021). Non-destructive methods for fruit quality evaluation. *Scientific Reports* (Vol. 11, Issue 1). https://doi.org/10.1038/s41598-021-87530-2

Du, Z., Zeng, X., Li, X., Ding, X., Cao, J., & Jiang, W. (2020). Recent advances in imaging techniques for bruise detection in fruits and vegetables. *Trends in Food Science and Technology, 99*, 133–141. https://doi.org/10.1016/j.tifs.2020.02.024

Fadiji, T., Coetzee, C., Chen, L., Chukwu, O., & Opara, U. L. (2016). Susceptibility of apples to bruising inside ventilated CP packages during simulated transport damage. *Postharvest Biology and Technology, 118*, 111–119. https://doi.org/10.1016/j.postharvbio.2016.04.001

Fadiji, T., Kaseke, T., Lufu, R., Li, Z., Opara, U. L., & Fawole, O. A. (2023). Impact of Packaging on Bruise Damage of Fresh Produce. *Mechanical Damage in Fresh Horticultural Produce* (pp. 311–336). Springer Nature Singapore. https://doi.org/10.1007/978-981-99-7096-415

Grand View Research. (2018). U.S. Fruits and Vegetables Market Size. https://www.grandviewresearch.com/industry-analysis/us-fruit-vegetables-market

He, Y., Xiao, Q., Bai, X., Zhou, L., Liu, F., & Zhang, C. (2022). Recent progress of nondestructive techniques for fruits damage inspection: a review. *Critical Reviews in Food Science and Nutrition, 62*(20), 5476–5494. https://doi.org/10.1080/10408398.2021.1885342

Hosoya, N., Mishima, M., Kajiwara, I., & Maeda, S. (2017). Non-destructive firmness assessment of apples using a non-contact laser excitation system based on a laser-induced plasma shock wave. *Postharvest Biology and Technology, 128*, 11–17. https://doi.org/10.1016/j.postharvbio.2017.01.014

Jung, H.-M., & Park, J.-G. (2012). Effects of Vibration Stress on the Quality of Packaged Apples during Simulated Transport. *Journal of Biosystems Engineering, 37*(1), 44–50. https://doi.org/10.5307/jbe.2012.37.1.044

Kim, K. B., Lee, S., Kim, M. S., & Cho, B. K. (2009). Determination of apple firmness by nondestructive ultrasonic measurement. *Postharvest Biology and Technology, 52*(1), 44–48. https://doi.org/10.1016/j.postharvbio.2008.04.006

Lee, A., Shim, J., Kim, B., Lee, H., & Lim, J. (2022). Non-destructive prediction of soluble solid contents in Fuji apples using visible near-infrared spectroscopy and various statistical methods. *Journal of Food Engineering, 321* (January), 110945. https://doi.org/10.1016/j.jfoodeng.2022.110945

Li, Z., & Thomas, C. (2014). Quantitative evaluation of mechanical damage to fresh fruits. *Trends in Food Science and Technology*, *35*(2), 138-150. https://doi.org/10.1016/j.tifs.2013.12.001

Lin, M., Fawole, O. A., Saeys, W., Wu, D., Wang, J., Opara, U. L., Nicolai, B., & Chen, K. (2023). Mechanical damages and packaging methods along the fresh fruit supply chain: A review. *Critical Reviews in Food Science and Nutrition* (Vol. 63, Issue 30, pp. 10283–10302). Taylor and Francis Ltd. https://doi.org/10.1080/10408398.2022.2078783

Lu, Y., & Lu, R. (2017). Non-destructive defect detection of apples by spectroscopic and imaging technologies: a review. *Transactions of the ASABE*, *60*(5), 1765-1790.

Mahanti, N. K., Pandiselvam, R., Kothakota, A., Ishwarya S., P., Chakraborty, S. K., Kumar, M., & Cozzolino, D. (2022). Emerging non-destructive imaging techniques for fruit damage detection: Image processing and analysis. *Trends in Food Science and Technology*, *120* (December 2021), 418–438. https://doi.org/10.1016/j.tifs.2021.12.021

Mehl, P. M., Chen, Y. R., Kim, M. S., & Chan, D. E. (2004). Development of hyperspectral imaging technique for the detection of apple surface defects and contaminations. *Journal of Food Engineering*, *61*(1 SPEC.), 67–81. https://doi.org/10.1016/S0260-8774(03)00188-2

Nturambirwe, J. F. I., & Opara, U. L. (2020). ML applications to non-destructive defect detection in horticultural products. *Biosystems Engineering*, *189*, 60–83. https://doi.org/10.1016/j.biosystemseng.2019.11.011

Pathare, P. B., & Al-Dairi, M. (2021). Bruise Susceptibility and Impact on Quality Parameters of Pears During Storage. *Frontiers in Sustainable Food Systems*, *5*. https://doi.org/10.3389/fsufs.2021.658132

Shi, X., & Wu, X. (2019). Tomato processing defect detection using deep learning. *Proceedings-2019 2nd World Conference on Mechanical Engineering and Intelligent Manufacturing, WCMEIM 2019*, 728-732. https://doi.org/10.1109/WCMEIM48965.2019.00153

Singh, S. P., Burgess, G., & Xu, M. (1992). Bruising of apples in four different packages using simulated truck vibration. *Packaging Technology and Science*, *5*(3), 145–150. https://doi.org/10.1002/pts.2770050304

Solovchenko, A. E., Chivkunova, O. B., Gitelson, A. A., & Merzlyak, M. N. (2010). Non-Destructive Estimation Pigment Content, Ripening, Quality and Damage in Apple Fruit with Spectral Reflectance in the Visible Range. *Fresh Produce*, *1*, 91–102.

Suprijono, H., Kartikadarma, E., Yusianto, R., & Marimin, M. (2022). Defect Detection of Agricultural Commodities using Image Processing and Artificial Neural Networks. *2022 International Seminar on Application for Technology of Information and Communication: Technology 4.0 for Smart Ecosystem: A New Way of Doing Digital Business, ISemantic 2022*, 405–408. https://doi.org/10.1109/iSemantic55962.2022.9920445

Tian, S., & Xu, H. (2023). Mechanical-based and Optical-based Methods for Nondestructive Evaluation of Fruit Firmness. *Food Reviews International*, *39*(7), 4009–4039. https://doi.org/10.1080/87559129.2021.2015376

Van Zeebroeck, M., Van linden, V., Ramon, H., De Baerdemaeker, J., Nicolaï, B. M., & Tijskens, E. (2007). Impact damage of apples during transport and handling. *Postharvest Biology and Technology*, *45*(2), 157–167. https://doi.org/10.1016/j.postharvbio.2007.01.015

Vursavuş, K., & Özgüven, F. (2004). Determining the effects of vibration parameters and packaging method on mechanical damage in golden delicious apples. *Turkish Journal of Agriculture and Forestry*, *28*(5), 311–320. https://doi.org/10.3906/tar-0401-10

Walkowiak-Tomczak, D., Idaszewska, N., Łysiak, G. P., & Bieńczak, K. (2021). The effect of mechanical vibration during transport under model conditions on the shelf-life, quality and physico-chemical parameters of four apple cultivars. *Agronomy*, *11*(1). https://doi.org/10.3390/agronomy11010081

Chapter 4: Predicting Compression Strength Loss in Corrugated Paperboard Boxes Post-Transportation Vibrations Using ML Models

Abstract

Effective packaging design is essential for ensuring the safe transportation and delivery of products, minimizing damage, and maintaining product integrity throughout the supply chain. With a growing emphasis on sustainability, corrugated paperboards have become increasingly popular for packaging due to their recyclable nature and reduced environmental impact. During a distribution cycle, these packages undergo transportation vibrations from the shipping vehicle, which can affect their structural integrity. This study delves into the prediction of compression strength loss in corrugated paperboard boxes following exposure to simulated transportation vibration, a critical concern in the packaging industry. By leveraging advanced ML techniques, this research aims to develop efficient models that can predict the extent of compression strength degradation due to vibrational forces experienced during transit. The findings from this investigation have significant implications for optimizing packaging materials and design, ultimately enhancing the durability and reliability of packaging solutions in various industries. The study utilizes ML models, with a specific focus on the XGBoost algorithm, to predict the percentage of compression strength loss based on various parameters. These parameters include the dimensions of the box (length, width, and height), vibration intensity, vibration duration, vibration profile (following ISTA standards), and top load. Using a collected dataset from experimental tests encompassing a range of scenarios, the XGBoost model achieved a remarkable R^2 score of 0.93, indicating its efficacy in predicting compression strength loss. Such accuracy is crucial in guiding packaging design decisions to minimize damage and ensure product integrity during transportation. The feature importance analysis reveals that vibration characteristics dominate the predictive capability of the XGBoost model. Vibration duration is the most critical feature, significantly impacting the model's performance. Vibration intensity and vibration profile

also play important roles, while the physical dimensions of the CP box, such as width, length, and height, are less influential. This highlights the greater importance of vibration characteristics over physical dimensions in the predictions of model. This research contributes to the field of packaging dynamics and distributions by providing a reliable predictive model for CP box compression strength loss.

4.1 Introduction

During distribution, packages endure various loading conditions, and inadequate protection can result in damage to both the package and the product. Studies have shown that shipping packages in a unitized configuration significantly reduces damage levels compared to shipping individual parcels (Singh et al., 2014). However, this method may not be appropriate for all types of products, such as extremely delicate items or hazardous materials. Over the past decade, there has been a substantial increase in the number of individual packages shipped directly to consumers, emphasizing the need for durable packaging solutions that can withstand the challenges of individual distribution (Singh & Pratheepthinthong, 2000). CP, a global sustainable packaging material, is employed to residence and protect a vast array of commodities, ranging from delicate consumer items to robust industrial components (Zang et al., 2021). However, the structural integrity of these corrugated boxes can be compromised during transportation, particularly due to the effects of vibration (Garcia-Romeu-Martinez, 2007). The compressive strength of corrugated boxes is a crucial indicator of their performance and ability to withstand the demands of storage and distribution (Zang et al., 2021). Vibration, a frequent hazard during transportation, can impose significant damage on the packaged-product system, altering the structural characteristics of the corrugated material (Molnár & Böröcz, 2020). Understanding the extent and mechanisms of this

damage is essential for designing robust sustainable packaging solutions that can mitigate the adverse effects of vibration.

Packaging systems are subjected to random dynamic compressive loads resulting from vehicle-generated vibrations during transportation. The severity and level of dynamic compressive loads are affected by vibration levels, stack weight, and stack configurations (Garcia-Romeu-Martinez, 2007). The vibration levels play a crucial role, as higher vibrations can lead to increased stress and potential damage to the stacked items. The configuration of the stack itself is significant; the arrangement and stability of the items within the stack can affect how the loads are distributed and absorbed. The weight of the stack is a substantial factor, as heavier stacks are subject to greater compressive forces, especially during transportation. Depending on the properties of material and the design of the box, a box can tolerate these compressive loads for a sufficiently long period of time (Garcia-Romeu-Martinez, 2007). Vibration levels experienced by packaged goods during transportation have been the subject of extensive research (Böröcz & Molnár, 2020). Measurements of vibration in smaller stacks of packages, as opposed to larger unitized loads, have revealed that the intensity of vibration increases with the height of the stack and the degree of free movement permitted. Marcondes (Marcondes, 1992) studied the effects of static and dynamic load histories on the compression strength and shock absorption properties of corrugated fiberboard boxes. The results indicated that while static compression forces did not significantly impact the performance of boxes, dynamic compression forces had a notable effect, suggesting that previous load histories play a crucial role in the overall durability and integrity of packaging during transportation. Rouillard et al., (Rouillard et al., 2007) explored the impact of random dynamic compressive loads on the stiffness and damping characteristics of packaging systems during transportation. Using thermal imaging and Frequency Response Function (FRF) monitoring, the

results reveal that regions of elevated temperature in corrugated paperboard indicate structural failures, and there is a strong correlation between reduced system stiffness and temperature variations. The reduction of compression strength in CP boxes after transportation vibration is a significant concern, particularly for the packaging of agricultural products (Jung & Park, 2012). This issue is of paramount importance as it directly impacts the integrity and protection of the packaged goods, which can lead to significant economic losses and compromised product quality.

As the vehicles traverse various terrains and encounter differing road conditions, the boxes are subjected to a complex array of vibrations, impacts, and compressive forces. These dynamic loads can induce structural deformations and degradation of the paperboard material, ultimately leading to a diminished ability to withstand compressive stresses. Furthermore, the frequency and magnitude of these vibrations can vary significantly depending on the mode of transportation, the condition of the transportation infrastructure, and the specific characteristics of the packaged goods. To address this challenge, researchers have employed a complicated approach, combining experimental investigations, numerical simulations, and analytical modeling. Experimental studies have been conducted to quantify the reduction in compression strength under various transportation conditions, with a focus on understanding the relationship between the vibration parameters and the resulting structural changes in the CP. Packages are subjected to numerous loading conditions during the distribution process, and inadequate protection can result in damage to both the package as well as the product during shipment.

This research investigates the loss of compression strength in CP boxes subjected to top load as a consequence of exposure to transportation vibrations. A data analysis approach was applied in this study, incorporating advanced ML techniques. A ML model was developed to predict the loss of compression strength, offering a more accurate and efficient means of assessing

the impact of transportation vibrations on packaging integrity. This research combines multiple parameters such as box dimensions, vibration intensity, duration, profile, and top load to create a robust predictive model. In addition, the applied ML model ranked the influence of each factor, which is highly beneficial for efficient package design. The integration of ML algorithms enhances predictive capability, providing valuable insights for improving packaging design and durability. In Chapter 1, an introduction to ML is provided. The novelty of this study is found in its pioneering use of advanced ML techniques, specifically the XGBoost algorithm, to precisely predict compression strength loss in CP boxes after simulated transportation vibrations. This research uniquely combines multiple parameters such as box dimensions, vibration intensity, duration, profile, and top load to create a robust predictive model. In addition, the applied ML model ranked the influence of each factor, which is highly beneficial for efficient package design.

This study is organized as follows: In Section 4.2, we describe the experimental data collection, outline the collection process of the sample data set from the experimental tests, and provide a comprehensive description of the data set. Section 4.3 offers an overview of the ML models employed in this study. Section 4.4 evaluates the performance of each model and discusses the prediction results. Finally, Section 4.5 presents the key findings and conclusions derived from the study.

4.2 Experimental data collection and overview

The detailed steps for data collection and model construction are outlined in this section.

4.2.1 Experimental data collection

In this study, the critical parameters considered to affect the loss of compression strength of the CP box after transportation vibration were the dimensions of the box (length, width, and height), the characteristics of the vibration (truck's suspension system, duration, intensity), and the

weight placed on top of the box (top load). The input variables ($X = \{x_1, x_2, x_3, x_4, x_5, x_6, x_7\}$) and the output variable (Y) are detailed in Table 4.1. An ASTM standard-based compressive test procedure was used to determine the compressive strength of the CP box after the vibration tests. The single wall C-flute CP boxes with three sets of random dimensions of 12 × 10 × 8 inches, 16 × 12 × 10 inches, and 18 × 10 × 8 inches were prepared. The sample boxes have a bursting strength of 200 lbs., meaning the test boxes can endure 200 lbs./sq.in. of sidewall pressure before bursting. The samples were conditioned for 24 hours at 72°F and 50% relative humidity, as required by the test standard ASTM D642 (ASTM D642, 2000).

Table 4.1 An overview of parameters in this study

Parameter	Type	Unit
x_1: length (12, 16, 18)	input	inch
x_2: width (10, 12)	input	inch
x_3: height (8, 10)	input	inch
x_4: vibration intensity (0.3, 0.5, 0.7)	input	G*rms*
x_5: vibration duration (30, 60, 90)	input	minutes
x_6: vibration profile (Over-the-road, Air-ride)	input	ISTA-random-vibration profiles
x_7: top load (10, 25)	input	lbs.
Y: percentage of loss of compression strength	output	%

The laboratory simulation involved utilizing an electrohydraulic vibration table (Model 10000 Vibration Test System, Lansmont) to conduct vibration testing on packaging integrity. Two distinct vibration profiles were employed: ISTA 3A, representing an over-the-road profile (Truck with leaf-spring suspension system), and ISTA 3H (Truck with air-ride suspension system), simulating an air ride profile. These vibration profiles are presented in Power Spectral Density

(PSD) format. As shown in Figure 3.2, the vibration energies are significant for frequencies below 100 Hz.

Vibration tests were conducted with varying durations of 30, 60, and 90 minutes, and intensities of 0.3, 0.5, and 0.7 for each profile. The top load, a parameter used to simulate stack loading conditions, was set at 10 and 25 lbs. (see Figure 4.1). These parameters aimed to comprehensively replicate real-world transportation conditions, including both smooth and rough roads. The vibration spectrums were executed using a random vibration controller to ensure accuracy in simulating transportation environments. Each packaging sample was subjected to these conditions to evaluate their structural integrity and durability under different stress levels. The results provided a detailed understanding of how the boxes would perform during actual transit, helping to identify potential weaknesses and areas for improvement in packaging design. This approach ensured that the testing conditions closely matched real-life scenarios, making the findings highly relevant for practical applications.

Compression tests for CP boxes are commonly used in packaging to evaluate the critical buckling loads of the packages. Similar to other compression testers in engineering, a compression tester with a wider platen area applies vertical loads to a box. Initially, control compression tests were conducted on CP boxes before subjecting them to vibration tests, recording the buckling loads for each different box dimension. Following this, vibration tests were performed, and subsequent compression tests were conducted on the samples post-vibration. Each package compression test was repeated five times, using a new, untested box for each iteration, and the average values were recorded as the compression strength of the samples after vibration.

Figure 4.1. Experimental test setup using a vertical vibration shaker table. The top packages with two different weights serve as the top loads

4.3 Experimental data analysis

Figure 4.2 illustrates the relationship between the top load and the percentage loss in a compression strength of the box after the vibration. From the plot, it is evident that the average percentage loss is higher for a top load of 10 lbs. compared to a top load of 25 lbs. After analyzing the results, the average loss for a top load of 10 lbs. was approximately 14%, whereas for a top load of 25 lbs., the average loss was around 12%. This indicates that a higher top load might be associated with a lower percentage loss in the CP boxes. While a heavier top load applies larger amount of compression force to the package, it can restrict box's vibrations and jumps during a transportation random vibration. The impacts applied to the box during these jumps might affect the box compression strength more than the heavier top loads. This information could be crucial for optimizing packaging strategies to minimize loss during transportation or storage.

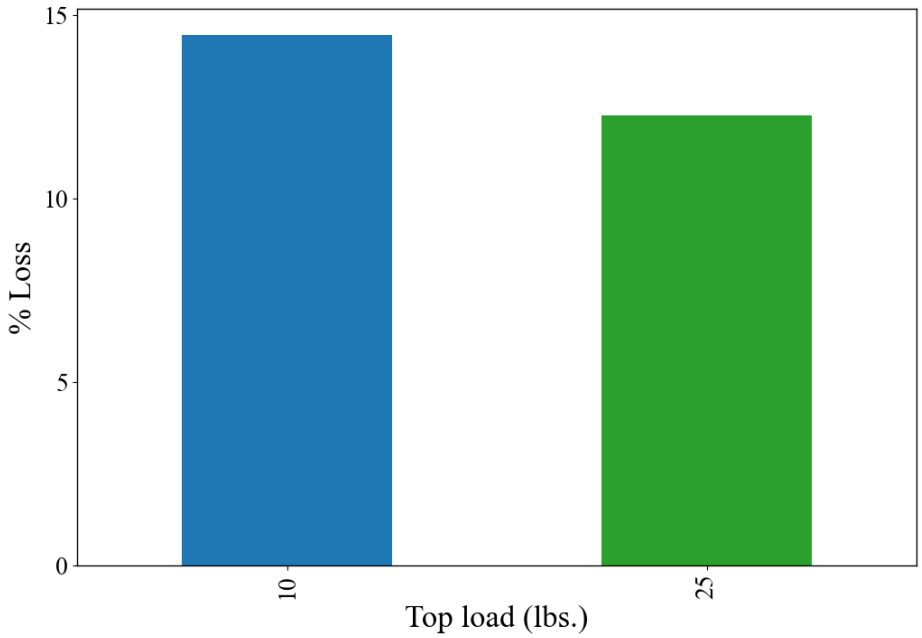

Figure 4.2. Effect of top load on percentage of loss of compression strength

Figure 4.3 illustrates the effect of different vibration profiles on the percentage loss of compression strength. The broad distribution of the Over-the-road profile suggests that the Over-the-road profile is associated with a higher and more variable percentage loss in compression strength. In contrast, the Air-ride vibration profile shows a much narrower range of loss percentages. This narrow distribution and lower median loss suggest that the Air-ride profile results in significantly less and more consistent loss in compression strength compared to the Over-the-road profile. Similar to other studies, this suggests that the Air-ride profile provides a smoother ride for packages causing less damage and better maintaining the integrity of packaged items during transportation.

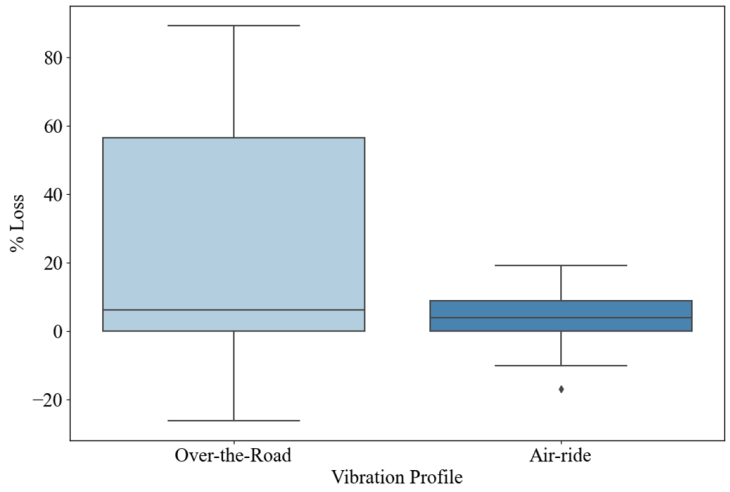

Figure 4.3. Effect of vibration profile on percentage of loss

4.3.1 Data preprocessing for ML models

The ML introduction is described in Chapter 1. In this study, the dataset was divided into training and testing sets, with 80% of the data allocated for training and the remaining 20% reserved for testing. The training set, comprising the majority of the data, is utilized to develop and train ML models, enabling them to learn the underlying patterns and relationships within the data. Conversely, the testing set is employed to evaluate the performance of these trained models, ensuring that they generalize well to new, unseen data. This division allows for a robust assessment of the predictive capabilities of the model and helps prevent overfitting, ultimately enhancing the reliability and accuracy of the findings of the study. To determine the variance ($\Delta\, CS$) in the compression strength (CS) of a package pre- and post-vibration testing, the following equation (Eq. 1) was employed:

$$\Delta\, CS\ = CS_{before} - CS_{after} \tag{1}$$

and the percentage of difference is calculated by given Eq. 2:

$$Percentage\ Difference\ = \left(\frac{\Delta\ CS}{CS_{before}}\right) \times 100 \quad (2)$$

A positive $\Delta\ CS$ indicates a decrease in compression strength after the vibration test. A negative $\Delta\ CS$ would indicate an increase in compression strength after the vibration test.

4.4 ML models used in this chapter

In this study, the selection of ML models to predict the loss of compression strength in CP boxes after vibration was guided by considerations of model performance, interpretability, and computational efficiency. Linear regression, decision tree regression, and XGBoost regression algorithms were chosen due to their distinct advantages and complementary strengths. Linear regression was selected for its simplicity and ease of interpretation, allowing for a straightforward understanding of the relationship between input features and the target variable. The decision tree regression algorithm was included for its ability to model complex, non-linear relationships and its intuitive decision-making process. XGBoost regression, an advanced ensemble technique, was employed for its high prediction accuracy and robustness against overfitting. Together, these models provided a comprehensive evaluation of the factors influencing compression strength loss, enabling a robust and reliable prediction framework.

4.4.1 Customized XGBoost regression model

In this study, the custom loss function in the XGBoost regression model is designed to address negative predictions (i.e., increase in compression strength after vibration), which are not mechanically feasible when predicting the percentage loss of compression strength in CP boxes after vibration. This customized loss function is important in the model as it handles negative values for the percentage loss, ensuring that the evaluation of the model is robust and realistic for the given circumstances. Including negative values in the dataset helps with the generalization of the model, as it provides a more comprehensive and realistic training set. This, in turn, can improve

the ability of the XGBoost model to generalize to unseen data and make more accurate predictions in real-world scenarios. The mathematical equation for this custom loss function combines the objective function of the XGBoost model with an additional penalty for negative predictions. Specifically, the function calculates the residuals (differences between the actual and predicted values) and adds a penalty term for any negative predictions. The penalty is set to ten times the absolute value of the negative prediction, ensuring that the model is heavily penalized for predicting negative values. The custom loss function L can be expressed as Eq. 6:

$$L(y_{true}, y_{pred}) = \frac{1}{n}\sum_{i=1}^{n}\left(y_{true,i}, y_{pred,i}\right)^2 + \frac{1}{n}\sum_{i=1}^{n} penalty\ (y_{pred,i}) \quad (6)$$

where i represents the index of each individual data point in the dataset, and n represents the total number of data points in the dataset. This customized approach helps the model to avoid making negative predictions by assigning a significant penalty, thus ensuring more realistic and logically consistent predictions for the percentage of loss. The penalty is defined as:

$$penalty\ (y_{pred,i}) = \begin{cases} 10\ \times |y_{pred,i}| & if\ y_{pred,i} < 0 \\ 0 & if\ y_{pred,i} \geq 0 \end{cases} \quad (7)$$

4.5 Results and discussions

This section provides a comprehensive analysis and interpretation of the prediction results for three distinct regression models: linear regression, decision tree regression, and XGBoost regression. Each model's performance is evaluated by comparing their predictive accuracy in estimating the loss of compression strength after vibration in CP boxes across various data points. The analysis highlights the strengths and weaknesses of each model, offering a detailed comparison to determine which model best predicts the loss of compression strength in different conditions. By examining the prediction results, we can visualize the effectiveness and reliability of the models, allowing for an in-depth understanding of their respective performance metrics.

4.5.1 Comparison of regression model predictions

The prediction plots in Figure 4.2 for each model are analyzed to evaluate their effectiveness in predicting the percentage of loss across various data points (test set). In all three plots, the blue line represents the actual percentage of compression strength loss, while the red dashed line shows the predicted percentage. The linear regression model (see Figure 4.2a) shows that it struggles to capture the true variability in the data. While it follows the general trend, it fails to predict the sharp increases and decreases accurately, for example at data points 11, 12, and 19, where the predicted values significantly underestimate the actual percentage of compression strength loss. This indicates that linear regression is not well-suited for capturing non-linear patterns in this dataset. Next, the decision tree regressor is examined as shown in Figure 4.2b. This model shows a closer alignment with the actual values across most data points, indicating a stronger fit than linear regression. It effectively captures the peaks and valleys in the data, closely following the actual percentage of loss even at higher values, such as at data points 11, 12, and 19. This performance of the model suggests it accurately reflects the variability and complexity in the dataset, outperforming the linear regression model. Finally, the XGBoost regressor plot (Figure 4.2c) demonstrates a high level of accuracy. The XGBoost model effectively captures both the overall trend and the specific peaks and valleys of the actual data. Its predictions are very close to the actual values, including the higher peaks at data points 11, 12, and 19. This indicates that XGBoost can handle the complex relationships in this data set more effectively than both the decision tree regressor and linear regression. Overall, these plots indicate that while the decision tree regressor performs well, the XGBoost regressor shows the best accuracy and reliability in predicting the percentage of loss, effectively capturing the complexity and variability in the data.

Linear regression, on the other hand, is less effective due to its inability to handle non-linear patterns and higher variability.

(a)

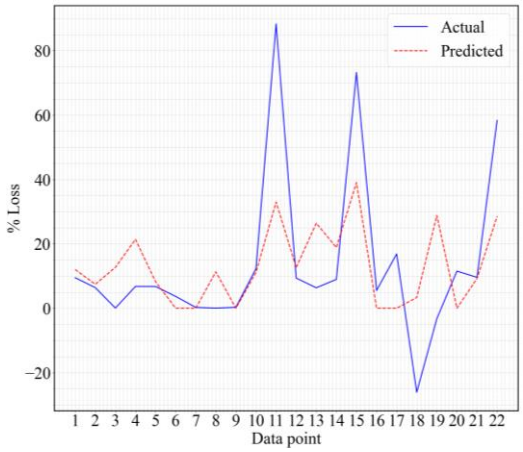

(b)

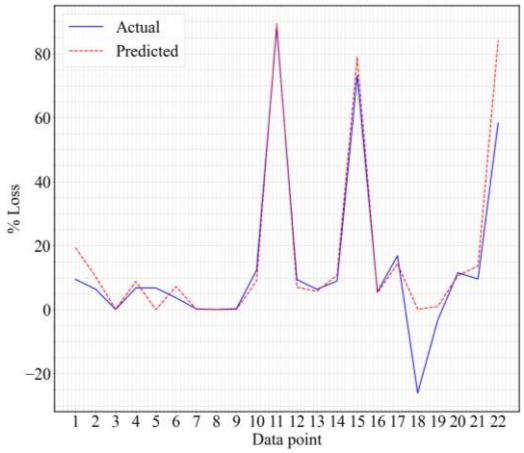

(c)

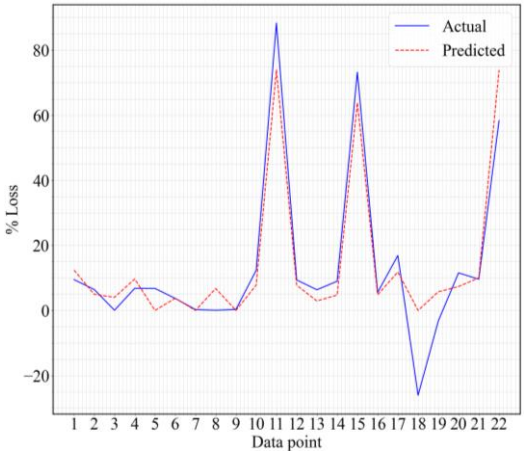

Figure 4.2. Prediction performance of (a) linear regression, (b) decision tree regression, (c) XGBoost regression model

4.5.2 Parameter importance

Figure 4.3, the bar chart illustrates the parameter importance scores for an XGBoost regression model, highlighting how each feature contributes to the predictions of the model. Among the features, "Vibration duration" has the highest importance score, 83, indicating it plays a critical role in the model's performance. Following closely is "Vibration intensity" and "Vibration profile," with scores at 67 and 57, respectively, emphasizing the significant impact of vibration-related features. "Top load" also shows considerable importance with a score of 51. On the other hand, the physical dimensions of the object, such as "Width," "Length," and "Height," of the CP box have lower importance scores of about 48, 27, and 10, respectively. Notably, "Height" is the least influential feature. This analysis underscores the predominance of vibration characteristics in the model's predictive capability compared to the physical dimensions of the CP box.

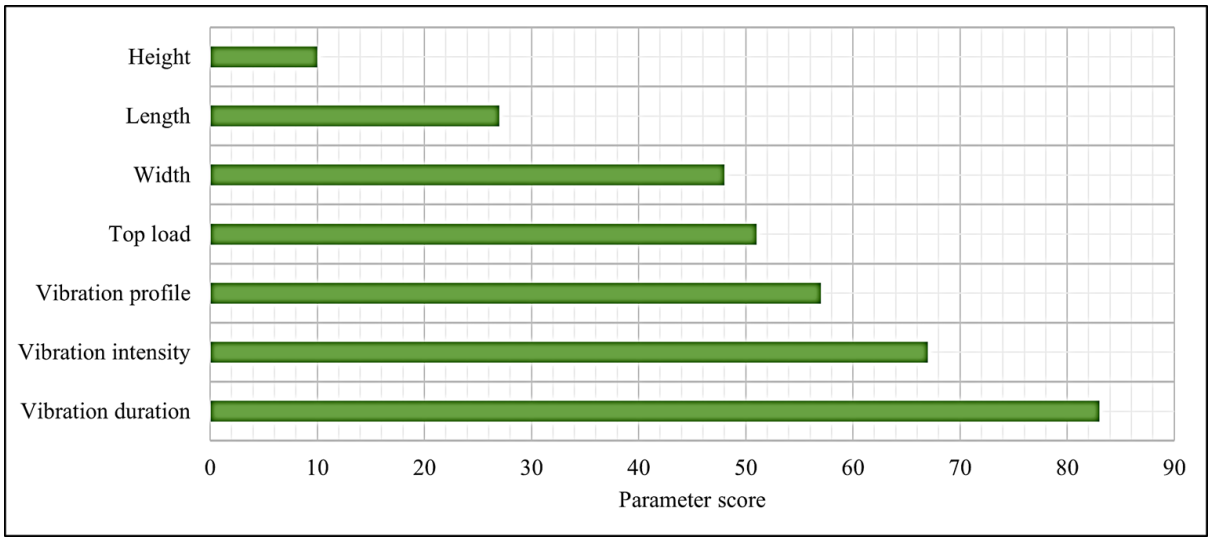

Figure 4.3. Parameter importance scores from XGBoost regression model analysis

4.5.3 Comparative analysis of model performance using evaluation metrics

Performance metrics for three regression models including linear regression, decision tree, and XGBoost are shown in Table 4.2. These models are evaluated using R^2, Mean Squared Error (MSE), Root Mean Squared Error (RMSE), and Mean Absolute Error (MAE). MSE measures the

average squared difference between predicted and actual values, RMSE provides the square root of the average squared differences, and MAE quantifies the average absolute difference, indicating the standard deviation of prediction errors. The XGBoost model demonstrates superior performance with an R^2 of 0.93, indicating that it explains approximately 93% of the variance in the data, significantly higher than linear regression (0.48) and decision tree (0.90). Furthermore, XGBoost achieves the lowest MSE (42.26), RMSE (6.51), and MAE (5.05), highlighting its accuracy in predictions. In contrast, the decision tree model, while performing better than linear regression, with an R^2 of 0.90 and moderate MSE (60.45) and RMSE (7.77), however does not match the performance of the XGBoost. Linear Regression lags considerably with an R^2 of 0.48, notably higher MSE (393.91), RMSE (19.84), and MAE (14.31), indicating it is the least effective among the three models for this particular dataset. Overall, these results underscore the effectiveness of XGBoost in regression tasks, outperforming both the decision tree and linear regression models.

Table 4.2. Performance metrics of ML models

	Linear Regression	Decision Tree	XGBoost
R^2	0.48	0.90	0.93
MSE	393.91	60.45	42.26
RMSE	19.84	7.77	6.51
MAE	14.31	4.16	5.05

4.6 Conclusion and future work

Developing a mechanics-based analytical or numerical model to predict the failure modes of corrugated paperboard (CP) boxes, with their complexities such as glued layers susceptible to humidity and temperature, is challenging. The results from experimental tests often do not follow a clear trend for these structures, making the application of ML models beneficial. This research

investigates the prediction of compression strength loss in CP boxes following exposure to simulated transportation vibration, utilizing physics informed ML models. This investigation specifically focused on key parameters that influence the structural integrity of packaging, including the dimensions of the box (length, width, and height), the intensity and duration of the vibration, the specific vibration profile (following ISTA standards), and the applied top load. These parameters were crucial in understanding the behavior of CP boxes under real-world transportation conditions. The primary objective was to develop a predictive model capable of estimating the percentage of compression strength loss that occurs in these boxes after experiencing vibration. The model was trained using a dataset that included variations in these parameters to ensure its robustness and generalizability. The XGBoost model emerged as a standout performer, achieving a remarkable accuracy with an R^2 score of 0.93. This high level of accuracy indicates that the model was able to effectively capture the complex relationships between the input parameters and the resulting compression strength loss. Such predictive capability is invaluable in the field of packaging professionals, as it can enable designers and engineers to optimize packaging designs to minimize damage and ensure product integrity during transportation. By providing a reliable method for predicting compression strength loss, this study contributes significantly to the field of packaging design and optimization. The insights gained can lead to more cost-effective and sustainable packaging solutions.

Future research could focus on several aspects, including refining the ML model by incorporating additional relevant features or exploring different algorithms to improve prediction accuracy. Additionally, investigating the impact of other environmental factors, such as humidity and temperature, on compression strength loss of CP boxes could enhance the model's predictive power. A newly installed multi-axis vibration shaker (IMV, Japan) in the School of Packaging at

MSU can be used to simulate transportation vibrations more realistically by including rotational vibrations.

REFERENCES

ASTM D642. (2000). Standard Test Method for Determining 1 Compressive Resistance of Shipping Containers, Components, and Unit Loads 1. *Test*, *00*(November), 1–6. https://doi.org/10.1520/D0642-20.

Böröcz, P., & Molnár, B. (2020). Measurement and analysis of vibration levels in stacked small package shipments in delivery vans as a function of free movement space. *Applied Sciences (Switzerland)*, *10*(21), 1–13. https://doi.org/10.3390/app10217821

Garcia-Romeu-Martinez, M. A., R. V., S. M. A., & C.-B. V. A. (2007). Monitoring the evolution of fatigue in CP under random loads. *Applied Mechanics and Materials*, *7*, 159–164.

Jung, H.-M., & Park, J.-G. (2012). Effects of Vibration Fatigue on Compression Strength of Corrugated Fiberboard Containers for Packaging of Fruits during Transport. *Journal of Biosystems Engineering*, *37*(1), 51–57. https://doi.org/10.5307/jbe.2012.37.1.051

Marcondes, J. A. (1992). Effect of load history on the performance of corrugated fiberboard boxes. *Packaging Technology and Science*, *5*(4), 179-187. https://doi.org/10.1002/pts.2770050403

Molnár, B., & Böröcz, P. (2020). Performance and analysis of unitized stacked load units under vibration simulation. *FME Transactions*, *48*(1), 96–101.

Rouillard, V., Lamb, M., & Sek, M. (2007). Determining fatigue progression in CP containers subjected to dynamic compression. *Proceedings of the 5th Australasian Congress on Applied Mechanics*. Brisbane, Qld.: Engineers Australia.

Singh, S. P., & Pratheepthinthong, S. (2000). Loss of compression strength in corrugated shipping containers shipped in the single parcel environment. *Journal of Testing and Evaluation*, *28*(4), 242-248.

Singh, P., Singh, J., Antle, J., Topper, E., & Grewal, G. (2014). Load securement and packaging methods to reduce risk of damage and personal injury for cargo freight in truck, container and intermodal shipments. *Journal of Applied Packaging Research*, *6*(1), 6.

Zang, S., Xu, L., & Sun, H. (2021). Research on Compressive Strength of High Strength Corrugated Box Based on Finite Element Analysis. *Integrated Ferroelectrics*, *213*(1), 21–34. https://doi.org/10.1080/10584587.2020.1728730

Chapter 5: Overall Conclusion

This dissertation has explored the transformative potential of applying ML techniques to enhance the design, durability, and sustainability of packaging systems, particularly in the context of dynamic distribution hazards. The research presented in each chapter tackles distinct challenges within the packaging distribution system. By employing mechanics-based analysis and data-driven ML models, three studies in this dissertation seek to predict buckling strength of ventilated corrugated paperboards plates featuring cutouts with different size, location, and shape; predict bruise damage to apple fruit and packaging subjected to vibrational forces during transportation; and forecast compression strength loss in corrugated paperboard boxes post-transportation vibrations. These ML solutions play a pivotal role in advancing packaging technology, offering substantial contributions to the field. ML predictive models offer significant cost and time advantages over traditional experimental testing in package dynamics and distribution hazards. By leveraging experimental and simulation datasets and advanced algorithms, ML models in this study can analyze and predict the damage of packaging under compressive load conditions without the need for extensive physical trials. In chapter 2, the development of machine learning models to predict the buckling strength of VCP plates with I) single circular, diamond, and square shaped cutouts and II) with multiple circular cutouts provides insights into how various factors, such as size, location, and shape of the cutouts impact the buckling load of ventilated CP plates. The model presented in this chapter serves as a valuable tool for enhancing the design of VCP plates. It facilitates the creation of more efficient structures and configurations, thereby serving as a step in optimizing the overall design process. Moreover, this study increases the knowledge of VCP plates and enhances insights into damage mechanisms and structural failure, leading to potential improved strategies for optimizing VCP performance that do not sacrifice performance. In chapter 3, the application of ML solutions to predict bruise damage to packed apple fruit during

transportation demonstrated the significant impact of data-driven analysis on packaging configurations. By identifying influential factors including vibration intensity, vibration duration, vibration profile, type of package, and type of apples and providing insights into effective protection strategies, this study enhances the understanding of vibration and package characteristics that affect external bruising in packed apples. The result of this chapter showed that the random forest model achieving an R^2 of 0.927. This highlights the ML model's superior effectiveness in predicting damage of packed apple during transportation vibrations, which is a function of various mentioned factors together. The findings emphasize the role of ML in developing future tailored packaging solutions that meet specific apple protection requirements. In Chapter 4, ML models were utilized to predict compression strength loss, guiding the development of CP packaging that withstands dynamic stresses in transportation. Key parameters, such as box dimensions, vibration intensity and duration, vibration profile, and applied top load, were analyzed to develop a robust predictive model, with the XGBoost model achieving an R^2 of 0.9302. The ML model's feature importance analysis showed with measurements that vibration characteristics are more influential in box compression loss compared to box dimension factors. This research highlights the potential of ML predictive modeling in improving packaging designs and transportation characteristics to reduce CP box damages in transit.

Collectively, the chapters in this dissertation demonstrate how ML can be employed to address specific challenges such as VCP compression strength, damage of packed apple due to transportation vibration, and reduction of compression strength in CP box after vibration in packaging dynamics and distribution hazards. The integration of ML models provides a powerful predictive tool for the development of packaging designs, thereby enhancing product protection. While not all influential factors on the studied damages can be controlled perfectly in a design, the

ML-based feature importance provided enables package designers to tackle these challenges more strategically.

The findings of this research demonstrate that ML models can significantly benefit the packaging industry, suggesting that it can be a foundation technology in advancing packaging design and performance.

5.1 Future work

Future work may explore further applications of ML in packaging, expanding the scope of its impact on various aspects of packaging engineering. Two key factors should be noted in the future works, A) importance of varying temperature and humidity on the packaging structures during dynamic testing, and B) applying multi-axis vibration analysis which simulates transportation vibrations more realistically. The continued development and refinement of predictive models will contribute to the creation of more resilient, efficient, and sustainable packaging solutions, ultimately benefiting both manufacturers and consumers. This could involve the integration of advanced sensor technologies and real-time data analytics to enhance the precision of predictions related to packaging performance under diverse environmental conditions. Additionally, future research could focus on the development of adaptive packaging systems that automatically adjust their properties in response to changing external factors, thereby optimizing product protection and reducing waste. Collaborative efforts with other industries and academic institutions could also pave the way for innovative approaches to packaging design and supply chain management, leveraging interdisciplinary expertise to tackle complex challenges. Furthermore, considering the ethical and societal impacts of implementing ML in packaging will ensure that technological advancements are made responsibly, aligning with sustainability objectives.